Developmental and peripheral nerve injury-induced changes of afferent synapses in the somatosensory thalamus

Yuichi Takeuchi

DOCTOR OF PHYLOSOPHY

Department of Physiological Sciences
School of Life Science
The Graduate University for Advanced Studies

2009

Contents

Chapter 1: Postnatal development of afferent synapses in the somatosensory thalamus of mice
- Abstract 1
- Introduction 2
- Materials and Methods 5
- Results 14
- Discussion 21
- Figures 30

Chapter 2: Peripheral nerve injury-induced remodeling of afferent synapses in the somatosensory thalamus of mice
- Abstract 44
- Introduction 46
- Materials and Methods 48
- Results 56
- Discussion 71
- Figures 80

Chapter 3: General discussion
- Discussion 110
- Figures and Tables 116
- Future direction 118

Acknowledgements 113

References 120

Chapter 1: Development of afferent synapses in the somatosensory thalamus of mice

Abstract

Lemniscal synapses in the ventroposterior medial (VPM) thalamic nucleus are afferent synapses, at which somatosensory information from the trigeminal nuclei is transmitted. Functional development of lemniscal synapses has been already described on postnatal days 7 - 24 (P7 - 24) in mice; however, precise time course of the entire postnatal development remains unknown. Here, I propose three distinct stages of developmental remodeling at lemniscal synapses based on synaptic properties and innervation patterns of lemniscal fibers onto a relay neuron. My findings are as follows: (1) During the first stage (P0 - 6), the number of lemniscal fibers which innervate a relay neuron increases. The amplitude of total lemniscal EPSCs via both NMDA and AMPA receptors rapidly grows at the end of this stage. (2) During the second stage (P7 - 20), redundant lemniscal fibers are dramatically eliminated. As a result, a relay neuron becomes monoinnervated by P21. Silent lemniscal synapses disappear during this stage. The AMPAR/NMDAR ratio of EPSC gradually increases in a similar time course. Moreover, the decay time of AMPAR-mediated EPSCs becomes shorter during this stage. A switch of alternative splice variants of AMPA receptor subunits (from flip to flop) underlies the phenomenon. (3) During the third stage (P21~), all synaptic properties are stable, indicating that the development is already completed.

Introduction

Precise synaptic connections and appropriate synaptic transmission are essential for proper functions of the nervous system. During the postnatal development, precise synaptic connections are sculpted via excessive synaptic formation and subsequent synapse elimination in both the peripheral and central nervous systems (CNS) (Purves and Lichtman, 1980; Kano and Hashimoto, 2009). Appropriate synaptic transmission is also built up via postnatal maturation processes, which include strengthening of specific synapses, changes in release probability, and switches of postsynaptic receptors. Although it is obviously important to investigate such remodeling of well identified synapses throughout postnatal development, it has been done at only few synapses in the CNS for its complexity.

Lemniscal synapses in the ventroposterior medial (VPM) thalamic nucleus are afferent synapses, at which relay neurons receive the whisker-related somatosensory information from the trigeminal nuclei in rodents. The whisker sensory pathway of rodents is one of the most studied sensory pathways on its precise somatotopic organization and fast encoding of tactile sensation (Woolsey and van der Loos, 1970; Killackey et al., 1995; Ahissar et al., 2000; Krupa et al., 2004; Petersen, 2007; Fox, 2008). Lemniscal synapses are very unique in that a relay neuron is innervated by a few lemniscal axons and the synaptic transmission is very fast, reliable, and in an all-or-none fashion. We can developmentally count the number of lemniscal fiber innervation onto a relay neuron in *in vitro* slice

preparation with whole-cell patch-clamp methods, as it has been done at climbing fiber-Purkinje cell synapses (Hashimoto and Kano, 2005). Thus, the aim of the present chapter is to study the postnatal development of lemniscal synaptic connections and transmission.

Anatomically, the postnatal development of lemniscal synapses of rodents is well characterized at both light and electron microscopy levels. On late pregnancy, developing lemniscal fibers arrive at VPM and elaborate their arbors in the nucleus (Leamey and Ho, 1998; Jones, 2007). Around postnatal days 3 - 4 (P3 - 4), lemniscal fibers are segregated according to afferent information, resulting in the complex of functional cylindrical units called barreloid, each of which is an analogous structure to a large whisker on snout (Van Der Loos, 1976; Woolsey et al., 1979). The terminals of a lemniscal fiber from the principle sensory nucleus of trigeminal nerve are confined to the single cylindrical structure (Williams et al., 1994; Veinante and Deschênes, 1999). After the establishment of topographic map, the number of lemniscal synapses dramatically increases in the ultrastructure level between P9 and 13 (Matthews and Faciane, 1977; Yamakado, 1985). The synaptic complex with glia ensheathment called synaptic glomerulus, which is characteristic of lemniscal synapses, is built up to the mature structure by P13 (Špaček and Lieberman, 1974; Matthews and Faciane, 1977; Yamakado, 1985; De Biasi et al., 1996).

In contrast to these anatomical data, functional data are not sufficient to understand

the entire postnatal development. Just before the birth, weak synaptic transmission via lemniscal fibers becomes detectable (Leamey and Ho, 1998). Because strong synaptic transmission with high release probability has already observed as early as P7 (Arsenault and Zhang, 2006), significant development during the first postnatal week is suggested. During the second and the third postnatal weeks, developmental synapse elimination and a switch from NMDAR- to AMPAR-dominated transmission at lemniscal synapses have been reported (Arsenault and Zhang, 2006), which results in fast all-or-none transmission (Miyata and Imoto, 2006). The period during which Arsenault and Zhang studied lemniscal synapses presumably corresponds to a refinement stage of the development. In that period, other developmental processes such as changes in AMPA receptor subunit composition may also mediate the refinement. Hence, both during initial stages and refinement stages of the development, further functional studies are needed.

Here, I studied developmental changes of lemniscal synapses from just after birth to P39 using whole-cell patch-clamp recordings in brain slice preparations of mice. I found the substantial formation of synaptic connection and strengthening of lemniscal synapses during the first postnatal week. During the next two weeks, redundant lemniscal fibers were eliminated, and the kinetics of lemniscal EPSCs became faster. All properties of lemniscal synapses and morphological properties of relay neurons were stable after P21. Taken together, I conclude that the development of lemniscal fiber-relay neuron system is completed by P21.

Materials and Methods

Animals

All experiments described here were approved by the Animal Care and Use Committee of the National Institute for Physiological Sciences (Okazaki, Japan), and were performed according to the institutional guidelines concerning the care and handling of experimental animals. C57BL/6 Cr Slc mice (P0 - 39) of both sexes were used in this study. The strain was purchased from Nihon SLC (Hamamatsu, Japan). Mice were provided with a commercial diet (CE-2, Nihon Clea, Tokyo, Japan) and water *ad libitum* with controlled temperature, humidity, and lightning (12 h light/dark cycle).

Preparation

Mice were decapitated under deep anesthesia with isoflurane (Abbott Japan, Tokyo, Japan). Parasagittal 300-μm-thick slices containing the VPM (Arsenault and Zhang, 2006) were prepared using a microslicer (VT1200S; Leica, Nussloch, Germany) in an ice cold Na^+-free solution (in mM; 234 sucrose, 2.5 KCl, 1.25 NaH_2PO_4, 10 $MgCl_2$, 0.5 $CaCl_2$, 25 $NaHCO_3$, 0.5 *myo*-inositol, and 11 glucose) equilibrated with 95%O_2-5%CO_2. Slices were then transferred in an incubation chamber containing artificial cerebrospinal fluid (ACSF) (in mM; 125 NaCl, 2.5 KCl, 1.25 NaH_2PO_4, 1 $MgSO_4$, 2 $CaCl_2$, 26 $NaHCO_3$, and 20 glucose) equilibrated with 95%O_2-5%CO_2. The brain slices were kept at 32°C for 30 min, and then at room temperature

until just before the recording. Each slice was transferred into the submerge-type recording chamber (Sakmann and Stuart, 1995) and perfused by ACSF kept at 30 - 32°C at a rate of 2.5 - 3.0 ml min^{-1}. During experiments, 10 μM bicuculline methochrolide (Tocris Cookson, Bristol, UK) and 1 μM CGP55845 (Tocris Cookson) were added into the superfusate to block $GABA_A$ and $GABA_B$ receptors, respectively.

Whole-cell patch-clamp recordings of lemniscal EPSCs

Patch pipettes were made from borosilicate capillaries (O.D., 1.5 mm; I.D., 0.87 mm; Hilgenberg, Malsgeld, Germany or Harvard apparatus, Holliston, MA, U.S.A.). The resistance of patch pipettes was 2 - 5 MΩ when filled with an intracellular solution; (in mM) 120 $CsMeSO_3$, 10 HEPES, 1 EGTA, 2 $MgCl_2$, 0.1 $CaCl_2$, 20 NaCl, 5 QX-314, 2 ATP-Na_2, and 0.5 GTP-Na (pH = 7.3, 290 - 300 mOsm). 5% biocytin was also included for the cell labeling. Calculated and measured liquid junction potential (-13.0 mV) was not compensated unless otherwise noted.

Whole-cell voltage-clamp recordings were made from relay neurons in the VPM under visual guidance using an upright microscope (BX51WI, Olympus, Tokyo, Japan) with an infrared differential interference contrast video system (C3077-79 with C2741-62, Hamamatsu Photonics, Hamamatsu, Japan). The location of the VPM was validated according to the adult or the developing mouse brain atlas (Paxinos and Franklin, 2001; Paxinos et al.,

2007). Identification of relay neurons in the VPM was conducted by cytocromeoxidase staining and biocytin labeling. The pipette series resistance (Rs) was compensated by 50 - 90%. Cells were rejected if Rs increased above 20 MΩ.

Recordings and data acquisition were performed by using an EPC9 amplifier (HEKA Elektronik, Lambecht, Germany) with PULSE software (version 8.80, HEKA Elektronik) or a MultiClamp700A amplifier (MDS, Toronto, Canada) and Digidata 1322A (MDS) with pClamp8 software (MDS). When the EPC9 amplifier was used, signals were serially filtered at 10 kHz (-3 dB) by a three-pole Bessel filter and at 3 kHz (-3 dB) by a four-pole Bessel filter. When the MultiClamp700A amplifier was used, signals were filtered at 3 kHz (-3 dB) by a four-pole Bessel filter. Signals were digitized at 50 kHz. Data analysis was performed using IgorPro software (Wavemetrics, Lake Oswego, OR, U.S.A.).

Lemniscal fiber responses

To evoke lemniscal fiber-mediated EPSCs, I used a concentric electrode (tip diameter, 25 μm; IMB-160820, InterMedical, Nagoya, Japan). The stimulus electrode was placed on the medial lemniscal fiber bundle which was visually identified (Arsenault and Zhang, 2006). The electrical stimulation was consisted of bipolar square pulses (duration, 10 μs; interval, 100 μs) of constant currents (typically 10 - 400 μA), and delivered at 0.1 Hz via a biphasic isolator

(BSI-2, BAK Electronics, Oxford, UK). Test stimulations were delivered by paired-pulse stimulation with the interpulse interval of 50 ms.

The criteria of lemniscal EPSCs are as follows: (1) all-or-none or stepwise increments of EPSCs with the distinct threshold(s) in response to increasing stimulus intensity (Arsenault and Zhang, 2006; Miyata and Imoto, 2006); (2) paired-pulse depression (Castro-Alamancos, 2002; Miyata and Imoto, 2006); (3) faster rise and decay time than those of corticothalamic EPSCs (typically < 1ms and < 4 ms, respectively) (Miyata and Imoto, 2006); (4) Smaller coefficient of variation of amplitude of EPSCs than that of corticothalamic EPSCs (Miyata and Imoto, 2009). These criteria are similar to those of retinogeniculate synapses (Turner and Salt, 1998; Chen and Regehr, 2000; Granseth et al., 2002). At the very early developmental stage (P0 - 6), there has been no description on synaptic properties of lemniscal synapses. I confirmed that even at very early developmental stage these criteria are still valid in distinguishing lemniscal EPSCs from corticothalamic EPSCs (evoked by stimulation of internal capsule) (data not shown).

I monitored Rs throughout recordings by applying a short negative voltage pulse (-5 mV from holding potential for 10 ms), and recordings were discarded when Rs varied by > 20%. Only recordings taken under a low Rs condition (< 10 MΩ, compensated for up to 90%) were used in analyses of EPSC kinetics.

Numbers of lemniscal fibers onto a relay neuron were estimated by counting discrete steps of EPSCs both at -70 mV and +40 mV with the stimulus intensity ranged 10 - 400 μA with 1 - 50 μA increments (Chen and Regehr, 2000; Arsenault and Zhang, 2006; Hooks and Chen, 2006, 2008; Wang and Zhang, 2008). Before and after each threshold, several stimuli, 3-10 times, were delivered at the same intensity to confirm that the increment did not derive from the variation among the same number of fibers. At an early developmental stage (P0 - 9), the amplitude of each single fiber-mediated EPSC is so small that steps of EPSCs were sometimes not distinguishable, which led me conservative in counting. At the end of the counting, I confirmed the absence of extra lemniscal fiber inputs by a strong stimulation, the intensity of which was two-fold greater than the largest threshold. I also confirmed that each lemniscal fiber-mediated EPSC onto a relay neuron isolated by offline-subtraction is consistent with the criteria described above.

Total EPSCs (saturated EPSCs of a given relay neuron) and isolated each single lemniscal fiber-mediated EPSCs were subject to offline analyses using IgorPro. The amplitude of AMPAR- and NMDAR-mediated components was measured as peak height of EPSCs recorded at -70 mV and +40 mV, respectively. Because AMPAR-mediated component decays rapidly, the component is negligible when NMDAR-mediated component reaches its peak conductance (> 6 ms after the initial of EPSCs) (Arsenault and Zhang, 2006). The AMPA/NMDA ratio was defined as the ratio of the amplitude at -70 mV to that of at +40 mV.

The decaying phase of EPSCs at -70 mV and at +40 mV was fitted with a single exponential function to determine the decay time constant of AMPAR- and NMDAR-mediated components, respectively (Miyata and Imoto, 2006). But when an obvious NMDAR-mediated component was observed even at -70 mV, typically on P0 - 9, a double exponential function was used for fitting.

The contribution ratio

I defined the contribution ratio for each relay neuron as the ratio of amplitude of the largest single fiber-mediated lemniscal EPSCs to that of total (saturated) lemniscal EPSCs. This value was affected by both innervation patterns and competition among lemniscal fibers. The contribution ratio I defined here focuses on a surviving strong fiber during synapse elimination, whereas the disparity ratio demonstrated by Hashimoto and Kano (2003) focuses on one of the remaining weak fibers. I also tried to employ the disparity ratio to analyze the strength of remaining weak fibers, which seem to be eliminated within succeeding several days. However, the analysis could not make sense, because the number of experiments was insufficient especially on P11 - 18, during which a strong lemniscal fiber and a few weak lemniscal fibers innervate a relay neuron.

Pharmacological experiments

To investigate developmental switches of alternative splice variants of AMPA receptor subunits, I bath-applied cyclothiazide (CTZ) or 2-[2,6-Difluoro-4-[[2-[(phenylsulfonyl)amino]ethyl]thio]phenoxy]acetamide (PEPA) as inhibitors of AMPA receptor desensitization, each of which is selective for flip and flop variants of AMPA receptor subunits, respectively (Partin et al., 1994; Sekiguchi et al., 1997). I compared the mean of the area under the curve of 6 - 12 EPSCs just before and 4 - 5 min after drug application.

Cytochrome oxidase staining and biocytin labeling

Double staining of cytochrome oxidase (CO) and biocytin was conducted to analyze the morphology of the recorded cell and to confirm that the relay neuron was in the VPM. It was carried out according to Wiser and Callaway (1996) with small modification. After recordings, each slice was fixed by 4% paraformaldehyde in 0.1 M phosphate buffered saline (PBS) for 6 - 16 hr. The more aged the slice is, the longer fixation is needed. But the excessive fixation results in inactivation of cytochrome oxidase. Slices were rinsed three times in 0.1 M PBS, then three times in 0.05 M PBS. After that, slices were stained for CO by incubation in a solution containing 30 mg of cytochrome c, 20 mg of catalase, and 50 mg of diaminobenzidine (DAB; all from Sigma-Aldrich, St. Louis, MO, U.S.A.) per 100 ml of 0.05 M PBS, for 0.5 - 3 hr at 37°C. Slices were rinsed again three times in 0.05 M PBS, and then

incubated in 10% methanol and 3% H_2O_2 in 0.05M PBS for 30 min. Slices were rinsed again five times in 0.05 M PBS, and then incubated in a horseradish peroxidase (HRP)-conjugated avidin-biotin complex (ABC, Peroxidase Standard Kit Elite, Vector Laboratories, Burlingame, CA, U.S.A.) prepared in 0.05 M PBS and 0.75% Triton X-100, for 2 h. Slices were rinsed three times in 0.05 M PBS, submerged in 0.1% glutaraldehyde in PBS for 4 min, and then rinsed three times in 0.05 M PBS and two times in 0.05 M TBS. The intracellularly injected biocytin was revealed by reacting slices in a solution containing 50 mg of DAB, 2.8 ml of 1% $CoCl_2$, 2.0 ml of 1% nickel ammonium sulfate, and 1 ml of 0.3% H_2O_2 per 100 ml of 0.05 M TBS, for 5 min at 4°C. Slices were rinsed five times in 0.05 M TBS, two times in 0.05 M PBS, and two times in 0.1 PB. Finally, slices were mounted on gelatin-coated slide glasses, dehydrated and penetrated by a series of ethanol-xylene, and sealed by cover glasses with a mounting medium. Several relay neurons which were completely reconstructed were used for morphological analyses for each developmental stage. Projected images of relay neurons were drawn using a camera lucida. The pictures were digitized by a scanner, and then binarized and analyzed using ImageJ software (version 1.42, http://rsbweb.nih.gov/ij/).

Chemicals

$CsMeSO_3$, QX-314, ATP-Na_2, GTP-Na, and sucrose were purchased from Sigma-Aldrich. All other chemicals were purchased from Nacalai Tesque (Kyoto, Japan), Wako Pure Chemical Industries (Osaka, Japan), or Kanto Chemical (Tokyo, Japan), unless otherwise specified.

Statistics

All values are given as means ± S.E.M., unless otherwise noted. Data analyses and fitting procedures were performed by IgorPro. Several statistical tests were employed in accordance with experimental design (*see the Results section*). The significant level was set at 0.05. Statistical analyses were performed by EXCEL Statistics (version 6.0, ESUMI, Tokyo, Japan) or IgorPro.

Results

To understand the entire time course of developmental changes of the lemniscal fiber-relay neuron system, I recorded lemniscal EPSCs and analyzed the morphology of relay neurons from P0 to P39.

Innervation patterns of lemniscal fibers onto a relay neuron

I first examined the developmental change of lemniscal fiber innervations onto a relay neuron. The recorded relay neuron was clamped at -70 mV or +40 mV, and lemniscal EPSCs were evoked by electrical stimulation (Fig. 1*A*). At an early developmental stage, multiple steps of EPSCs with distinct thresholds were observed as the stimulus intensity was increased with small increments. I could estimate the number of lemniscal fiber inputs from the number of steps, as Zhang *et al*. (2006; 2008) did at this synapse. This counting method is used for other synapses in the CNS (Kano et al., 1995; Chen and Regehr, 2000). The number of lemniscal fiber inputs onto a given relay neuron increased during the first postnatal week, and it in turn decreased during the next two weeks (2.1 ± 0.2, 2.7 ± 0.3, 7.1 ± 0.6, 3.0 ± 0.5, 1.9 ± 0.2, 1.2 ± 0.1, 1.2 ± 0.1, and 1.1 ± 0.1 for P0-2, P4-5, P7-9, P11-13, P15-18, P21-25, P28-32, and P35-39, respectively) (Fig. 1*B*). This developmental change was statistically significant (**$P < 0.01$, Kruskal-Wallis test). The contribution ratio (*see Methods and Materials*) also varied consistently with the innervation pattern (figure not shown; **$P < 0.01$, one-way ANOVA,

values: 0.733 ± 0.06, 0.632 ± 0.05, 0.400 ± 0.05, 0.611 ± 0.10, 0.725 ± 0.07, 0.963 ± 0.02, 0.962 ± 0.02, and 0.984 ± 0.02, n=15, 11, 17, 14, 13, 28, 31, and 13 for P0-2, P4-5, P7-9, P11-13, P15-18, P21-25, P28-32, and P35-39, respectively). As a result of synapse elimination, 81.5% of relay neurons were innervated by only one lemniscal fiber on P21 - 25. After P21, the number of lemniscal fiber inputs did not vary ($P = 0.74$, Kruskal-Wallis test), suggesting that the majority of relay neurons receive only one lemniscal fiber during the mature period.

Silent lemniscal synapses during the postnatal development

A silent synapse is defined as "a synapse in which an EPSC is absent at the resting membrane potential but becomes apparent on depolarization" (Kerchner and Nicoll, 2008). At an early postnatal stage (P0 - 9), silent lemniscal synapses were frequently observed. A representative trace of a silent lemniscal synapse from a P2 mouse was shown at Fig. 2*A*. The percentage that a relay neuron received at least one silent lemniscal fiber was about 50% during the first two postnatal weeks; however, the value decayed during the next week, reaching zero by P21 (Fig. 2*B,* values (%): 52, 33, 60, 43, 10, 0, 0, and 0 for P0-2, P4-5, P7-9, P11-13, P15-18, P21-25, P28-32, and P35-39, respectively). Difference in the percentage among the developmental stages was statistically significant (**$P < 0.01$, chi-square test for independence). This observation is consistent with previous studies which reported the

developmental disappearance of silent synapses at other synapses in the CNS (Durand et al., 1996; Wu et al., 1996; Isaac et al., 1997; Rumpel et al., 1998; Chen and Regehr, 2000).

Developmental changes in EPSC amplitude

There was a clear difference in amplitude between immature and mature lemniscal EPSCs (Fig. 3*A*). Total (saturated) NMDAR- and AMPAR-mediated EPSCs rapidly developed around P6 (Fig. 3*B*, left). Total NMDAR-mediated EPSCs then gradually declined, whereas AMPAR-mediated EPSCs gradually increased (Fig. 3*B*, left; $^{**}P < 0.01$ for both NMDA and AMPA, one-way ANOVA, values (nA): on NMDA, 0.21 ± 0.05, 0.44 ± 0.10, 1.99 ± 0.45, 1.10 ± 0.30, 1.53 ± 0.36, 0.81 ± 0.14, 1.31 ± 0.19, and 0.90 ± 0.29, on AMPA, 0.08 ± 0.01, 0.18 ± 0.04, 2.02 ± 0.49, 2.46 ± 0.68, 2.70 ± 0.54, 2.57 ± 0.32, 2.84 ± 0.42, and 2.52 ± 0.77 for P0-2, P4-5, P7-9, P11-13, P15-18, P21-25, P28-32, and P35-29, respectively). On the other hand, the amplitude of single fiber-mediated EPSCs goes through different developmental transition from that of total lemniscal EPSCs. “Single fiber” means one of the lemniscal fibers onto a relay neuron, each of which corresponds to one of the multiple EPSC steps observed in figure 1. Both NMDAR- and AMPAR-mediated, single fiber-evoked EPSCs gradually increased by P21 (Fig. 3*B*, right; $^{**}P < 0.01$ for both NMDA and AMPA, one-way ANOVA, values (nA): on NMDA, 0.10 ± 0.01, 0.17 ± 0.03, 0.33 ± 0.04, 0.45 ± 0.12, 0.73 ± 0.14, 0.73 ± 0.12, 1.10 ± 0.15, and 0.80 ± 0.28, on AMPA, 0.05 ± 0.01, 0.08 ± 0.01, 0.48 ±

0.08, 1.10 ± 0.25, 1.60 ± 0.30, 2.10 ± 0.30, 2.54 ± 0.36, and 2.30 ± 0.73 for P0-2, P4-5, P7-9, P11-13, P15-18, P21-25, P28-32, and P35-39, respectively). During the second and third postnatal weeks, the amplitude of AMPAR-mediated EPSCs more greatly increased than that of NMDAR-mediated EPSCs (Fig. 3*B*). As a result, the AMPA/NMDA ratios of both total and single fiber-mediated EPSCs gradually increased (Fig. 3*C*; $^{**}P < 0.01$ for both total and single, one-way ANOVA, values: on total, 0.77 ± 0.16, 0.45 ± 0.05, 1.13 ± 0.22, 2.11 ± 0.39, 2.46 ± 0.52, 3.95 ± 0.75, 2.85 ± 0.33, and 4.05 ± 0.81, on single, 0.95 ± 0.18, 0.62 ± 0.09, 1.36 ± 0.14, 2.39 ± 0.35, 2.58 ± 0.33, 3.84 ± 0.69, 2.70 ± 0.28, and 3.89 ± 0.78 for P0-2, P4-5, P7-9, P11-13, P15-18, P21-25, P28-32, and P35-39, respectively). The AMPA/NMDA ratios reached the mature level by P21.

Developmental speeding of lemniscal EPSCs

Developmental shortening in decay time of lemniscal EPSCs was observed for both NMDAR- and AMPAR-mediated EPSCs (Fig. 4*A*, *C*, respectively). The shortening occurred during the second and third postnatal weeks for both NMDAR- and AMPAR-mediated EPSCs (Fig. 4*B*, *D*, respectively). These changes in decay time constant were statistically significant ($^{**}P < 0.01$, one-way ANOVA, values (ms): on NMDA, 85.9 ± 11.3, 91.7 ± 8.1, 137.2 ± 10.0, 93.1 ± 5.8, 54.1 ± 3.4, 45.5 ± 3.2, 49.1 ± 2.4, and 44.4 ± 3.9, on AMPA, 5.0 ± 0.9, 4.8 ± 0.5, 8.9 ± 1.4, 2.7 ± 0.4, 1.6 ± 0.2, 1.6 ± 0.2, 1.3 ± 0.2, and 1.7 ± 0.3 for P0-2, P4-5, P7-9, P11-13,

P15-18, P21-25, P28-32, and P35-39, respectively). The shortening in decay time of NMDAR-mediated lemniscal EPSCs have already been reported that it is due to the switch of receptor subunits from NR2B to NR2A (Arsenault and Zhang, 2006). On the shortening in decay time of AMPAR-mediated lemniscal EPSCs, I conducted the following experiment.

A developmental switch of alternative splice variants of AMPA receptor subunits

Each AMPA receptor subunit has alternative splice variants (flip and flop), which have relatively slow and fast kinetics, respectively (Sommer et al., 1990; Hollmann and Heinemann, 1994; Mosbacher et al., 1994; Quirk et al., 2004). Thus, I hypothesized that the developmental speeding of AMPAR-mediated EPSCs is due to a switch from flip to flop. I employed here two inhibitors of AMPA receptor desensitization, CTZ and PEPA, which were selective for the flip and flop, respectively (Partin et al., 1994; Sekiguchi et al., 1997). I measured the areas enclosed by the baselines and the EPSCs (Nakagawa et al., 1999), which will be referred to as the integrated EPSCs hereafter. Bath-applied 100 μM CTZ potentiated the integrated EPSCs of both immature and mature lemniscal fibers (Fig. 5*A*). The potentiating effect on immature EPSCs (182.6 ± 25.3%) was significantly larger than that on mature EPSCs (60.5 ± 11.5%) (Fig. 5*C*; $*P < 0.05$, two-tailed Student's *t*-test). In contrast, bath-applied 100 μM PEPA tends to more powerful to mature EPSCs (53.0 ± 10.2%) than to immature EPSCs (5.6 ± 10.2%) (Fig. 5*B*). The difference in percent potentiation, however, was not statistically significant

(Fig. 5*C*; $P = 0.34$, two-tailed Student's *t*-test, n = 4 and 10 for P7-9 and P21-32, respectively). These results suggest the developmental switch from flip to flop splice variants of AMPA receptor subunits.

No change of paired-pulse ratio during the postnatal development

The paired-pulse ratio of lemniscal EPSCs, which mainly reflects the probability of transmitter release (Manabe et al., 1993; Zucker and Regehr, 2002; Pan and Zucker, 2009), was investigated during the postnatal developmental period. Lemniscal EPSCs from P7 - 25 mice exhibited paired-pulse depression as previously reported, which presumably suggest a high release probability at lemniscal synapses (Fig. 6*A*, *B*) (Arsenault and Zhang, 2006; Miyata and Imoto, 2006). In addition, I found that even just after the birth, lemniscal EPSCs exhibited paired-pulse depression (Fig. 6*B*), whereas corticothalamic EPSCs showed paired-pulse facilitation (data not shown). The extent of paired-pulse depression was not different among the developmental stages ($P = 0.83$, one-way ANOVA, values: 0.51 ± 0.03, 0.55 ± 0.03, 0.52 ± 0.02, 0.52 ± 0.03, 0.56 ± 0.05, 0.53 ± 0.02, 0.56 ± 0.02, and 0.58 ± 0.03 for P0-2, P4-5, P7-9, P11-13, P15-18, P21-25, P28-32, and P35-39, respectively). These results suggest that the release probability of transmitter at lemniscal synapses is high even just after the birth and stable during the postnatal development period.

Morphological development of relay neurons

Finally, I investigated the morphological development of relay neurons. Biocytin-labeled relay neurons were visualized by DAB reaction and reconstructed their projected images using camera lucida. Just after the birth, relay neurons were quite small (Fig. 7*A*), and the gradual development was then observed on both somatic and dendritic areas (Fig. 7*A*, *B*). These developmental changes were statistically significant (**$P < 0.01$ for both soma and dendrite, one-way ANOVA, values (μm^2): on soma, 97.7 ± 23.9, 132.2 ± 13.9, 232.8 ± 24.0, 239.9 ± 23.5, 216.8 ± 42.0, 188.5 ± 16.1, 202.1 ± 22.1, and 195.1 ± 25.2, on dendrite, 240.2 ± 93.4, 740.2 ± 107.8, 1879.7 ± 302.4, 2062.2 ± 220.3, 2415.2 ± 307.5, 3014.5 ± 362.0, 3313.4 ± 318.6, and 3147.3 ± 506.6 for P0-2, P4-5, P7-9, P11-13, P15-18, P21-25, P28-32, and P35-39, respectively, n = five for each age). I found that the development of the soma was already finished on P7, whereas that of dendrites continued to grow during the first three postnatal weeks (Fig. 7*A*, *B*). After P21, both soma and dendrite did not obviously develop ($P = 0.88$ and 0.84 for soma and dendrite, respectively, one-way ANOVA). These results suggest that morphological development of relay neurons is completed by P21.

Discussion

In this chapter, the precise developmental time course of lemniscal synapses and morphology of relay neurons in the VPM are described. I found three distinct stages of the postnatal development of lemniscal synapse-relay neuron system, which are "Growth stage", "Refinement stage", and "Mature stage" (*see Fig. 23 in chapter 3*). Details in each stage are summarized in the following paragraph.

Formation and maturation of the lemniscal synapse-relay neuron system

In the "Growth stage" (P0 - 6), topographic map is initially built up on P0 - 3. Massive lemniscal fibers are then actively recruited by a relay neuron around P6, resulting in an increase in amplitude of both AMPAR- and NMDAR-mediated EPSCs. Soma size of a relay neuron becomes larger on the end of this stage. In the "Refinement stage" (P7 - 21), redundant lemniscal fibers are eliminated, and surviving lemniscal fibers are strengthened, so that monoinnervation is established by P21. Shortening of decay time of AMPAR-mediated EPSCs is observed during this stage. A switch of alternative splice variants of AMPA receptors from flip to flop underlies the phenomenon. Dendrites of a relay neuron gradually grow up during the first three postnatal weeks and finish their growth at the end of this stage. In the "Mature stage" (P21~), all synaptic properties and morphology of relay neurons are stable. Thus, I conclude that the development of lemniscal fiber-relay neuron system is

completed by P21.

Functional and anatomical maturation of lemniscal synapses

As noted above, I found the time course of functional development of lemniscal synapses, which includes “Growth stage” and “Refinement stage”. This two step development is well consistent with previous anatomical studies, which report establishment of the barreloid structure and maturation of neuropile in the VPM (Yamakado, 1985; De Biasi et al., 1996). In the Growth stage, the barreloid structure is established first around P3 – 5 (Yamakado, 1985; Muñoz et al., 1999). After that, each relay neuron actively recruits new lemniscal fiber inputs around P6, which is consistent with the anatomical increase of lemniscal synapses in number (Matthews and Faciane, 1977; Yamakado, 1985). In the Refinement stage, the surplus lemniscal fibers are eliminated, whereas a surviving lemniscal fiber is strengthened. As a result, total lemniscal EPSCs of a relay neuron increases rather than deceases (Fig. 3). This is also well consistent with anatomical studies that the number of lemniscal synapses is not reduced during this stage (Matthews and Faciane, 1977; Yamakado, 1985). In this stage, lemniscal fiber contacts a relay neuron via multiple synaptic glomeruli, each of which is characterized by multiple synapses with glia ensheathment (Špaček and Lieberman, 1974; Matthews and Faciane, 1977; Yamakado, 1985; De Biasi et al., 1996), which presumably contributes to strengthening of the surviving lemniscal fiber.

Notably, at an early stage of barreloid structure formation (P0 - 3), the barreloid can be altered by afferent information (Woolsey et al., 1979; Belford and Killackey, 1980). After the closure of the critical period, a relay neuron actively recruits multiple lemniscal fibers. Hence, during P0 - 3, the determination of general map has priority over the strengthening of lemniscal transmission.

Elimination of lemniscal synapses

During the second and third postnatal weeks, the number of lemniscal fibers onto a given relay neuron decreases, whereas dendrites of relay neurons gradually develop until P21 (Fig. 1 and 7).

These results suggest that synapse elimination process is actively controlled with independent control from dendritic growth. In general, appropriate neural activities sculpt appropriate neural circuits (Katz and Shatz, 1996). Along with the dogma, several studies have shown activity-driven synapse elimination. For example, if mice once experience normal sensory inputs (e.g. eye opening, onset of whiskering), following normal sensory inputs accelerate the subsequent elimination of afferent synapses in the thalamus (Hooks and Chen, 2006, 2008; Wang and Zhang, 2008). Furthermore, in the cerebellum and neuromuscular junction, neural activities could promote of synapse elimination (Thompson, 1983; Sanes and Lichtman, 1999; Buffelli et al., 2003; Lorenzetto et al., 2009). Properly patterned neural

activity is also necessary for synapse elimination (Andjus et al., 2003; Hooks and Chen, 2006). Thus, synapse elimination observed here should be driven by intact sensory experience during the second and third postnatal weeks.

Molecular mechanisms of synapse elimination of lemniscal synapses remain unknown. However, in the visual thalamus, elimination of retinogeniculate synapses is disturbed by dysfunction or knockout of various molecules, including a metabotropic glutamate receptor (mGluR1) (Narushima et al., 2008), immune-related molecules (class 1 MHC, C1q) (Huh et al., 2000; Stevens et al., 2007), and a transcription factor (MeCP2) (Chen, 2009). Therefore, these molecules may underlie the developmental elimination of lemniscal synapses. Furthermore, a series of sophisticated studies on the cerebellum demonstrate that the mGluR1 - Gαq - PLCβ4 - PKCγ cascade following parallel fiber inputs onto Purkinje cells is essential for elimination of climbing fiber synapses onto a Purkinje cell (Kano et al., 1995; Kano et al., 1997; Offermanns et al., 1997; Kano et al., 1998). Because the mGluR1 - PLCβ4 cascade following corticothalamic inputs is also functional in the somatosensory thalamus (Miyata et al., 2003), the cascade may be important for elimination of lemniscal synapses.

Robustness of the step-counting method

The number of innervating lemniscal fibers onto a given relay neuron in this study is well consistent with that in previous studies (Arsenault and Zhang, 2006; Wang and Zhang, 2008).

There are two concerns about the step-counting method employed here to underestimate the number of inputs. First, as Wang and Zhang (2008) pointed out, several lemniscal fibers on each relay neuron may have been lost during preparation, because relay neurons have radial dendrites. However, because lemniscal synapses are located mainly on soma or proximal dendrites whenever they can be identified as lemniscal synapses (Peschanski et al., 1984; Williams et al., 1994; De Biasi et al., 1996), the loss of inputs may be relatively minor. The other concern is about underestimation of the number of lemniscal inputs especially at early postnatal day (P0 - 5). I found that EPSCs evoked by stimulation on lemniscal fiber bundle exhibited paired-pulse depression in the same extent of mature lemniscal EPSCs (Fig. 6), which is distinguishable from EPSCs evoked by stimulation on internal capsule (presumably, corticothalamic EPSCs) exhibited paired-pulse facilitation. Hence, although I cannot completely rule out the possibility that some lemniscal EPSCs exhibit paired-pulse facilitation at P0 - 5, the majority of immature lemniscal EPSCs presumably exhibit paired-pulse depression. Thus, although there may be slight underestimation in number, the present data on the number of lemniscal fibers can be plausible.

Development of NMDAR- and AMPAR-mediated EPSCs and maturation of lemniscal synapses

The developmental time courses of NMDAR- and AMPAR-mediated lemniscal EPSCs were

not identical. I found a small AMPA/NMDA ratio (Fig. 3*C*) and abundant silent synapses (Fig. 2) at early postnatal days, both of which are frequently observed throughout the immature CNS (Liao et al., 1995; Durand et al., 1996; Wu et al., 1996; Isaac et al., 1997; Rumpel et al., 1998; Chen and Regehr, 2000; Futai et al., 2001; Cathala et al., 2003; Lo and Erzurumlu, 2007; Kerchner and Nicoll, 2008). The abundant NMDA receptors at the immature CNS are required for synaptic transmission (Liu and Chen, 2008) and refinement of neural circuits (Schlaggar et al., 1993; Fox et al., 1996).

The subsequent switch from NMDAR-dominant synaptic transmission to AMPAR-dominant synaptic transmission gradually occurred by P21 (Fig. 3), which is well consistent with previous reports on maturation of synapses in the CNS (Chen and Regehr, 2000; Futai et al., 2001; Cathala et al., 2003; Arsenault and Zhang, 2006). The switch during the second and third postnatal weeks seems to be reasonable, because mice start active whiskering around P11 - 12, which requires the precise temporal cording for tactile discrimination (Carvell and Simons, 1990; Jones et al., 2004; Montemurro et al., 2007; Petersen et al., 2008). In addition, the small contribution of NMDA receptors to synaptic transmission ensures high fidelity of transmission even with high frequency presynaptic spike trains (Futai et al., 2001; Cathala et al., 2003). The increase in AMPAR/NMDAR ratio of lemniscal EPSC may be an experience-dependent process, because a reduced AMPAR/NMDAR ratio of lemniscal EPSC is observed in whisker-deprived mice (Wang and

Zhang, 2008). The AMPAR/NMDAR ratio of lemniscal EPSC is also reduced in adenylyl cyclase 1 knockout mice, which suggest that adenylyl cyclase 1 is involved in the maturation of lemniscal synapses (Wang et al., 2009).

Developmental speeding of EPSCs mediated by switches of glutamate receptors

Fast and reliable synaptic transmission resulting in a small jitter of postsynaptic action potentials is observed at adult lemniscal synapses, auditory and vestibular sensory synapses in the brainstem, mossy fiber-granule cell synapses in the cerebellum, etc (Babalian et al., 1997; Futai et al., 2001; Cathala et al., 2003; Koike-Tani et al., 2005; Montemurro et al., 2007; Rancz et al., 2007; Bagnall et al., 2008; Petersen et al., 2008; Englitz et al., 2009; Tolnai et al., 2009). Such fast transmission is required physiological functions (e.g. tactile discrimination, sound localization, and vestibulo-ocular reflex). Generally, fast synaptic transmission is established through developmental speedings of postsynaptic currents. In the present study, I found that the decay time of lemniscal EPSCs is shortened on both NMDAR- and AMPAR-mediated components during the second postnatal weeks (Fig. 4). On NMDA receptors, it has been revealed that the speeding of NMDAR-mediated EPSCs is mediated by the receptor switch from NR2B-dominant to NR2A-dominant compositions (Arsenault and Zhang, 2006). On AMPA receptors, the results in figure 5 clearly demonstrate that flip-type subunits are developmentally down-regulated, whereas flop-type subunits are up-regulated, as

reported at calyx-of-Held synapses (Koike-Tani et al., 2005). The expression of flip-type splice variants correlates with that of GluR2 subunits (Geiger et al., 1995). The GluR2 subunit is the one of the four subunits (GluR1 - 4) which consist AMPA type glutamate receptors (Hollmann and Heinemann, 1994). In the thalamus, developmental progress in inward rectification of AMPAR-mediated EPSCs is observed at retinogeniculate synapses (dos Louros et al., 2009). In addition, anatomical studies have revealed that GluR2 mRNA is abundant at immature thalamus (Pellegrini-Giampietro et al., 1992), and that GluR2 subunit is absent and GluR4 (flop type) subunit is abundant at mature thalamus (Keinänen et al., 1990; Young et al., 1995; Jones et al., 1998) (Yamasaki, 2009; *personal communication*). Thus, it is probable that GluR2-containing AMPA receptors developmentally decrease, whereas fast flop-type ones increase at lemniscal synapses. However, the kinetics, the conductance, the inward rectification, and pharmacological properties of native AMPA receptors can be modulated by transmembrane AMPA receptor regulatory proteins (TARPs) (Tomita et al., 2003; Turetsky et al., 2005; Tomita et al., 2006; Cho et al., 2007; Soto et al., 2007). The switch from GluR2-flip to GluR4-flop subunits should be further investigated by an electron microscopic analysis and a single cell RT-PCR analysis.

Morphological development of relay neuron

Apparently, neurons have various morphologies and develop their neurites during postnatal

development (Cajal, 1995). Relay neurons in the VPM have radial dendrites (Harris, 1986; Cajal, 1995). Brown *et al.* (1995) and Zantua *et al*. (1996) have already reported the morphological development by filling relay neurons with Lucifer yellow via grass pipettes. In the present study, I also investigated the morphological development by biocytin labeling of a relay neuron and CO staining for the neuropile. General morphology, soma development, dendritic development (Fig. 7), and the number of primary dendrites (data not shown) of relay neurons were almost consistent with previous reports (Brown et al., 1995; Zantua et al., 1996). A gradual increase in intensity of CO staining (data not shown) temporally agree with the maturation of neuropile in the barreloid at the second postnatal week (Yamakado, 1985). Gradual elongation of dendrites even after the excessive innervations of lemniscal fibers (Fig. 1, 7) indicates the delayed maturation of neural units to integrate information. As Brown *et al*. (1995) pointed out, a territory of mature dendrites of a relay neuron is larger than the diameter of each barreloid (about 70 - 100 μm) (Fig. 7) (Van Der Loos, 1976). The development of dendrites across a barreloid (Fig. 7) is temporally parallel with the developmental increase of corticothalamic synapses, which preferentially located on distal dendrites of relay neurons (Matthews and Faciane, 1977; Peschanski et al., 1984). Therefore, these observations may indicate transvibrissae information processing via the thalamocortical loop.

Figures

Figure 1. Formation and elimination of lemniscal synapses during postnatal development

A, Representative traces of lemniscal fiber-mediated EPSCs (lemniscal EPSCs) under voltage clamp conditions at +40 mV or -70 mV. Several raw traces with different stimulus intensities are superimposed at each holding potential. An arrow indicates the synapse elimination process. *B*, Summary histograms showing the number of discrete steps of EPSCs. Numbers of recorded cells are 22, 14, 18, 17, 13, 27, 22, and 11 for P0-2, P4-5, P7-9, P11-13, P15-18, P21-25, P28-32, and P35-39, respectively.

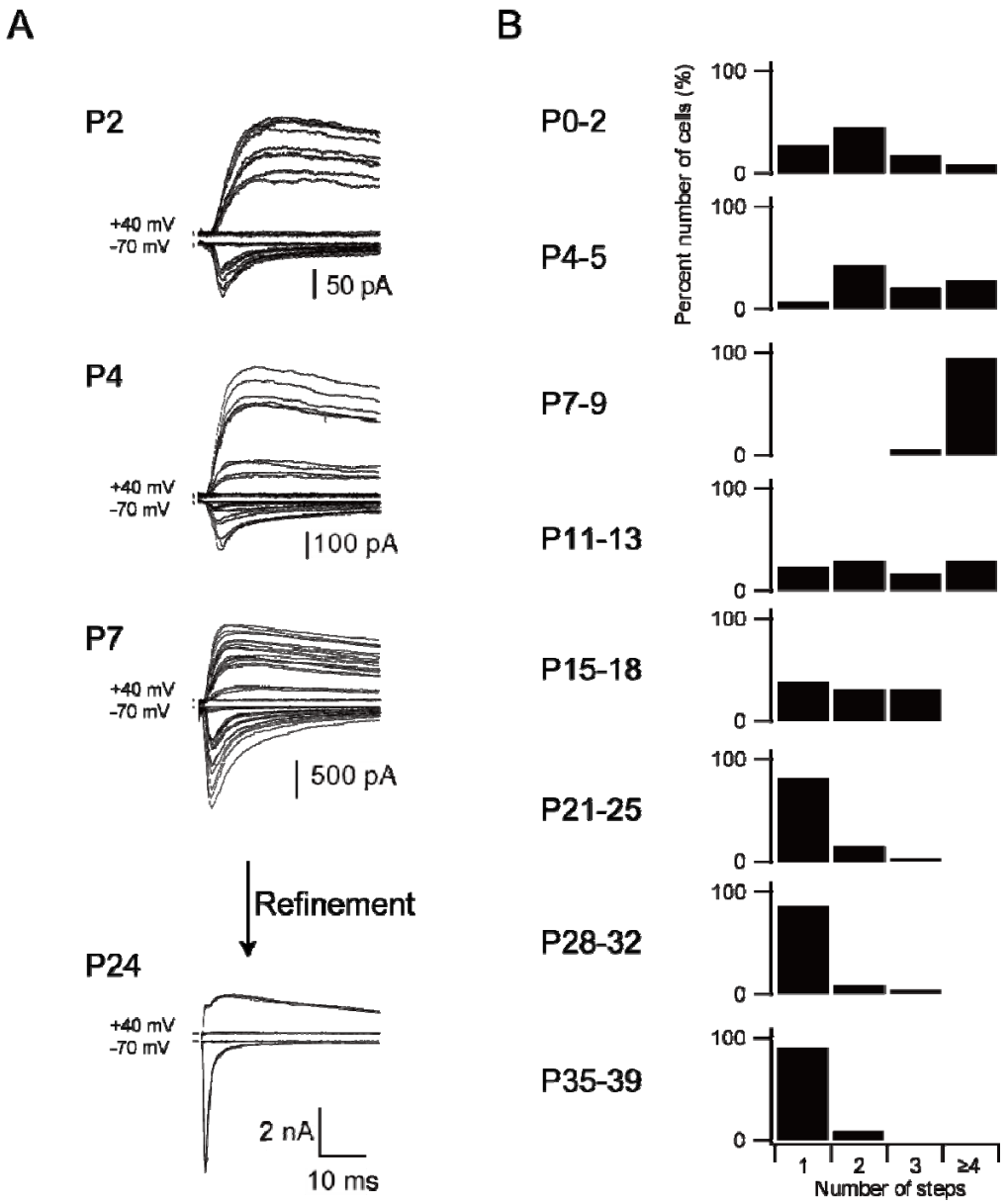
A
P2
+40 mV
-70 mV
50 pA
P4
+40 mV
-70 mV
100 pA
P7
+40 mV
-70 mV
500 pA
Refinement
P24
+40 mV
-70 mV
2 nA
10 ms
B
P0-2
P4-5
P7-9
P11-13
P15-18
P21-25
P28-32
P35-39
Percent number of cells (%)
100
0
1
2
3
≥4
Number of steps

Figure 1

Figure 2. Silent synapses observed during early postnatal development

A, A representative trace of silent lemniscal fiber-mediated EPSCs recorded at P2. *B*, The percentage that a relay neuron receives at least one silent lemniscal fiber is plotted against age. Numbers of recorded cells are 23, 15, 15, 14, 10, 27, 19, and 7 for P0-2, P4-5, P7-9, P11-13, P15-18, P21-25, P28-32, and P35-39, respectively.

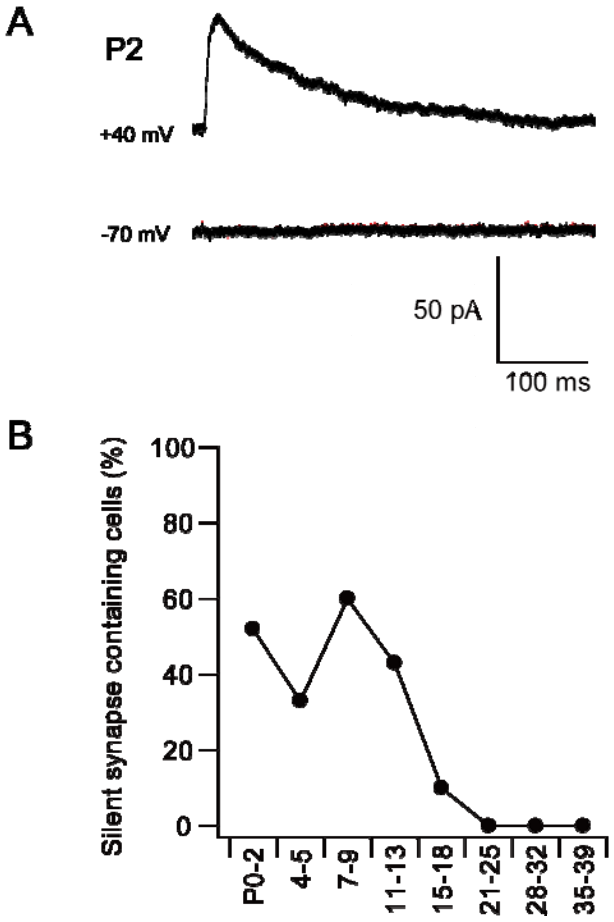
A
P2
+40 mV
-70 mV
50 pA
100 ms
B
Silent synapse containing cells (%)
100
80
60
40
20
0
P0-2
4-5
7-9
11-13
15-18
21-25
28-32
35-39

Figure 2

Figure 3. Postnatal development of NMDAR- and AMPAR-mediated lemniscal EPSCs

A, Representative traces recorded from P4 and P31 mice are shown in the same calibration. Several raw traces with different stimulus intensities are superimposed at each holding potential. *B*, Developmental changes in amplitude of NMDAR-mediated (+40 mV) and AMPAR-mediated (-70 mV) lemniscal EPSCs. The amplitude indicates the peak amplitude of total (saturated) lemniscal EPSCs onto a relay neuron (left) or single fiber-mediated lemniscal EPSCs (right). Numbers of recorded cells are 21, 14, 18, 16, 13, 27, 31, and 11. Numbers of recorded fibers for NMDAR-mediated EPSCS are 47, 35, 122, 43, 19, 30, 33, and 10. Numbers of recorded fibers for AMPAR-mediated EPSCS are 32, 32, 98, 40, 24, 33, 36, and 12. *C*, Developmental changes in AMPAR/NMDAR ratio in total (left) or single fiber-mediated (right) lemniscal EPSCs. Numbers of recorded cells for total are 20, 14, 18, 14, 10, 29, 28, and 9. Numbers of recorded single fiber-mediated EPSCs are 28, 32, 87, 37, 21, 31, 36, and 11. All numbers of experiments are for P0-2, P4-5, P7-9, P11-13, P15-18, P21-25, P28-32, and P35-29, respectively. Each column represents the mean ± S.E.M.

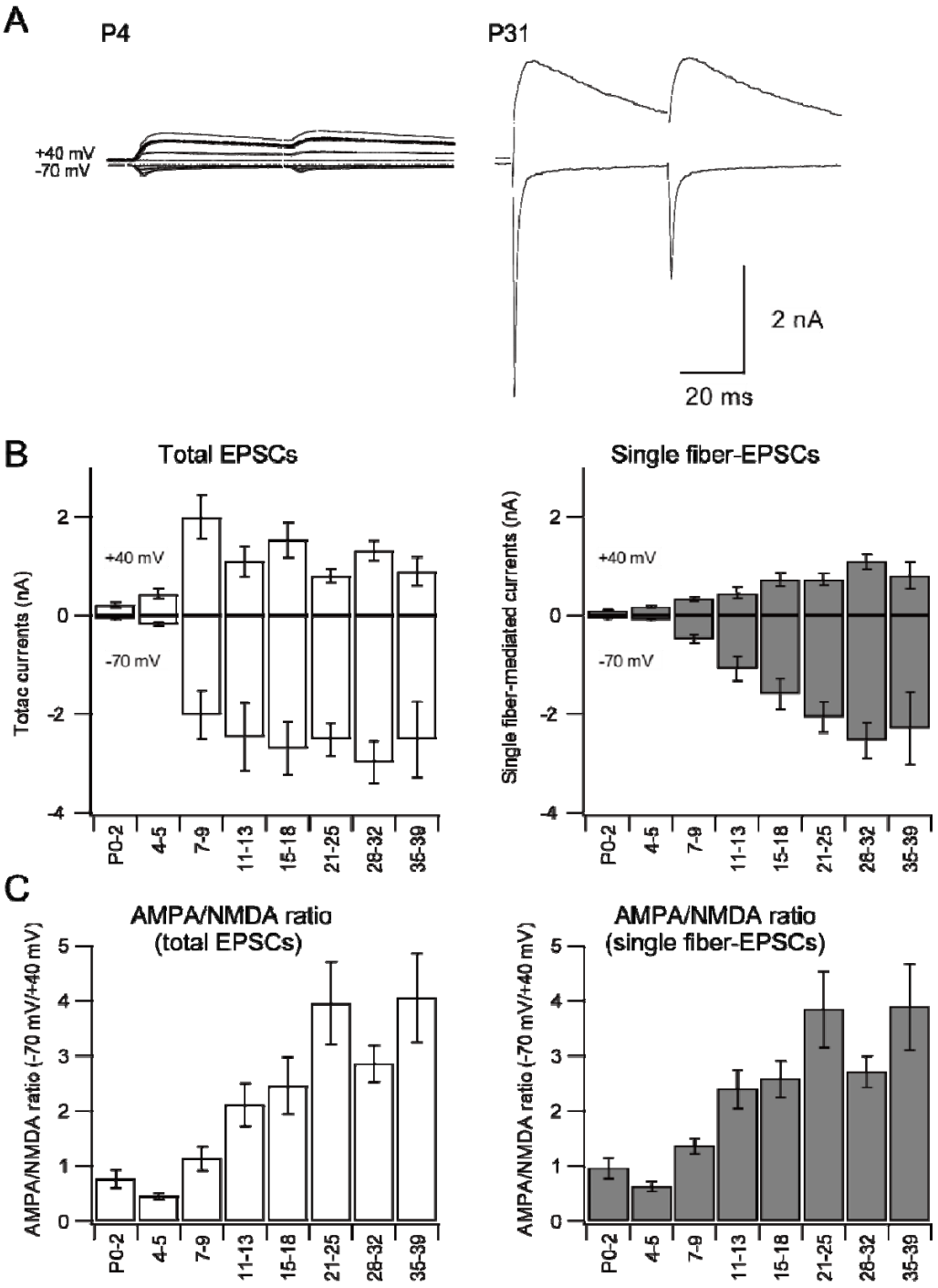
A
P4
P31
+40 mV
-70 mV
2 nA
20 ms
B
Total EPSCs
Single fiber-EPSCs
Totac currents (nA)
Single fiber-mediated currents (nA)
+40 mV
-70 mV
P0-2
4-5
7-9
11-13
15-18
21-25
28-32
35-39
C
AMPA/NMDA ratio
(total EPSCs)
AMPA/NMDA ratio
(single fiber-EPSCs)
AMPA/NMDA ratio (-70 mV/+40 mV)

Figure 3

Figure 4. Developmental speeding of lemniscal EPSCs

A, Representative traces of single fiber-mediated lemniscal EPSCs from both immature and mature mice (thin and thick traces, respectively). Traces are normalized by their peak height (642 pA and 1400 pA for P7 and P39, respectively). The holding potential was at +40 mV. *B*, Developmental time course of decay time constants of EPSCs recorded at +40 mV. Numbers of recorded lemniscal fibers are 19, 4, 48, 31, 17, 22, 28, and 5 for P0-2, P4-5, P7-9, P11-13, P15-18, P21-25, P28-32, and P35-39, respectively. *C*, Same as (A) but at -70 mV. Peak currents are 401 pA and 6402 pA for P7 and P29, respectively. *D*, Developmental time course of decay time constants of EPSCs recorded at -70 mV. Numbers of recorded lemniscal fibers are 28, 32, 87, 37, 21, 31, 36, and 11 for P0-2, P4-5, P7-9, P11-13, P15-18, P21-25, P28-32, and P35-39, respectively. Each column represents the mean ± S.E.M.

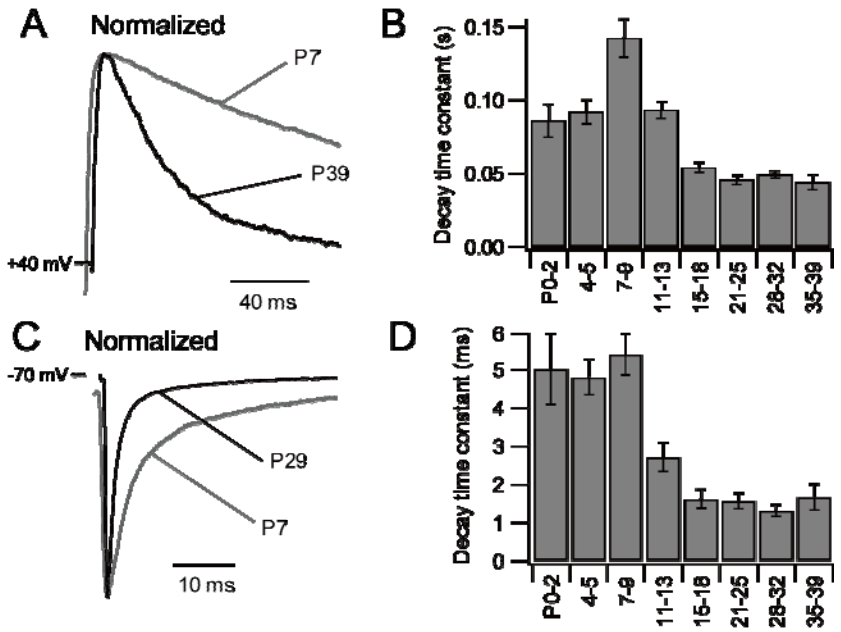
A
Normalized
P7
P39
+40 mV
40 ms
B
Decay time constant (s)
0.15
0.10
0.05
0.00
P0-2
4-5
7-9
11-13
15-18
21-25
28-32
35-39
C
Normalized
-70 mV
P29
P7
10 ms
D
Decay time constant (ms)
6
5
4
3
2
1
0
P0-2
4-5
7-9
11-13
15-18
21-25
28-32
35-39

Figure 4

Figure 5. A developmental switch of splice variant of AMPA receptor subunits

Cyclothiazide (CTZ) and PEPA are inhibitors of AMPA receptor desensitization and selective for flip and flop splice variants of AMPA receptor subunits, respectively. *A*, Representative traces of lemniscal EPSCs in the presence of 100 μM CTZ (thick line) are overlaid with control traces (thin line). Each trace is the average of six individual raw traces. *B*, Same as (A) but in the presence of 100 μM PEPA instead of CTZ. *C*, Percent increments of area under the curve by CTZ and PEPA. Each column represents the mean ± S.E.M. Statistical significance was tested by two-tailed Student's *t*-test. $*P < 0.05$.

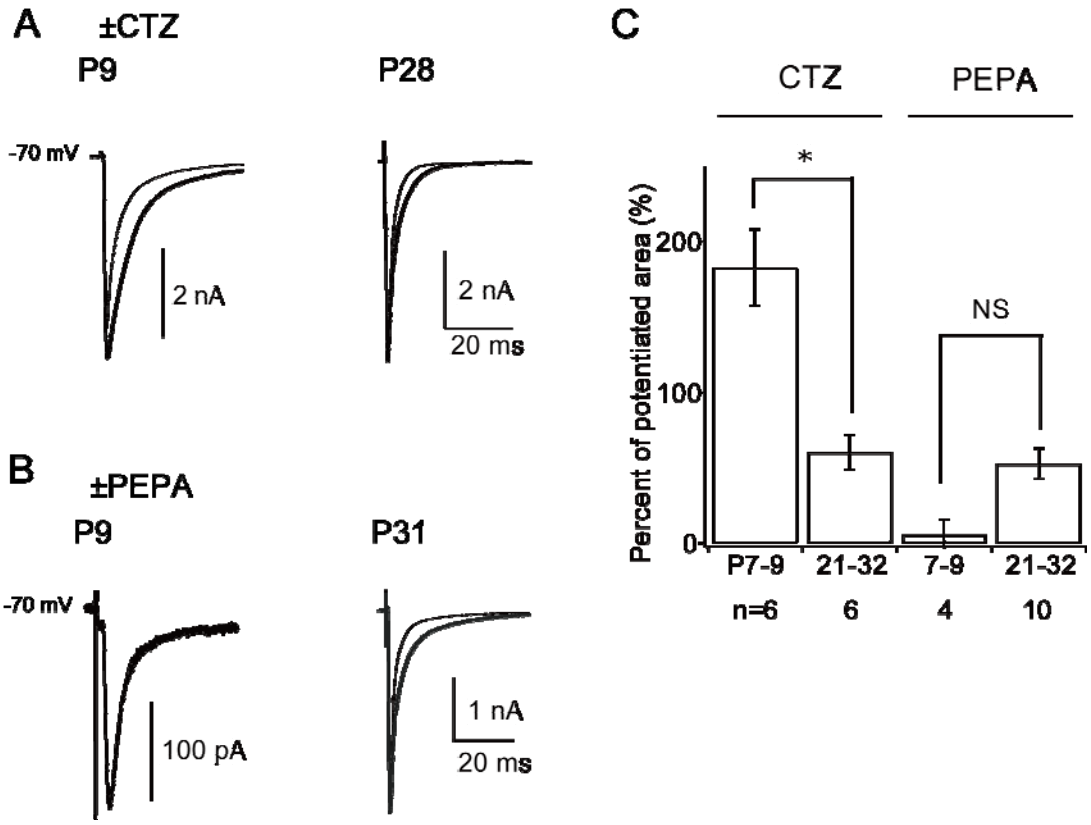
A
±CTZ
P9
P28
-70 mV
2 nA
2 nA
20 ms
B
±PEPA
P9
P31
-70 mV
100 pA
1 nA
20 ms
C
CTZ
PEPA
*
NS
Percent of potentiated area (%)
200
100
0
P7-9
21-32
7-9
21-32
n=6
6
4
10

Figure 5

Figure 6. No change of paired-pulse ratio during postnatal development

A, Representative traces of single fiber-mediated lemniscal EPSCs evoked by paired-pulse stimulation. The interpulse interval is 50 ms. Thin and thick traces are from P7 and P22, respectively. Traces are normalized by their peak height of first EPSCs (348 pA and 4775 pA for P7 and P22, respectively). *B*, Means of the paired-pulse ratio (2^{nd} EPSCs/1^{st} EPSCs) during postnatal development. Error bars represent S.E.M. Numbers of analyzed fibers are 27, 29, 78, 40, 24, 33, 36, and 12 for P0-2, P4-5, P7-9, P11-13, P15-18, P21-25, P28-32, and P35-39, respectively.

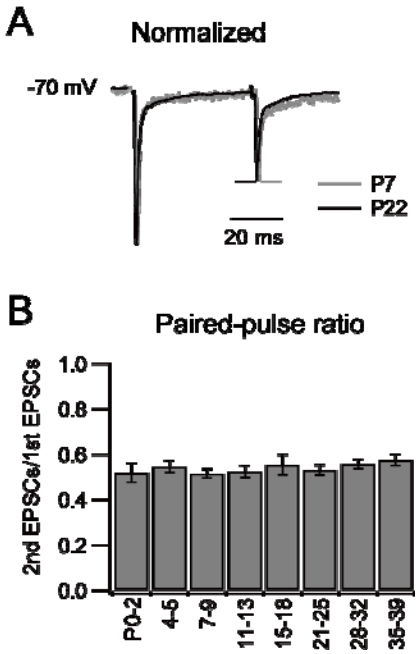
A
Normalized
-70 mV
P7
P22
20 ms
B
Paired-pulse ratio
2nd EPSCs/1st EPSCs
1.0
0.8
0.6
0.4
0.2
0.0
P0-2
4-5
7-9
11-13
15-18
21-25
28-32
35-39

Figure 6

Figure 7. Morphological development of relay neurons

A, Camera lucida reconstructed projection images of relay neurons during postnatal development. Red traces represent putative axons of relay neurons. *B*, Time course of the mean of projected somatic and dendritic areas. Each point represents the mean ± S.E.M. of five separate cells.

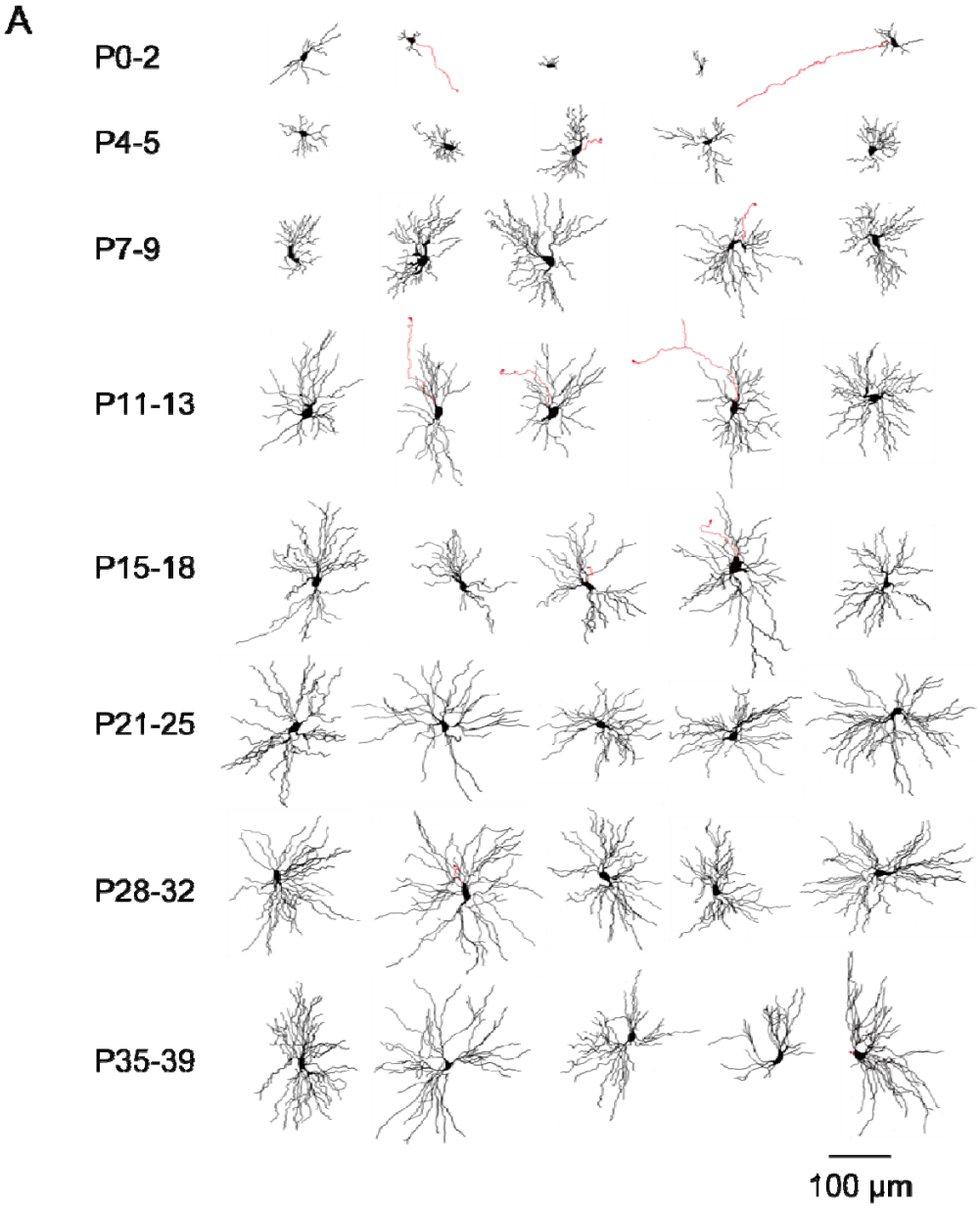
A
P0-2
P4-5
P7-9
P11-13
P15-18
P21-25
P28-32
P35-39
100 μm
B
Soma area (μm2)
200
100
0
3000
2000
1000
0
Dendritic area (μm2)
soma
dendrite
P0-2
4-5
7-9
11-13
15-18
21-25
28-32
35-39

Figure 7

Chapter 2: Peripheral nerve injury-induced remodeling of afferent synapses in the somatosensory thalamus of mice

Abstract

Functional remodeling in the somatosensory thalamus after deafferentation has been described in *in vivo* experimental studies, but precise synaptic mechanisms for the remodeling have not been investigated in *in vitro* systems yet. Here, I show peripheral nerve cut-induced remodeling of lemniscal synapses (afferent synapses in the somatosensory thalamus) using whole-cell patch-clamp recordings in brain slice preparations of mice. One week after complete transection of the infraorbital nerve (IONC) of mice on P21, multiple reinnervation of lemniscal fibers onto a thalamic relay neuron is observed. The IONC operation decreased the amplitude of single fiber-mediated EPSCs, but not the amplitude of total lemniscal EPSCs of a given relay neuron. Multiple innervating lemniscal fibers are classified into two distinct populations; “Strong fibers” with a shorter decay time and larger amplitude of AMPAR-mediated lemniscal EPSCs, and “Weak fibers” with a longer decay time and smaller amplitude. A cluster analysis and innervation patterns of the two types of fibers suggest that Weak fibers are putative newly-recruited fibers. Moreover, current-voltage relationships and pharmacological analyses suggest that the IONC operation up-regulates GluR2-containing and flip-type AMPA receptors at the postsynaptic sites of Weak fibers. In contrast, no change is observed on NMDAR-mediated EPSCs. Paired-pulse ratio and coefficient of variation of

AMPAR-mediated lemniscal EPSCs are elevated at Weak fiber synapses. These results suggest that the IONC operation can induce remodeling of lemniscal synapses with the change of AMPA receptor compositions even after maturation of the lemniscal synapses.

Introduction

A one of the most intriguing features of the central nervous system (CNS) is the ability to change itself according to afferent information. The changes include long-term plastic changes of synaptic transmission (Allen et al., 2003; Bender et al., 2006; Clem et al., 2008) and rewiring of neural circuits (Rhoades et al., 1997; Sengelaub et al., 1997; Florence et al., 1998; Jain et al., 2000; Hooks and Chen, 2006, 2008; Yamahachi et al., 2009). Such changes can properly alter the CNS but sometimes improperly, for example, resulting in maladaptation such as phantom sensation (Flor et al., 2006; Giummarra et al., 2007). Thus, studies on synaptic basis underlying such plastic changes after deafferentation is important to understand both appropriate and pathological changes.

Lesion of the afferent pathway can reorganize the receptive field in the somatosensory thalamus (Davis et al., 1998; Jones and Pons, 1998; Florence et al., 2000; Graziano et al., 2008). Such reorganization also occurs in the somatosensory cortex after the deafferentation (Merzenich et al., 1984; Pons et al., 1991; Manger et al., 1996), and the extent of reorganization correlates the extent of phantom pain (Ramachandran and Hirstein, 1998; Grüsser et al., 2001). Several lines of reports suggest that the reorganization of the receptive field in the somatosensory thalamus affects that in the somatosensory cortex (Jones and Pons, 1998; Kaas et al., 1999; Florence et al., 2000; Jones, 2000). Thus, remodeling in the thalamus after the deafferentation is likely to be initial neural mechanisms by which phantom sensation

or such occurs. However, it remains unknown how synapses change in the thalamus after the deafferentation.

The whisker-related somatosensory pathway of rodents is one of the most studied pathways. Along the pathway, afferent synapses in the thalamus (lemniscal synapses) are candidates for loci the remodeling of which accounts for that of the thalamus. Topographic map formation along the whisker-related axis can be disrupted by the lesion or the blockade of axonal transport rather than activity of peripheral sensory nerve during the neonatal period (Chiaia et al., 1992; Henderson et al., 1992; Chiaia et al., 1996). Moreover, developmental elimination of lemniscal synapses is partially disrupted by whisker deprivation from a particular critical period (postnatal days 12 - 13), but not after the critical period (Arsenault and Zhang, 2006; Wang and Zhang, 2008). These reports suggest that developmental changes of lemniscal synapses are subject to afferent information; however, it is unknown how lemniscal synapses are changed by complete transection of peripheral sensory nerves even after they become mature.

In the present study, I examined the remodeling of lemniscal synapses in the whisker-related somatosensory thalamus after complete transection of peripheral nerve on P21, by which lemniscal synapses become mature (*see chapter 1*). I found marked remodeling in the VPM after the deafferentation, including multiple reinnervation of lemniscal fibers onto a relay neuron.

Materials and Methods

Animals

All experiments described here were approved by the Animal Care and Use Committee of the National Institute for Physiological Sciences (Okazaki, Japan) and Tokyo Women's Medical University (Tokyo, Japan) and were performed according to the institutional guidelines concerning the care and handling of experimental animals. C57BL/6 Cr Slc mice (postnatal days 21 -32) (P21 - 32) of both sexes were used in this study. The strain was purchased from Nihon SLC (Hamamatsu, Japan). Mice were provided with a commercial diet (CE-2, Nihon Clea) and water *ad libitum* with controlled temperature, humidity, and lightning (12 h light/dark cycle).

Infraorbital nerve cut (IONC) operation

Mice on P21 were anesthetized by intraperitoneal administration of ketamine (80 mg/kg, Daiichi Sankyo Company, Tokyo, Japan) and xylazine (10 mg/kg, Sigma-Aldrich). The infraorbital nerve (a part of the maxillary nerve passing through the infraorbital canal, which convey somatosensory information from the maxillary region) of the left side face was exposed under a dissecting microscope according to a rodent anatomical chart (Greene, 1955). The infraorbital nerve was completely transected using sterilized fine scissors and the cutting planes were separated at a distance > 1.0 mm to prevent regeneration. For a sham operation,

the infraorbital nerve was exposed without the transection. The skin then was sutured by silken threads. Physiological saline (0.2 ml per animal) was subcutaneously injected for maintenance.

Whisker deprivation

All large vibrissae on the left side snout were repeatedly deprived every day from P21 to the recording day. This method is similar to that employed by Fox and others (Fox, 1992; Li et al., 1995). Briefly, mice were anesthetized by isoflurane. Under a dissecting microscope, vibrissae were carefully removed using fine tweezers by applying slow, steady tension to the base of the vibrissa until the vibrissa slipped out of the follicle. This procedure does not induce any damage on the sensory nerve endings (Li et al., 1995).

Preparation

Parasagittal brain slices containing the VPM were prepared from the right hemisphere of brain. All other procedures were same as the developmental study (*see chapter 1*)

Whole-cell voltage-clamp recordings of lemniscal EPSCs

Somatic whole-cell voltage-clamp recordings were made from relay neurons in the VPM. Lemniscal EPSCs were evoked by electrical stimulation of the medial lemniscal fiber bundle

(*for in detail, see chapter 1*). To isolate pure AMPAR- or NMDAR-mediated component, some experiments were conducted in the presence of 100 - 200 μM $_{D}$- or $_{DL}$-APV (Tocris Cookson) or 20 μM NBQX (Tocris Cookson).

Evoked miniature EPSCs

To analyze input specific miniature EPSCs, I recorded Sr^{2+}-induced delayed miniature EPSCs (Dodge et al., 1969; Goda and Stevens, 1994; Oliet et al., 1996; Silver et al., 1998; Bekkers and Clements, 1999; Chen and Regehr, 2000; Wang and Zhang, 2008). I first recorded the single fiber-mediated lemniscal EPSCs in the presence of 100 μM $_{DL}$-APV. Slices then were perfused by modified ACSF substituting 4 mM Sr^{2+} ions for Ca^{2+} ions. The holding potential was set at -90 mV to increase the driving force. A time window for analysis was 100 - 500 ms after stimulus. Miniature EPSCs were detected and analyzed by a semi-automated IgorPro procedure.

Current-voltage relationships of AMPAR-mediated EPSCs

To preserve intracellular polyamine, which induces an inward rectification of AMPAR-mediated currents, the pipette solution includes 100 μM spermine (Sigma-Aldrich) (Bowie and Mayer, 1995; Isa et al., 1995). Single fiber-mediated lemniscal EPSCs were recorded in the presence of 200 μM $_{D}$-APV. Current-voltage relationships were investigated

by recordings of EPSCs at various holding potentials ranged ±60 mV in 10 mV steps. The liquid junction potential was compensated (estimated as -13 mV). The rectification index was defined as the ratio of the EPSC amplitude at +40 mV to that of -40 mV (Isa et al., 1995; Wang and Zhang, 2008).

Current-voltage relationships of NMDAR-mediated EPSCs

Single fiber-mediated lemniscal EPSCs were recorded in the presence of 20 μM NBQX. Current-voltage relationships were investigated by recordings of EPSCs at various holding potentials ranged from +40 mV to -100 mV in 10 mV decrements. The liquid junction potential was compensated.

Pharmacological experiments

Single fiber-mediated lemniscal EPSCs were recorded in the presence of 100 μM $_{DL}$-APV at -70 mV. After establishment of stable recordings, 1 mM spermine (Sigma-Aldrich) (Isa et al., 1996; Washburn and Dingledine, 1996) or 100 μM pentobarbital (Dainippon Sumitomo Pharma, Osaka, Japan) (Yamakura et al., 1995; Liu and Cull-Candy, 2000) was bath-applied for 5 min. The average percent inhibition in amplitude of EPSCs 4-5 min after application was analyzed. For CTZ and PEPA application, the experimental design and analysis were same as chapter 1.

Paired-pulse ratio and coefficient of variation analyses

A series of paired-pulse stimulations were conducted, the interpulse intervals of which were ranged from 30 to 1000 ms, while single fiber-mediated lemniscal EPSCs were recorded in the presence of 100 μM $_{DL}$-APV at -70 mV. The paired-pulse ratio is the ratio of amplitude of second EPSCs to that of first EPSCs. The coefficient of variation of amplitude of EPSCs was calculated from 30 consecutive single fiber-mediated lemniscal EPSCs.

Cytochrome oxidase staining and biocytin labeling

(*Same as chapter 1*)

VGluT2-immunostaining

The following procedures were conducted at room temperature unless otherwise specified. Mice on P28 (sham- or IONC-operated on P21) were anesthetized by intraperitoneal administration of 80 mg/kg pentobarbital (Dainippon Sumitomo Pharma) and perfused transcardially with cold physiological saline followed by 4% paraformaldehyde in 0.1 M PBS (pH 7.4). After removal, the brains were postfixed for overnight, infiltrated with a series of sucrose 10 - 30% in 0.1 M PBS, blocked by O.C.T. Compound (Sakura Finetek USA, Torrance, CA, U.S.A.), and frozen in dry ice. The blocks of the thalamus were sectioned

coronally at 20 μm by cryostat at -18°C. Sections were collected in cold antifreeze solution (30% ethylenglycol and 20% glycerol in 0.02 M PBS). Sections were then rinsed three times in 0.1 M PBS, mounted on gelatin-coated slide glasses, and air-dried for 30 min. Sections were rinsed three times in 0.1 M PBS, incubated in 0.3% H_2O_2 to quench endogenous peroxidases, washed three times in 0.1 M PBS, and blocked by 10% normal goat serum (NGS) and 0.3% Triton X-100 in 0.1 M PBS for 1 h. Sections were then incubated three overnights at 4°C with primary antibody (guinea pig polyclonal anti-mouse VGluT2, dilution, 1:200, VGluT2-GP-Af-240-1, Frontier Science, Hokkaido, Japan) (Miyazaki et al., 2003) prepared with 2%NGS and 0.3% Triton X-100 in 0.1 M PBS. Sections then were washed three times in 0.1 M PBS, incubated for 2 h with secondary antibody (biotinylated goat anti-guinea pig IgG, dilution, 1:250, BA-7000, Vector Laboratories) prepared with 2%NGS and 0.3% Triton X-100 in 0.1 M PBS. Sections were washed in 0.1 M PBS, and incubated at room temperature for 1 h with HRP-AB regent (ABC kit elite, Vector Laboratories). After that, sections were washed three times in 0.1 M PBS, three times in 0.05 M TBS, pre-incubated for 6 min with H_2O_2-lacking DAB solution (0.1 mg/ml DAB and 2 mg/ml nickel ammonium sulfate in 0.05 M TBS), and developed with 0.003% H_2O_2 containing DAB solution at 4°C for 9 min. Sections were then washed three times in 0.05 M TBS, once in 0.1 M PBS, once in 0.1 PB, dehydrated, penetrated, and coverslipped with a mounting medium. In some experiments, sections were incubated with 1% methyl green (Sigma-Aldrich) for 30 min for nuclear stain

just before dehydration. Images were taken by using a upright microscope (BX51; Olympus) equipped with a digital camera (DP70; Olympus) with a same exposure time, 2 ms. Images were then subject to auto-level-correction in Photoshop software (version 10.0.1, Adobe Systems, San Jose, CA, U.S.A.), auto-binarized, and analyzed for area using ImageJ. Counting of VGluT2-immunoreactive boutons or methyl green-stained nuclei was assisted by Cell Counter plugin for ImageJ (http://rsbweb.nih.gov/ij/plugins/cell-counter.html).

Chemicals

SYM 2206 was purchased from Tocris Cookson. All other chemicals were from Nacalai Tesque (Kyoto, Japan), Wako Pure Chemical Industries (Osaka, Japan), or Kanto Chemical (Tokyo, Japan), unless otherwise specified.

Cluster analyses

Each decay time constant of single fiber-mediated lemniscal EPSCs was plotted against its amplitude. The distribution was analyzed by two-dimensional histogram (ordinate bin, 0.2 ms; abscissa bin, 0.2 nA). Because the histogram exhibited obvious two clusters, the histogram was fitted with a summation of two independent Gaussians:

$$f(x,y) = w0 \cdot \exp\left(\frac{-1}{2\left(1-w1^2\right)}\left(\left(\frac{x-w2}{w3}\right)^2 + \left(\frac{y-w4}{w5}\right)^2 - \frac{2\cdot w1\,(x-w2)\,(y-w4)}{w3\cdot w5}\right)\right)$$
$$+ w6 \cdot \exp\left(\frac{-1}{2\left(1-w7^2\right)}\left(\left(\frac{x-w8}{w9}\right)^2 + \left(\frac{y-w10}{w11}\right)^2 - \frac{2\cdot w7\,(x-w8)\,(y-w10)}{w9\cdot w11}\right)\right)$$

where w0 - 11 are coefficients. Initial guess of the 12 coefficients was supported by outcomes of the KMeans analysis using an IgorPro built-in function. The "best" values of the coefficients were then calculated by the Levenberg-Marquardt least-squares method. To define a threshold of EPSC amplitude which well separates the first and second Gaussian components, I defined a contamination ratio as a ratio of contamination of the first Gaussian component to the rightward than the threshold or the second Gaussian component to the leftward than the threshold. Each Gaussian was weighted.

Statistics

All values are given as means ± S.E.M. unless otherwise noted. Data analyses and fitting procedures were performed by IgorPro (Wavemetrics). Several statistical tests were employed in accordance with experimental design (*see the Results section*). The significant level was set at 0.05. Statistical analyses were performed by EXCEL Statistics (version 6.0, ESUMI, Tokyo, Japan) or IgorPro.

Results

Here, to investigate whether the complete loss of afferent inputs induces remodeling in the mature VPM as in the visual thalamus, I made complete transection of the left infraorbital nerve on P21, and then characterized lemniscal EPSCs on P28 - 32.

Infraorbital nerve cut-induced multiple reinnervation of lemniscal fibers onto a relay neuron

First, I investigated the number of lemniscal fiber inputs onto a relay neuron in the same way as in chapter 1. In this post-maturation period (P28-32), most of relay neurons of both intact and sham groups were innervated by a single lemniscal fiber (Fig. 8*A*, *B*, 87.1% and 87.0% for intact and sham, respectively). In contrast, 68.5% of relay neurons of the IONC group received multiple innervation of lemniscal fibers (Fig. 8*A*, *B*). Distributions of the numbers of lemniscal inputs were significantly different between the sham and IONC groups (Fig. 8*B*; $^{**}P < 0.01$, Kolmogorov-Smirnov two-sample test). The contribution ratios, which reflect both elimination and competition of lemniscal fibers, were also significantly different between the sham and IONC groups (Fig. 8*C*, *D*; $^{**}P < 0.01$, two-tailed Welch's *t*-test, values: 0.95 ± 0.13 and 0.75 ± 0.24 for sham and IONC, respectively). Moreover, the IONC operation induced silent lemniscal synapses, which were never observed in the intact and sham groups on P28-32 (Fig. 9 and Fig. 2 in chapter 1). Because the mono-innervation pattern

is already established by P21 (*see chapter 1*), the multiple innervation observed after the IONC operation indicates reinnervation of lemniscal fibers.

No significant increase in density of lemniscal fiber boutons in the VPM

The IONC-induced multiple innervation may be additive, resulting in an increase in number of lemniscal fiber boutons in the VPM. Therefore, I conducted immunostaining using an antibody against the type 2 vesicular glutamate transporter (VGluT2), which is a specific marker of lemniscal fiber boutons (Miyazaki et al., 2003; Graziano et al., 2008). First, I prepared VGluT2-immunostained coronal sections of the VPM (Fig. 10*A*). Images were taken and auto-binarized. However, the ratios of signal area to the ROI area in the VPM were not different between the sham and IONC groups (data not shown, $P = 0.92$, two-tailed Student's *t*-test, values: 0.17 ± 0.02 and 0.17 ± 0.01 for sham and IONC, respectively). I also counted VGluT2-immunoreactive boutons in the VPM but again found no significant difference (Fig. 10*C*; $P = 0.38$, two-tailed Student's *t*-test, values ($10^3/mm^2$): 12.8 ± 0.7 and 13.6 ± 0.7 for sham and IONC, respectively). Next, I conducted VGluT2-immunostaining with methyl green nuclear staining (Fig. 10*B*) and calculated the number of VGluT2-immunoreactive boutons per cell. However, no difference was again observed between the sham and IONC groups (Fig. 10*D*; $P = 0.79$, two-tailed Student's *t*-test, values: 3.1 ± 0.2 and 3.3 ± 0.4 for sham and IONC, respectively). These results suggest that the IONC operation does not increase lemniscal fiber

boutons in the VPM, which may be consistent with the results that total (saturated) lemniscal EPSCs are not different between sham and IONC groups (Fig. 11).

The IONC operation reduces amplitude of single fiber-mediated lemniscal EPSCs

The amplitudes of NMDAR-mediated (+40 mV) and AMPAR-mediated (-70 mV) components of single fiber-mediated and total (saturated) lemniscal EPSCs were compared between the sham and IONC groups. The amplitude of NMDAR-mediated component of single fiber-mediated lemniscal EPSCs was significantly decreased by the IONC operation (1.23 ± 0.11 to 0.75 ± 0.09 nA) (Fig. 11*A*, *B*; $^{**}P < 0.01$, two-tailed Student's *t*-test), but not total lemniscal EPSCs (1.16 ± 0.08 to 1.11 ± 0.09 nA) (Fig. 11*A*, *B*; $P = 0.78$, two-tailed Student's *t*-test). The same is true for AMPAR-mediated EPSCs; single fiber-mediated EPSCs were decreased (2.47 ± 0.15 to 1.38 ± 0.11 nA) (Fig. 11*C*, *D*; $^{**}P < 0.01$, two-tailed Student's *t*-test), but not total lemniscal EPSCs (2.67 ± 0.22 to 2.34 ± 0.22 nA) (Fig. 11*C*, *D*; $P = 0.27$, two-tailed Student's *t*-test). These results are consistent with the anatomical evidence (Fig. 10) and may suggest the compensatory innervations of multiple lemniscal fibers.

Strong and Weak fibers in the IONC-operated group

For further understanding of the properties of lemniscal synapses after the IONC operation, I investigated the distributions of amplitude of AMPAR-mediated component of single

fiber-mediated lemniscal EPSCs. As a result, it was found that the distributions from sham and IONC were significantly different (Fig. 12*A*; $^{**}P < 0.01$, Kolmogorov-Smirnov two-sample test, n = 98 and 199 for sham and IONC, respectively). In addition, I found that no sham fiber was below 500 pA in amplitude at -70 mV, whereas 39% of IONC fibers were smaller than 500 pA, which may be putative newly-recruited fibers. Thus, I defined tentatively 500 pA as a threshold that separates Weak fibers and Strong fibers in the IONC group, and then assessed its validity.

The IONC operation not only reduced the amplitude of lemniscal EPSCs but also prolonged the decay time of AMPAR-mediated lemniscal EPSCs (Fig. 15). Hence, I plotted the decay time constant against the amplitude for each single fiber-mediated lemniscal EPSC and investigated their correlation (Fig. 12*B*). As a result, the decay time significantly correlated with its amplitude in the IONC group ($^{**}P < 0.01$, two-tailed, *t*-test on correlation coefficient, correlation coefficient = -0.28, n = 179), but not in the sham group ($P > 0.05$, correlation coefficient = -0.11, n = 90). Pooled data still retained the correlation ($^{**}P < 0.01$, correlation coefficient = -0.34, n = 269). From these results and seeing the distribution of pooled data, I hypothesized that the pooled data consisted of two populations; the first population with slower decay time and smaller amplitude, and the second population with faster decay time and larger amplitude. Thus, the distribution of pooled data was fitted with a summation of two independent Gaussian surfaces (Fig. 12*C* left). Because the first Gaussian

component with slower decay time and smaller amplitude exclusively consisted of IONC fibers (Fig. 12*C* center), while the second Gaussian component consisted of both sham and IONC fibers (Fig. 12*C* right), the first Gaussian might be a newly-recruited population. After that, the most reasonable threshold level that distinguishes the two Gaussian components was searched (Fig. 12*D*, *E*). At 500 pA, the first Gaussian component is 0.91 in cumulative probability, whereas the second is only 0.13 (Fig. 12*D*). Moreover, contamination ratios (*see Methods and Materials*) on the first and second components are only 0.09 and 0.13, respectively. Hence, I employed 500 pA as the threshold of Strong and Weak fibers.

Distinct innervation patterns of lemniscal fibers onto a relay neuron between sham and IONC-operated groups

Because the reasonable threshold that well defines Strong and Weak fibers could be determined, I next tried to establish further classifications of innervation using the threshold. The most prominent innervation pattern in the sham group was innervation by only one Strong fiber (S only, 86.7%), and the other pattern was by multiple Strong fibers (SS) (Fig. 13*A*, *C*). On the other hand, the most prominent innervation pattern in the IONC group was innervation by combination of one Strong fiber and a single or multiple Weak fiber(s) (SW, 37.3%) (Fig. 13*B*, *C*). Moreover, it was found that the majority of relay neurons in the IONC group received at least one Strong fiber (92.2%, SW + SS + S only) (Fig. 13*C*). These results

suggest that Weak fibers, which are exclusively observed in the IONC group, are newly-recruited lemniscal fibers after the IONC operation.

The small AMPA/NMDA ratio at Weak fiber synapses

I compared the amplitudes of EPSCs of sham fibers, Strong fibers in the IONC group (IONC-S), and Weak fibers in the IONC group (IONC-W). IONC-W fibers had significantly smaller EPSCs in amplitude in both AMPAR- and NMDAR-mediated components than those of sham and IONC-S fibers (Fig. 14*B*; $^{**}P < 0.01$, multiple *t*-test with Bonferroni correction following ANOVA, two-tailed, values (nA): on AMPA, 2.47 ± 0.15, 2.09 ± 0.14, and 0.24 ± 0.01, on NMDA, 1.23 ± 0.11, 0.90 ± 0.11, and 0.18 ± 0.02 for sham, IONC-S, and IONC-W, respectively). IONC-S fibers tended to have smaller EPSCs than sham fibers, but the difference was not statistically significant owing to Bonferroni correction (Fig. 14*B*). The mean of AMPA/NMDA ratios at IONC-W synapses was significantly smaller than that of sham and IONC-S fibers (Fig. 14*C*; $^{*}P < 0.05$ vs. sham; $^{**}P < 0.01$ vs. IONC-S, two-tailed, multiple *t*-test with Bonferroni correction following ANOVA, values: 3.32 ± 0.38, 3.52 ± 0.47, and 1.35 ± 0.14 for sham, IONC-S, and IONC-W, respectively). Because the small AMPA/NMDA ratio at IONC-W synapses is similar to that observed around P7-9 (Fig. 3 in chapter 1), Weak fibers seem to be immature fibers.

Prolonged decay time of AMPAR-mediated EPSCs at Weak fiber synapses

The decay time constants of purely AMPAR-mediated EPSCs were compared among the three fiber groups. The mean of decay time constants of IONC-W EPSCs was significantly larger than that of sham and IONC-S EPSCs (Fig. 15; $^{**}P < 0.01$, two-tailed, multiple *t*-test with Bonferroni correction following one-way ANOVA, values (ms): 1.68 ± 0.12, 1.94 ± 0.09, and 2.84 ± 0.18 for sham, IONC-S, and IONC-W fibers, respectively), but there was no difference in 10-90% rise time of EPSCs among the fiber groups (data not shown; $P = 0.83$, one-way ANOVA, values (ms): 0.51 ± 0.03, 0.52 ± 0.03, and 0.54 ± 0.03 for sham, IONC-S, and IONC-W, respectively). The result indicates that the prolonged decay time is not a result of dendritic filtering (Hashimoto et al., 2009).

Analyses of asynchronously-released miniature EPSCs

To determine whether the reduced amplitude and the prolonged decay time of AMPAR-mediated lemniscal EPSCs derive from presynaptic or postsynaptic changes, I conducted the analysis of evoked miniature EPSCs from each lemniscal fiber. First, single fiber-mediated lemniscal EPSCs were recorded. Slices then were perfused by modified ACSF substituting 4 mM Sr^{2+} ions for Ca^{2+} ions, while a single lemniscal fiber was stimulated at 0.1Hz, resulting in asynchronous miniature EPSCs following a synchronous EPSC from the stimulated fiber (Fig. 16A). I analyzed 2173, 1572, and 1211 miniature EPSCs for sham,

IONC-S, and IONC-W fibers, respectively (pooled data from 12, 8, and 7 cells, respectively). The amplitudes of miniature EPSCs from both IONC-S and -W fibers were significantly smaller than those from sham fibers (Fig. 16*B*, *C*; $^{**}P < 0.01$, Kolmogorov-Smirnov two-sample test). The decay time constants of miniature EPSCs from IONC-W fibers were significantly larger than those from sham fibers, whereas the rise time constants were identical (Fig. 16*C, E, F*; $^{**}P < 0.01$ for decay; $P > 0.05$ for rise, Kolmogorov-Smirnov two-sample test). These results suggest that the reduced amplitude and the prolonged decay time of AMPAR-mediated lemniscal EPSCs after the IONC operation, at least partially, derive from postsynaptic changes.

No contribution of kainate (KA) receptors-mediated components to lemniscal EPSCs after the IONC operation

It might be possible that an appearance of KA receptors prolongs the decay time of lemniscal EPSCs after the IONC operation, because KAR-mediated EPSCs in native synapses have a long decay time (Castillo *et al.*, 1997; Kidd and Isaac, 1999; Li *et al.*, 1999; Bureau *et al.*, 2000; Kidd and Isaac, 2001; Wu *et al.*, 2005a; Miyata and Imoto, 2006, 2009). Miyata and Imoto (2006) have reported that lemniscal EPSCs are lacking of a KAR-mediated component. Thus, if KA receptors appear at the postsynaptic membrane of IONC-W fibers after the IONC operation, persistent KAR-mediated EPSCs could be observed after selective blockades of

AMPA and NMDA receptors.

However, no KAR-mediated component was observed at IONC-W EPSCs after bath application of 100 μM SYM 2206 (a selective blocker of AMPA receptors which does not block KA receptors) (Pelletier et al., 1996) in the presence of 100 μM $_{DL}$-APV. The SYM2206 completely blocked APV-resistant EPSCs (figure not shown, 99.3 ± 0.5% inhibition, n = six), and the extent of which was not different from that after the subsequent application of 20 μM NBQX (AMPA/Kainate blocker). Hence, there appears to be no appearance of KA receptors at IONC-W synapses after the IONC operation.

Relatively abundant GluR2 containing AMPA receptor compositions at IONC Weak fiber synapses

As another possibility, switches of AMPA receptor compositions may account for the prolonged decay time of EPSCs after the IONC operation, because kinetics of AMPAR-mediated currents largely depends on its subunit compositions (Mosbacher et al., 1994; Quirk et al., 2004). To elucidate the nature of AMPA receptors at the postsynaptic membrane of each fiber, I investigated current-voltage (I-V) relationships of AMPAR-mediated EPSCs in the presence of 200 μM $_{D}$-APV (Fig. 17*A*-*C*). Consistently with previous reports (Arsenault and Zhang, 2006; Miyata and Imoto, 2006; Wang and Zhang, 2008), AMPAR-mediated EPSCs of sham fibers exhibited a strong inward rectification (Fig.

17*A*, *B*), suggesting that these were mainly mediated by GluR2-lacking, Ca^{2+}-permeable subunit compositions (Liu and Zukin, 2007). EPSCs of IONC-S were almost identical with those of sham in I-V relationship (Fig. 17*A*, *B*). However, EPSCs of IONC-W exhibited a relatively weak inward rectification compared with that of sham and IONC-S (Fig. 17*A*, *B*; $^{**}P < 0.01$ both vs. sham and IONC-S, two-way repeated ANOVA, n = 11, 14, and 10 for sham, IONC-S, and IONC-W, respectively). The mean of rectification indexes (ratio of +40 mV to -40 mV) of IONC-W was significantly larger than that of sham and IONC-S (Fig. 17*C*; $^{*}P < 0.05$ vs. sham; $^{**}P < 0.01$ vs. IONC-S, two-tailed, multiple *t*-test with Bonferroni correction following ANOVA, values: 0.29 ± 0.03, 0.26 ± 0.02, and 0.44 ± 0.05 for sham, IONC-S, and IONC-W, respectively). Given these results, it is possible that GluR2-containing AMPA receptors are relatively abundant at IONC-W synapses. I confirmed the possibility by pharmacological experiments using spermine and pentobarbital, which were specific inhibitors for GluR2-lacking and -containing AMPA receptors, respectively (Yamakura et al., 1995; Isa et al., 1996; Washburn and Dingledine, 1996; Liu and Cull-Candy, 2000). Bath-applied 1 mM spermine less efficiently inhibited EPSCs of IONC-W than those of sham and IONC-S (Fig. 17*D*, *E*; $^{**}P < 0.01$, two-tailed, multiple *t*-test with Bonferroni correction following ANOVA, values (%): 57.7 ± 3.6, 63.0 ± 2.9, and 37.0 ± 5.6 for sham, IONC-S, and IONC-W, respectively). Conversely, bath-applied 100 μM pentobarbital more efficiently inhibited EPSCs of IONC-W than those of sham and IONC-S (Fig. 17*D*, *E*; $^{*}P < 0.05$,

two-tailed, multiple *t*-test with Bonferroni correction following ANOVA, values (%): 8.3 ± 1.8, 9.2 ± 2.4, and 30.0 ± 11.1 for sham, IONC-S, and IONC-W, respectively). Collectively, it is probable that GluR2-containing AMPA receptors were relatively abundant at IONC-W synapses.

Relatively abundant flip-type splice variants of AMPA receptors at IONC-W synapses

Two alternative splice variants of each AMPA receptor subunit (flip or flop) determine kinetics and sensitivity to chemicals of functional AMPA receptors (Sommer et al., 1990; Hollmann and Heinemann, 1994; Mosbacher et al., 1994; Partin et al., 1994; Sekiguchi et al., 1997; Quirk et al., 2004). Because expression of flip-type subunits, the kinetics of each of which was slow, correlates with that of the GluR2 subunit (Geiger et al., 1995), I hypothesized that flip-type splice variants are abundant at IONC-W synapses as GluR2 subunits are.

As in chapter 1, I employed two inhibitors of AMPA receptor desensitization, CTZ and PEPA, which were selective for flip and flop, respectively (Partin et al., 1994; Sekiguchi et al., 1997). As expected, bath-applied 100 μM CTZ more effectively potentiate EPSCs of IONC-W than those of sham and IONC-S (Fig. 18*A*, *B*; $*P < 0.05$ vs. sham; $P = 0.08$ vs. IONC-S, two-tailed, multiple *t*-test with Bonferroni correction following ANOVA, values (%): 39.6 ± 11.3, 52.3 ± 7.2, and 111.8 ± 28.8 for sham, IONC-S, and IONC-W, respectively).

By contrast, bath-applied 100 μM PEPA tended to less effective at IONC-W synapses than at sham and IONC-S synapses, but not statistically significant (Fig. 18*C*, *D*; $P = 0.36$ vs. sham; $P = 0.62$ vs. IONC-S, two-tailed, multiple *t*-test with Bonferroni correction following ANOVA, values (%): 62.7 ± 26.6, 50.4 ± 20.1, and 37.7 ± 8.3 for sham, IONC-S, and IONC-W, respectively). Taken together, these results indicate the relative abundance of flip type splice variants at IONC-W synapses, which can contribute to slower kinetics of IONC-W EPSCs.

No change of NMDA receptor compositions after the IONC operation

Next, I investigated possible changes of NMDA receptor compositions after the IONC operation. Because NR2A-containing NMDA receptors dominate at lemniscal synapses at the intact mature condition (Arsenault and Zhang, 2006; Miyata and Imoto, 2006), a possible appearance of NR2C or D-containing receptors could release the magnesium blockade of NMDA receptors at negative potentials. In addition, a possible appearance of NR2B, C, or D-containing receptors could prolong decay time of EPSCs.

However, I-V curves of EPSCs of the three types of lemniscal fibers were almost superimposed (Fig. 19*A*, *B*; $P = 0.16$, two-way repeated ANOVA). Moreover, no difference was observed in decay time of EPSCs among the three types of fibers (Fig. 19*C*, *D*; $P = 0.81$, one-way ANOVA, values (ms): 53.2 ± 3.3, 54.6 ± 2.8, and 50.8 ± 4.4 for sham, IONC-S, and

IONC-W, respectively). Thus, there appears to be no change in property of NMDA receptors after the IONC operation.

The elevated paired-pulse ratio and coefficient of variation of IONC-W EPSCs

To assess presynaptic properties of the three types of lemniscal fibers, two types of experiments were employed, paired-pulse stimulation and coefficient of variation analyses. The paired-pulse ratio (the 2^{nd} EPSCs/the 1^{st} EPSCs) negatively correlates with the probability of transmitter release (Manabe et al., 1993; Zucker and Regehr, 2002; Pan and Zucker, 2009). I found that the paired-pulse ratio of IONC-W EPSCs was larger than that of sham and IONC-S EPSCs, especially at short interpulse intervals (Fig. 20*A*, *B*; $*P < 0.05$ vs. sham; $**P < 0.01$ vs. IONC-S, two-way repeated ANOVA, n = 6, 10, and 6 for sham, IONC-S, and IONC-W, respectively). Further, I analyzed the coefficient of variation calculated from amplitude of 30 consecutive EPSCs of each fiber. As a result, the mean of the value of IONC-W was significantly larger than that of sham and IONC-S (Fig. 20*C*, $**P < 0.01$, two-tailed, multiple *t*-test with Bonferroni correction following one-way ANOVA, values: 0.048 ± 0.005, 0.051 ± 0.006, and 0.147 ± 0.021 for sham, IONC-S, and IONC-W, respectively). It is accepted that coefficient of variation of EPSC amplitude reflects both the release probability of transmitter and the number of release site (del Castillo and Katz, 1954; Manabe et al., 1993). Thus, together with the result of paired-pulse stimulation, it seems

likely that IONC-W synapses have lower release probability and fewer release sites of transmitter than those of sham and IONC-S synapses.

No effect of whisker deprivation on lemniscal fiber innervation

To investigate whether the lack of sensory inputs causes multiple reinnervation of lemniscal fibers, I removed all large whiskers on the left side snout from P21 to the recording day (Fig. 12*A*), when I counted the number of lemniscal fibers onto a given relay neuron. As a result, there was no difference in number of lemniscal fiber inputs onto a given relay neuron between intact and deprived animals (Fig. 21*B*, *C*; $P = 0.74$, Wilcoxon-Mann-Whitney two-sample rank test, values: 1.16 ± 0.08 and 1.17 ± 0.08 for intact and deprived groups, respectively). Therefore, the lack of whisker-mediated sensory inputs is not sufficient to induce the multiple reinnervation of lemniscal fibers onto a relay neuron.

No morphological change of relay neuron after deafferentation

Finally, I investigated whether the deafferentation employed here (IONC and whisker deprivation) induces morphological changes of relay neurons in the VPM (e.g. shrinkage or unusual development) with a biocytin labeling technique. As a result, I could not detect any morphological change of relay neurons on both soma and dendrite (Fig. 22; $P = 0.75$ for soma; $P = 0.58$ for dendrite, one-way ANOVA, values (μm^2): on soma, 175.1 ± 19.9, 192.8 ±

23.4, and 180.4 ± 10.7, on dendrite, 3174.1 ± 310.5, 3225.7 ± 314.4, and 2829.7 ± 336.3 for sham, IONC, and whisker deprivation, respectively). The morphology of relay neurons was well consistent with previous studies (Brown et al., 1995; Zantua et al., 1996).

Discussion

In this study, IONC-induced remodeling of mature lemniscal synapses was examined using electrophysiological and immunohistochemical techniques. The findings are as follows: (1) The IONC operation induces multiple reinnervation of lemniscal fibers onto a relay neuron. (2) The IONC reduces the amplitude of single fiber-mediated lemniscal EPSCs, but not that of total lemniscal EPSCs. (3) Weak fibers observed after the IONC are presumably newly-recruited (Weak fibers). (4) The IONC operation induces changes in AMPA receptor compositions at Weak fiber synapses, but no change in NMDA receptor compositions. (5) The IONC operation elevated the paired-pulse ratio and the coefficient of variation of EPSC amplitude at Weak fiber synapses.

Multiple reinnervation of lemniscal fibers onto a relay neuron

The present results clearly demonstrate that additional lemniscal fibers are recruited by relay neurons after the IONC operation (Fig. 8). Mechanisms whereby such reinnervation of lemniscal fibers occurs presumably are sprouting of lemniscal fibers in the VPM. Active axonal sprouting after deafferentation along the somatosensory pathway has been reported in both the spinal cord (Sengelaub et al., 1997; Jain et al., 2000) and the cortex (Florence et al., 1998). Moreover, several papers have pointed out that it is likely to occur at the thalamus (Jones and Pons, 1998; Kaas et al., 1999; Jones, 2000). In the visual thalamus, indeed,

reinnervation of retinogeniculate axons onto a relay neuron is induced by dark rearing even after developmental synapse elimination has been finished (Hooks and Chen, 2006, 2008). Sprouting of lemniscal fibers to adjacent relay neurons can remodel wiring in the VPM. Because recordings here were conducted one week after the IONC operation, sprouting lemniscal fibers could be expanded within a limited area (e.g. within a single barreloid structure). This is well consistent with the fact that CO-stained barreloid structures, which are visualized as the expansion of lemniscal fiber bundle, are not obviously changed after the IONC operation (data not shown).

Mechanisms underlying the multiple reinnervation of lemniscal fibers

Mechanisms underlying the multiple reinnervation of lemniscal fibers are unknown. However, since whisker deprivation did not induce the multiple reinnervation of lemniscal fibers (Fig. 21), I can conclude, at least, that the lack of whisker-mediated sensory inputs is not sufficient for the remodeling. Because gentle whisker deprivation employed here does not induce any damage on sensory nerve endings (Li et al., 1995), IONC-induced nerve injury itself or shutoff of axonal transport by complete transection might induce the reinnervation of lemniscal fibers. In fact, there was a significant activation of microglia in the principle sensory nucleus of trigeminal nerve after the IONC operation which emits lemniscal fibers toward the VPM (data not shown). Activation of microglia is also observed in the dorsal horn

of the spinal cord after peripheral nerve injury (Coull et al., 2003; Tsuda et al., 2003; Coull et al., 2005). Activated microglia releases brain derived neurotrophic factor, which is critical for developmental or plastic change in wiring of synaptic connection in the CNS (e.g. synaptogenesis or reinnervation of climbing fiber in the cerebellum) (Letellier et al., 2007; Sherrard et al., 2009). Taken together, I speculate that IONC-induced nerve injury results in activation of microglia in the principle sensory nucleus of trigeminal nerve, and the subsequent brain derived neurotrophic factor signal cascade might induce the reinnervation of lemniscal fibers in the VPM.

Weak fibers are putative newly-recruited fiber.

The results in figure 12 suggest that the IONC operation induces a new population of lemniscal fibers with smaller amplitude and slower decay time of AMPAR-mediated EPSCs. I defined the new population as Weak fibers, and the remaining as Strong fibers. Weak fibers had immature synaptic properties (small AMPA/NMDA ratio, Fig. 14; slow decay time of AMPAR-mediated EPSCs, Fig. 15; reduced inward rectification, Fig. 17; and high sensitivity to cyclothiazide). These results well agree with the report of Hooks and Chen (2006) that reinnervation of retinogeniculate fibers resulted in small EPSC amplitude and a small AMPA/NMDA ratio of retinogeniculate EPSCs. Moreover, since 92.2% of relay neurons in the IONC group were innervated at least one Strong fiber, Strong fibers in the IONC group

(IONC-S) are assumed to be preexisting fibers, whereas Weak fibers in the IONC group (IONC-W) are newly-recruited fibers.

Reduced amplitude of EPSCs after the IONC operation

Both IONC-S and IONC-W fibers had smaller amplitude of evoked EPSCs compared with that of sham fibers (Fig. 14). As a result, total (saturated) currents recorded from a given relay neuron were not different between the sham and IONC groups, even though extra lemniscal fibers were recruited (Fig. 11). The IONC operation also reduced amplitude of miniature lemniscal EPSCs both from IONC-S and IONC-W fibers (Fig. 16). This is well consistent with the report that small miniature lemniscal EPSCs is observed after whisker deprivation (Wang and Zhang, 2008). Studies on synaptic scaling suggest that a reduction in sensory input or a cessation of synaptic activity results in global up-regulation of synaptic gain for homeostasis (Desai et al., 2002; Goel and Lee, 2007; Turrigiano, 2008). Thus, the reduction in amplitude of miniature lemniscal EPSCs observed in this study can be the input specific modification. Other excitatory inputs, corticothalamic synapses may be potentiated after IONC or whisker deprivation. Taken together, silencing of sensory inputs may induce input-specific reduction in amplitude of lemniscal EPSCs, which in turn induce compensatory reinnervation of lemniscal fibers.

Altered AMPA receptor properties at IONC-W synapses

At IONC-W synapses, putative newly-generated synapses, the longer decay time of AMPAR-mediated EPSCs was observed (Fig. 15, 16). Data from current-voltage relationships of AMPAR-mediated lemniscal EPSCs and pharmacological experiments (Fig. 17, 18) suggest that altered compositions of postsynaptic AMPA receptors. Because NMDARs compositions were not altered (Fig. 19), it is suggested that AMPA and NMDA receptors are differently regulated.

The GluR2 subunit is a critical determinant of the nature of AMPAR-mediated currents; GluR2-lacking AMPA receptors exhibit a strong inward rectification, whereas GluR2-containing ones do not (Verdoorn et al., 1991; Burnashev et al., 1992). Thus, the strong inward rectification of AMPAR-mediated EPSCs at sham and IONC-S synapses indicates relatively little GluR2-containing AMPA receptors at these synapses. This is well consistent with anatomical data that the adult VPM is lacking of the GluR2 subunit mRNA and protein (Keinänen et al., 1990; Young et al., 1995; Jones et al., 1998) (Yamasaki, 2009; *personal communication*). In contrast, the reduced inward rectification of AMPAR-mediated EPSCs at IONC-W synapses indicates relatively abundant GluR2-containing AMPA receptors at the synapses (Fig. 17*A*-*C*). The reduced sensitivity to spermine and the increased sensitivity to pentobarbital of EPSCs at IONC-W synapses further support the idea (Fig. 17*D*-*G*).

By the way, the adult VPM has more abundant expression of flop-type alternative

slice variants of AMPA receptor subunits than that of flip-type ones (Young et al., 1995). The abundant flop-type expression in the mature VPM probably contributes to the fast decay time of lemniscal EPSCs and the higher sensitivity to PEPA rather than to CTZ (Fig. 5 in chapter 1) (Mosbacher et al., 1994; Sekiguchi et al., 1997; Quirk et al., 2004). After the IONC operation, the sensitivity to CTZ of IONC-W EPSCs was increased to suggest the up-regulation of the flip-type splice variants at IONC-W synapses (Fig. 18) (Partin et al., 1994). These results are well consistent with that GluR2 expression correlates with that of flip-type splice variants (Geiger et al., 1995).

In addition to receptor subunit compositions and splice variants, the association of transmembrane AMPAR regulatory proteins (TARPs) with AMPA receptors also modifies properties of AMPA receptors. Association with TARPs increases the conductance and slows the kinetics of AMPA receptors (Tomita et al., 2003; Turetsky et al., 2005; Cho et al., 2007). In the presence of TARPs, AMPA receptors become less sensitive to polyamine block (e.g. spermine), resulting in reduced inward rectification of AMPAR-mediated currents (Cho et al., 2007; Soto et al., 2007). Moreover, TARPs increase the sensitivity to CTZ and PEPA of AMPA receptors (Tomita et al., 2006). Anatomically, the mature thalamus exhibits a low level of TARPs expression except stargazin (γ2); the modest expression of stargazin is observed (Allen, 2003; Tomita et al., 2003). Thus, increased association of TARPs with AMPA receptors at IONC-W synapses may account for the latter part of the present results (Fig. 15 -

18). However, although I do not totally exclude the possibility, no change in 10 - 90% rise time (Fig. 16) and PEPA sensitivity (Fig. 18) are more suggestive of increased GluR2-flip subunits at IONC-W synapses.

The elevated paired-pulse ratio and coefficient of variation at IONC-W synapses

Both the paired-pulse ratio and the coefficient of variation of EPSC amplitude were larger at IONC-W synapses than those at sham and IONC-S synapses (Fig. 20). These results suggest that release probability of transmitter is reduced at IONC-W synapses (Manabe et al., 1993; Zucker and Regehr, 2002; Pan and Zucker, 2009). Fewer number of release sites at IONC-W fiber synapses calculated from the amplitudes of evoked and miniature EPSCs (data not shown) also could contribute to the elevated value of coefficient of variation (del Castillo and Katz, 1954; Manabe et al., 1993). Reduced desensitization which is due to up-regulated flip splice variant or increased TARP association might contribute to the elevated paired-pulse ratio (Chen et al., 2002; Tomita et al., 2006; Cho et al., 2007). Saturation of AMPA receptors may not contribute to the difference in paired-pulse ratio, because weaker saturation results in a decrease in paired-pulse ratio (Wadiche and Jahr, 2001; Foster et al., 2005). Absence of spermine in the pipette solution excluded the contribution of use-dependent relief from polyamine block to paired-pulse ratio (Bowie et al., 1998; Rozov et al., 1998). Taken together, at the IONC-W synapses, the release probability is presumably reduced, and the number of

release site should be small.

Remodeling of lemniscal synapses after the IONC operation and deafferentation-induced reorganization in the thalamus

Because the present experiments after the IONC operation were limited to a subacute phase, the phenomena observed here might be quite different from mechanisms which underlie functional changes reported by *in vivo* long-term experiments ranged from a month to 20 years after deafferentation (Sengelaub et al., 1997; Jones and Pons, 1998; Jain et al., 2000; Graziano and Jones, 2009). Although the multiple innervation may be transient as in neuromuscular junctions (Brown et al., 1981; Rich and Lichtman, 1989), pilot data revealed that the multiple innervation of lemniscal fibers were retained at least two weeks after the IONC operation (data not shown). Considering previous studies in the CNS (Rossi *et al.*, 1991b), the multiple innervation of lemniscal fibers may survive for a long time, be consolidated, and then contribute to plastic changes of receptive fields in the thalamus and change in somatic sensation (Pons et al., 1991; Davis et al., 1998; Jones and Pons, 1998; Jones, 2000; Jain et al., 2008).

Summary

In this chapter, IONC operation-induced changes of lemniscal synapses were reported. The

IONC operation induced the multiple reinnervation of lemniscal fibers onto a relay neuron in the VPM. IONC-W fibers which may be newly-recruited lemniscal fibers have distinct pre- and postsynaptic properties, including GluR2-containing-like AMPAR-mediated EPSCs, compared with those of sham or preexisting fibers. These remodeling may underlie functional changes of the thalamus observed in *in vivo* and pathological sensations after deafferentations.

Figures

Figure 8. Infraorbital nerve cut-induced multiple reinnervation of lemniscal fibers onto a relay neuron.

A, Representative traces of lemniscal EPSCs recorded one week after sham or the IONC operation under voltage clamp conditions at both +40 mV and -70 mV. Several raw traces with different stimulus intensities are superimposed at each holding potential. *B*, Summary histogram showing the number of discrete EPSC steps. *C*, Arrows beside traces represent the amplitude of saturated currents (left) and of single fiber currents from the strongest fiber (right). *D*, Summary bar graph showing the mean of contribution ratio (*see Methods and Materials in chapter 1*) for each group. Each column represents the mean ± S.E.M. Statistical significance was tested by two-tailed Student's *t*-test. $^{**}P < 0.01$.

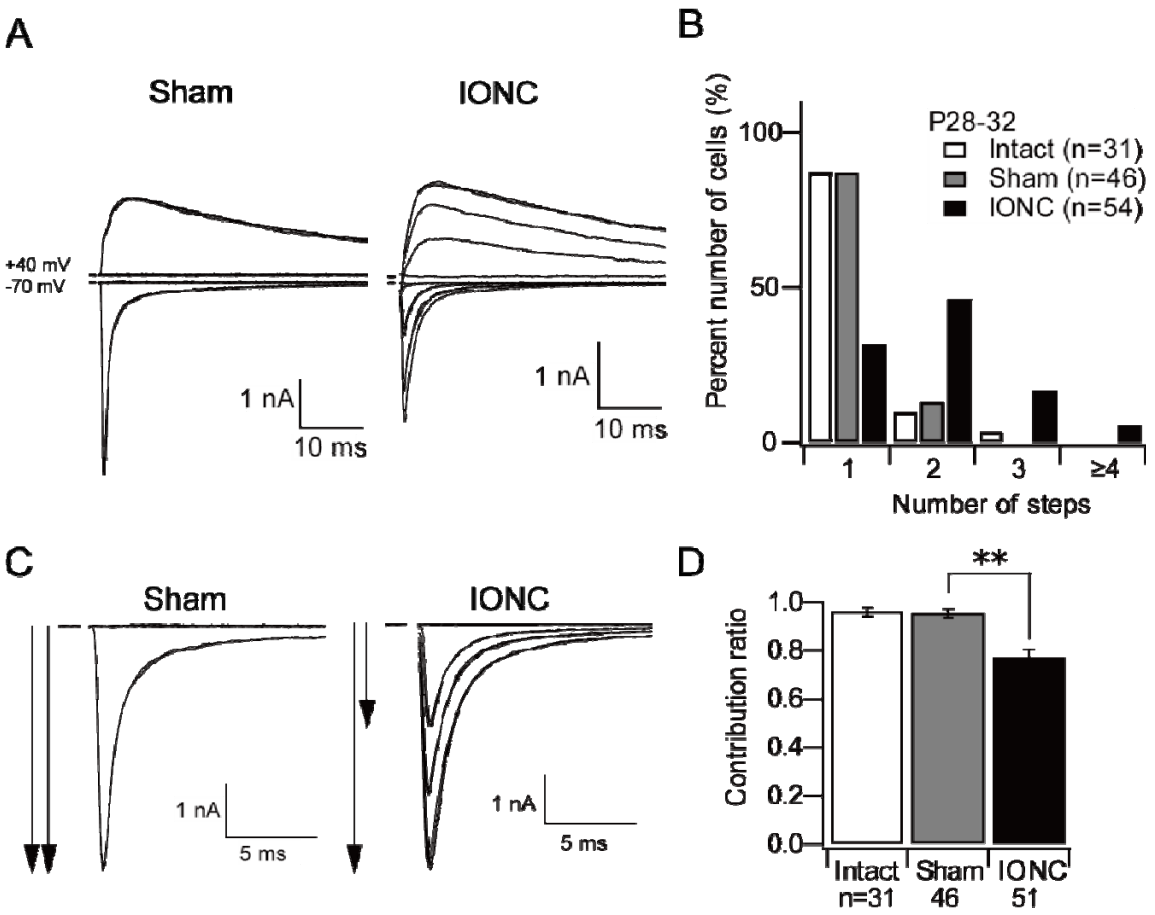
A
Sham
IONC
+40 mV
-70 mV
1 nA
10 ms
1 nA
10 ms
B
Percent number of cells (%)
100
50
0
P28-32
Intact (n=31)
Sham (n=46)
IONC (n=54)
1
2
3
≥4
Number of steps
C
Sham
IONC
1 nA
5 ms
1 nA
5 ms
D
**
Contribution ratio
1.0
0.8
0.6
0.4
0.2
0.0
Intact
n=31
Sham
46
IONC
51

Figure 8

Figure 9. IONC-induced silent synapses

A representative trace of IONC-induced silent lemniscal EPSCs. Two of fifty-four relay neurons were innervated by a silent lemniscal fiber after the IONC operation. There was no silent synapse containing cell in sham-operated group.

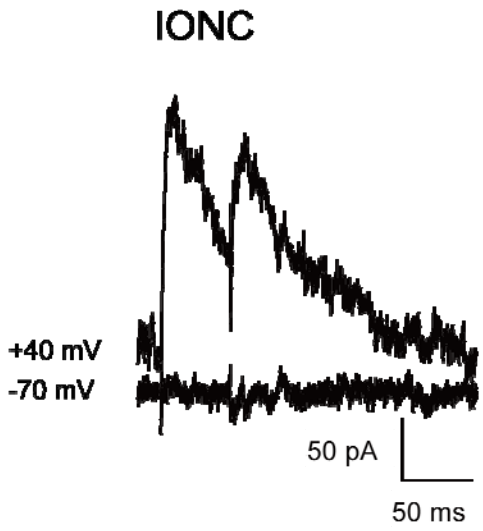

Figure 9

Figure 10. Quantification of density of lemniscal fiber boutons in the VPM nucleus

A, Representative images of immunostaining against VGluT2, which results in selective staining against presynaptic lemniscal fiber boutons in the VPM nucleus. *B*, Representative images of double staining of lemniscal fiber boutons and nuclei in the VPM nucleus by VGluT2-immunostaining (magenta) and methyl green (green), respectively. *C*, Summary bar graph showing the mean of numbers of VGluT2-immunoreactive boutons in the VPM nucleus. Each column represents the mean ± S.E.M. of six separate mice. Statistical significance was tested by two-tailed Student's *t*-test. NS: $P > 0.05$. *D*, The ratios of the number of VGluT2-immunoreactive boutons to the number of methyl green positive nuclei in VPM nucleus. Each column represents the mean ± S.E.M. of three separate mice. Statistical significance was tested by two-tailed Student's *t*-test. NS: $P > 0.05$.

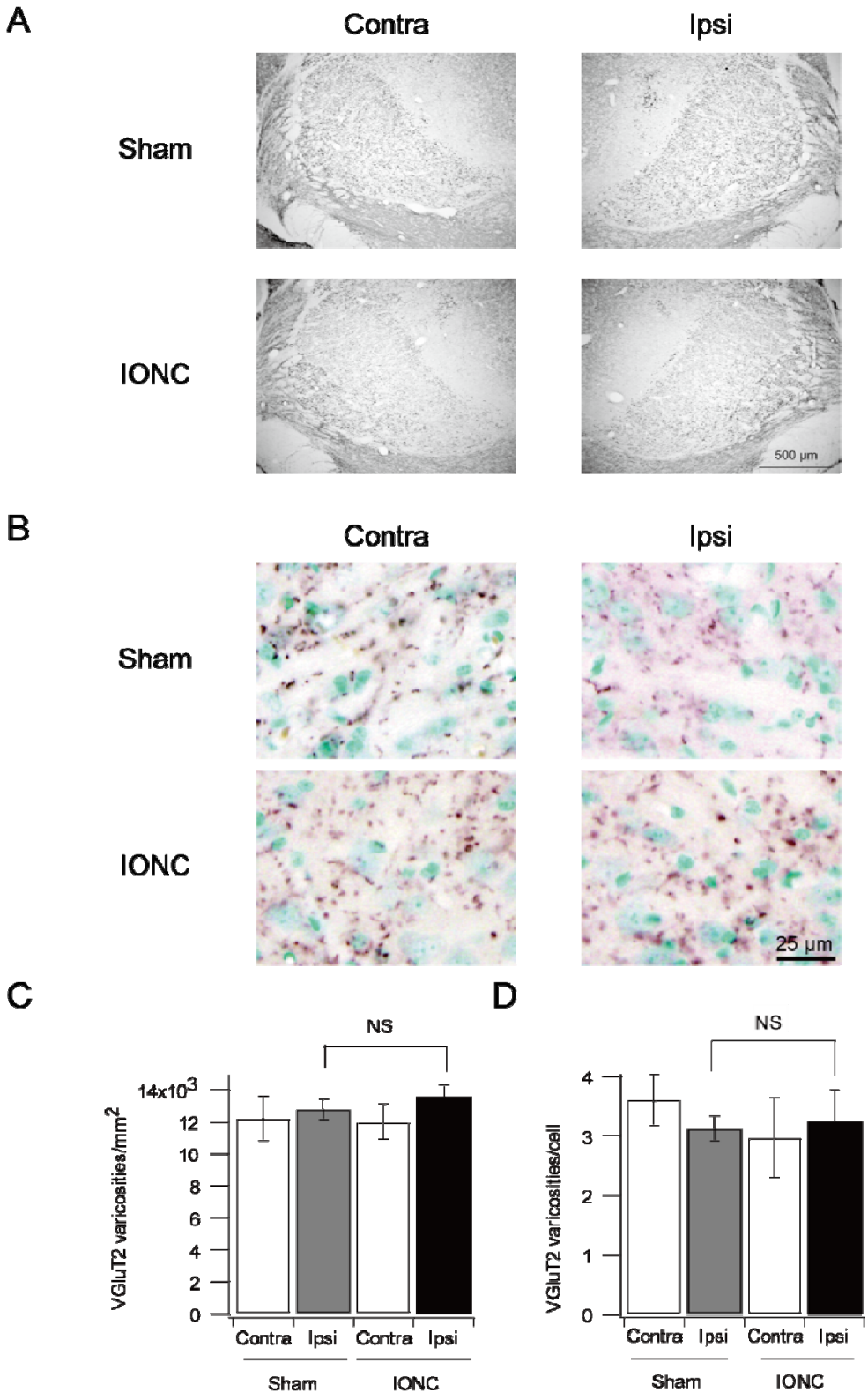
A
Contra
Ipsi
Sham
IONC
500 μm
B
Contra
Ipsi
Sham
IONC
25 μm
C
NS
14x10^3
12
10
8
6
4
2
0
VGluT2 varicosities/mm^2
Contra
Ipsi
Contra
Ipsi
Sham
IONC
D
NS
4
3
2
1
0
VGluT2 varicosities/cell
Contra
Ipsi
Contra
Ipsi
Sham
IONC

Figure10

Figure 11. IONC reduces the amplitude of single fiber-mediated lemniscal EPSCs.

A, *C*, Representative traces of lemniscal EPSCs from both sham- and IONC-operated mice are shown in the same calibration. The holding potential was at +40 mV (A) or -70 mV (C). Several raw traces with different stimulus intensities are superimposed. *B*, *D*, Summary bar graphs showing the mean of amplitude of single fiber-mediated (left) and total lemniscal fiber-mediated (right) EPSCs. The holding potential was at +40 mV (B) or -70 mV (D). Each column represents the mean ± S.E.M. Statistical significance was tested by two-tailed Student's *t*-test. $^{**}P < 0.01$.

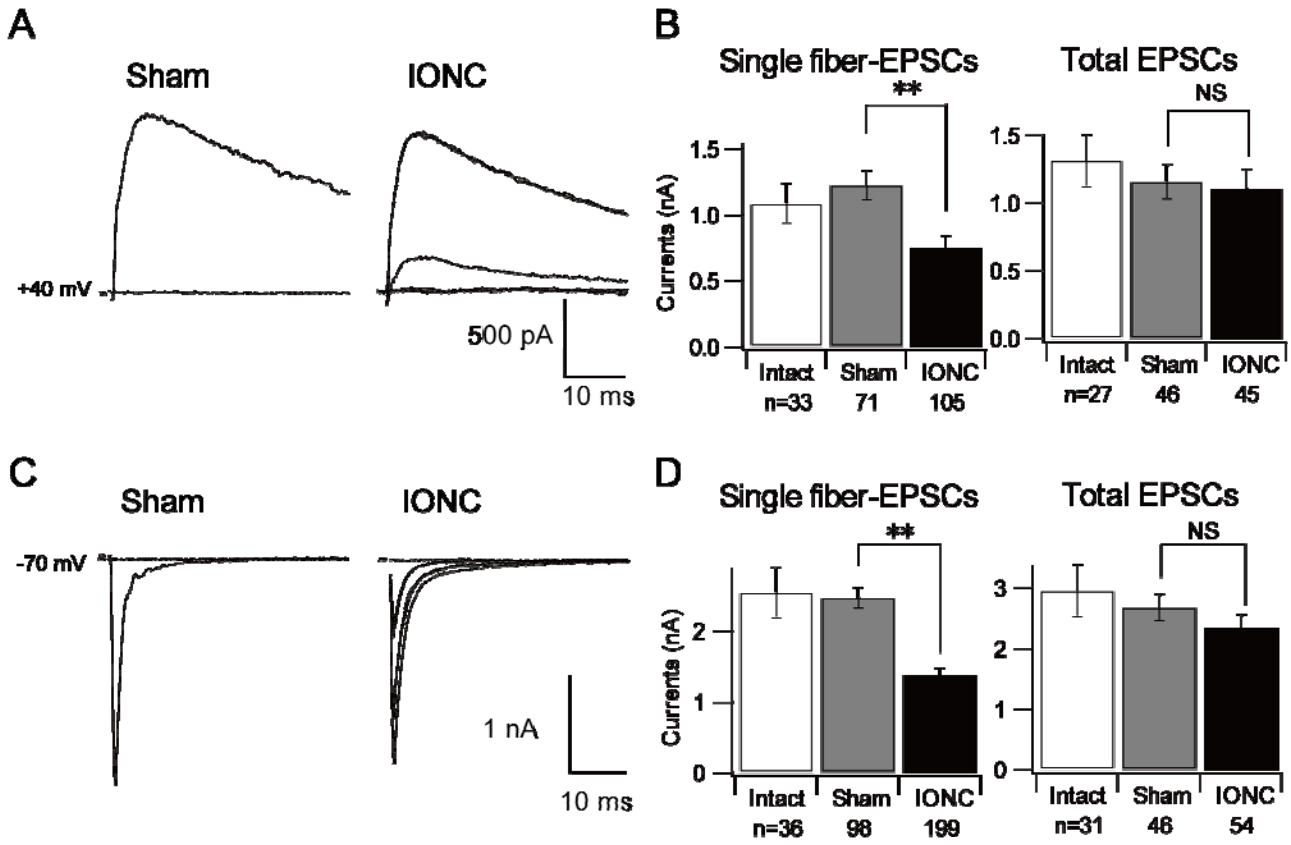
A
Sham
IONC
+40 mV
500 pA
10 ms
B
Single fiber-EPSCs
Total EPSCs
**
NS
Currents (nA)
1.5
1.0
0.5
0.0
Intact
Sham
IONC
n=33
71
105
n=27
46
45
C
Sham
IONC
-70 mV
1 nA
10 ms
D
Single fiber-EPSCs
Total EPSCs
**
NS
Currents (nA)
3
2
1
0
Intact
Sham
IONC
n=36
98
199
n=31
46
54

Figure 11

Figure 12. Distributions of single fiber-mediated lemniscal EPSCs amplitude, cluster analysis, and its validation

Single fiber-mediated lemniscal EPSCs were recorded at -70 mV. The fibers then were classified by their amplitude and decay time constant. *A*, Histograms showing distributions of single fiber-mediated lemniscal EPSC amplitude recorded from sham (left) and IONC (right) groups. Red dashed lines indicate the threshold which separates Strong and Weak fibers. *B*, Decay time constant of lemniscal EPSCs is plotted against its amplitude. Each marker represents an individual lemniscal fiber. *C*, Data from sham and IONC groups were pooled. The pooled distribution then was fitted with summation of two independent Gaussian surfaces (left, red). After that, first (green) and second (magenta) The Gaussian surfaces were represented at center and right panels, respectively. *D*, Cumulative probability distribution of each Gaussian is plotted as a function of EPSC amplitude which determines the cutting plane. *E*, The contamination ratio (*see Material and Methods*) is plotted as a function of threshold (EPSC amplitude). Each Gaussian was weighted. Arrow indicates the 500 pA, the threshold between Strong and Weak fibers which I employed.

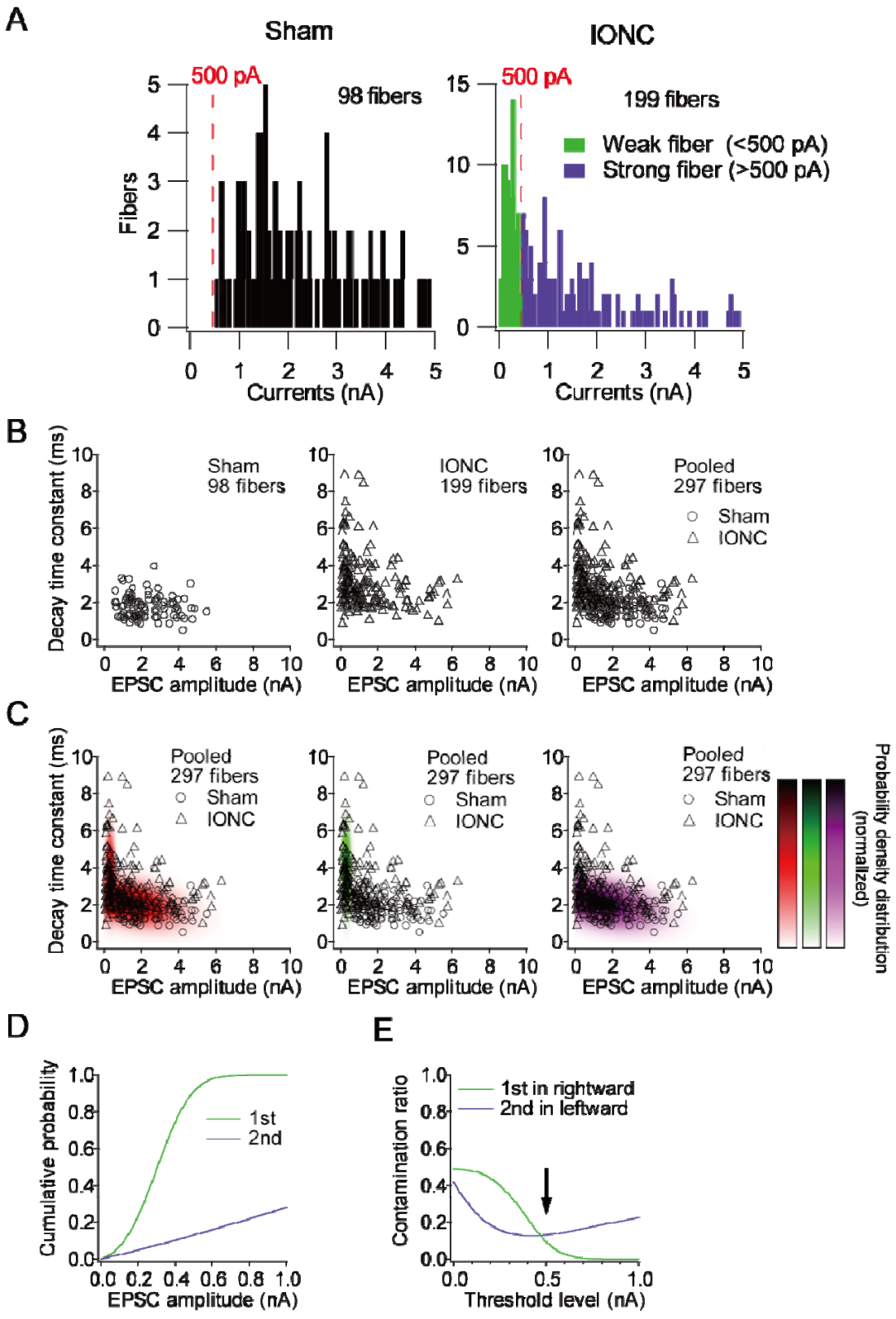
A
Sham
IONC
500 pA
98 fibers
199 fibers
Weak fiber (<500 pA)
Strong fiber (>500 pA)
Fibers
Currents (nA)
B
Sham
98 fibers
IONC
199 fibers
Pooled
297 fibers
Sham
IONC
Decay time constant (ms)
EPSC amplitude (nA)
C
Probability density distribution
(normalized)
D
Cumulative probability
1st
2nd
E
1st in rightward
2nd in leftward
Contamination ratio
Threshold level (nA)

Figure 12

Figure 13. Different innervation patterns of lemniscal fibers onto a relay neuron between sham and IONC groups.

Each relay neuron was classified into S only, W only, SS, SW, or WW by the amplitude of lemniscal fibers which innervated the cell. S only and W only indicate the single innervations of Strong and Weak fiber, respectively. SS and WW indicate innervations of multiple Strong fibers and multiple Weak fibers, respectively. SW indicates hybrid multiple innervations of Strong and Weak fibers. *A*, *B*, Representative innervation patterns are shown from sham (A) and IONC (B) groups. Several raw traces with different stimulus intensities are superimposed. *C*, Proportions of cellular type of each operation group are shown. Numbers of analyzed cell are 46 for sham and 54 for IONC groups.

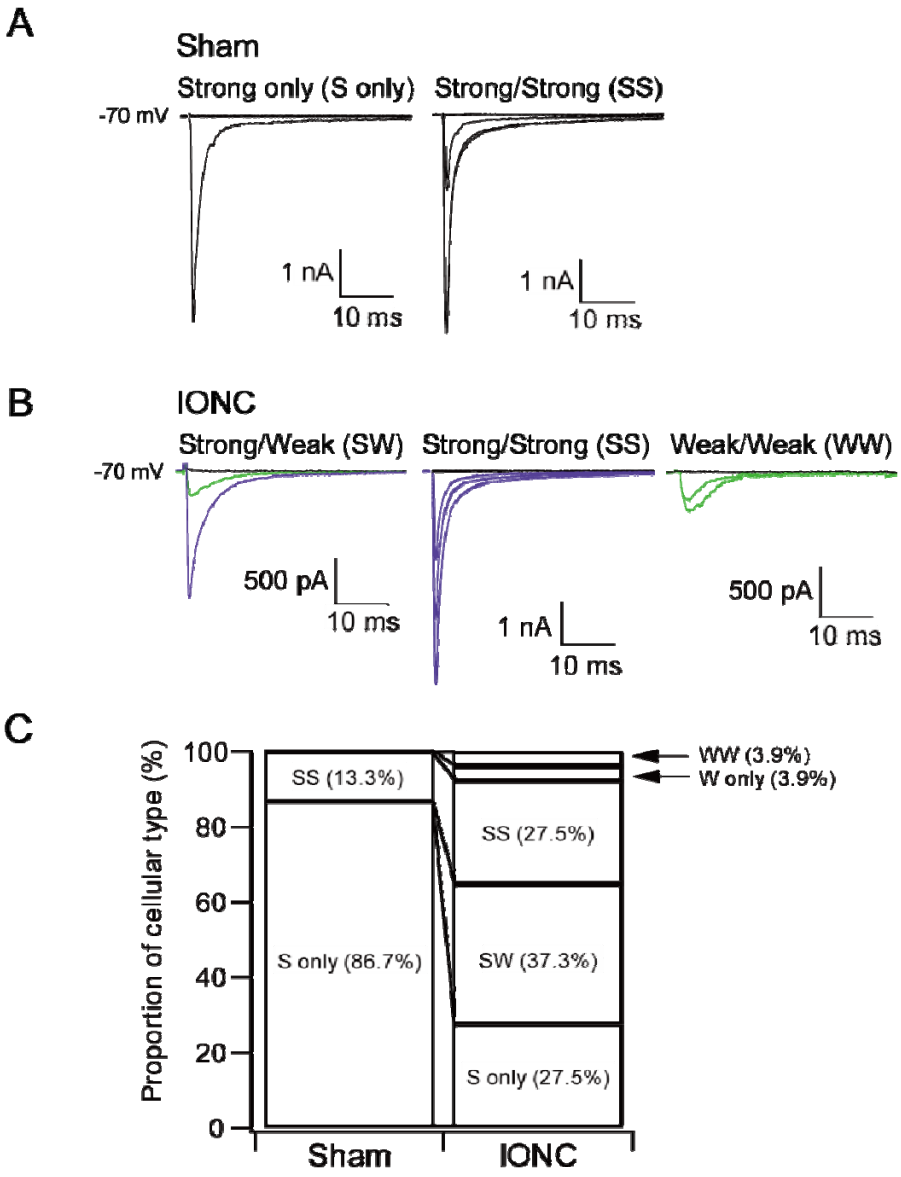
A
Sham
Strong only (S only)
Strong/Strong (SS)
-70 mV
1 nA
10 ms
1 nA
10 ms
B
IONC
Strong/Weak (SW)
Strong/Strong (SS)
Weak/Weak (WW)
-70 mV
500 pA
10 ms
1 nA
10 ms
500 pA
10 ms
C
Proportion of cellular type (%)
100
80
60
40
20
0
SS (13.3%)
S only (86.7%)
SS (27.5%)
SW (37.3%)
S only (27.5%)
WW (3.9%)
W only (3.9%)
Sham
IONC

Figure 13

Figure 14. The small AMPA/NMDA ratio at Weak fiber synapses

A, Representative traces of sham (black), IONC-S (magenta), and IONC-W (green) fiber-mediated EPSCs. Several raw traces with different stimulus intensities are superimposed. The holding potential was +40 mV or -70 mV. *B*, Summary bar graphs showing the mean of amplitude of single fiber-mediated lemniscal EPSCs. AMPAR-mediated EPSCs were recorded at -70 mV (left). NMDAR-mediated EPSCs were recorded at +40 mV (right). *C*, Summary bar graph showing the mean of AMPA/NMDA ratios (-70 mV/+40 mV) from single fiber- mediated lemniscal EPSCs. All error bars represent S.E.M. Statistical significance was tested by multiple *t*-test with Bonferroni correction following one-way ANOVA. **P* < 0.05; ***P* < 0.01 (two-tailed).

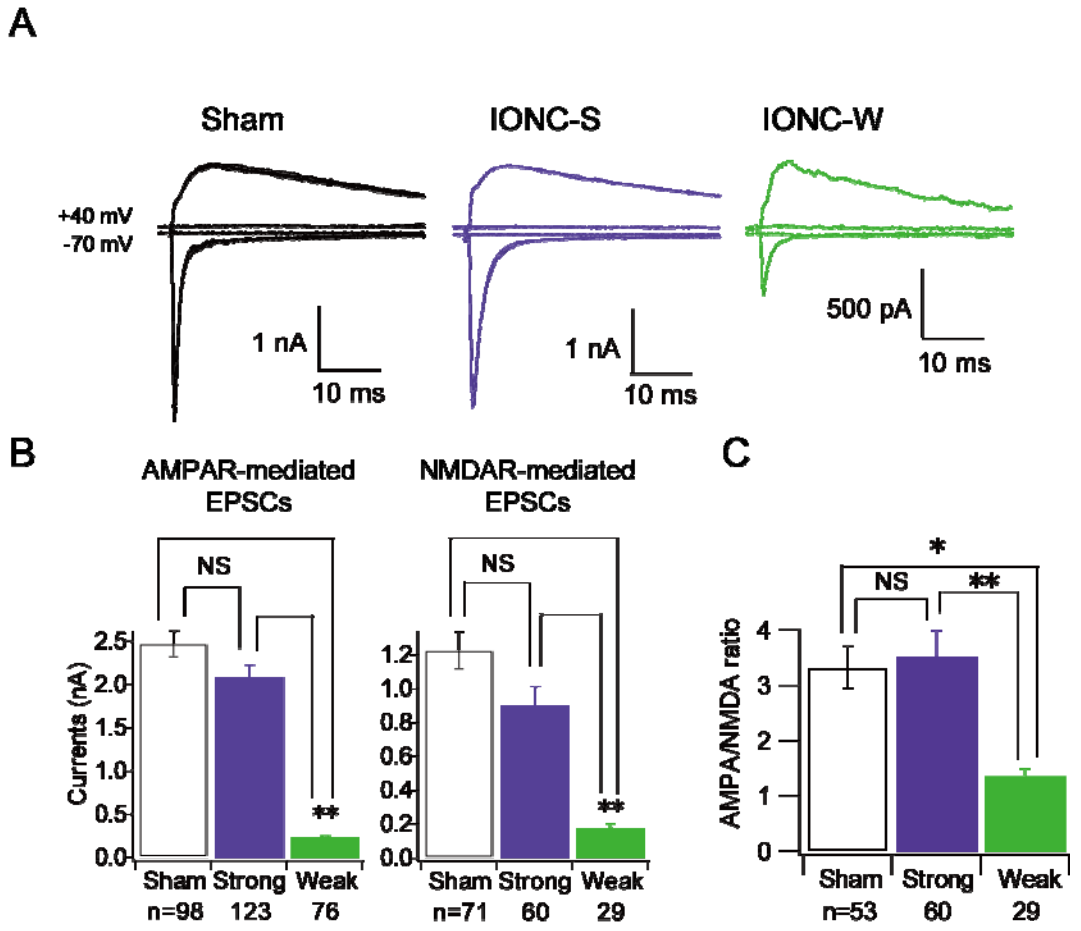
A
Sham
IONC-S
IONC-W
+40 mV
-70 mV
1 nA
10 ms
1 nA
10 ms
500 pA
10 ms
B
AMPAR-mediated EPSCs
NMDAR-mediated EPSCs
NS
NS
**
**
Currents (nA)
2.5
2.0
1.5
1.0
0.5
0.0
1.2
1.0
0.8
0.6
0.4
0.2
0.0
Sham Strong Weak
n=98 123 76
Sham Strong Weak
n=71 60 29
C
*
NS
**
AMPA/NMDA ratio
4
3
2
1
0
Sham Strong Weak
n=53 60 29

Figure 14

Figure 15. Prolonged decay time of AMPAR-mediated EPSCs at Weak fiber synapses

A, Representative traces of AMPAR-mediated lemniscal EPSCs in the presence of 100 μM APV. Each trace is normalized by its peak amplitude (2633, 1436, and 551 pA for sham, IONC-S, and IONC-W fiber, respectively). The holding potential was at -90 mV. *B*, Summary bar graph showing the mean of decay time constants of AMPAR-mediated EPSCs. Error bars represent S.E.M. Statistical significance was tested by multiple *t*-test with Bonferroni correction following one-way ANOVA. $^{**}P < 0.01$ (two-tailed).

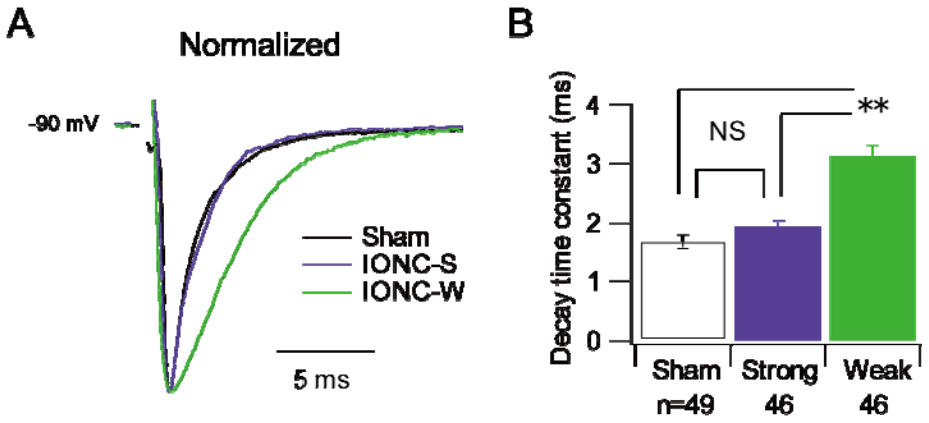
A
Normalized
-90 mV
Sham
IONC-S
IONC-W
5 ms
B
Decay time constant (ms)
0
1
2
3
4
NS
**
Sham
n=49
Strong
46
Weak
46

Figure 15

Figure 16. Asynchronous release of miniature event from an individual lemniscal fiber

A, Representative traces of AMPAR-meditated asynchronous miniature EPSCs evoked by stimulation of single lemniscal fiber in the presence of 4 mM Sr^{2+} ions instead of Ca^{2+} ions. The ACSF included 100 μM APV. The holding potential was at -90 mV. *B*, Averaged traces of miniature EPSCs. Traces of 1517, 1341, and 1015 events were averaged for sham, IONC-S, and IONC-W fibers, respectively. Data from 12, 8, and 7 cells were pooled for sham, IONC-S, and IONC-W, respectively. *D*, Same as (B), but normalized by their amplitude. *C*, *E*, *F*, Cumulative probabilities of amplitude, decay time constants, and 10 - 90% rise time are shown at (C), (E), and (F), respectively.

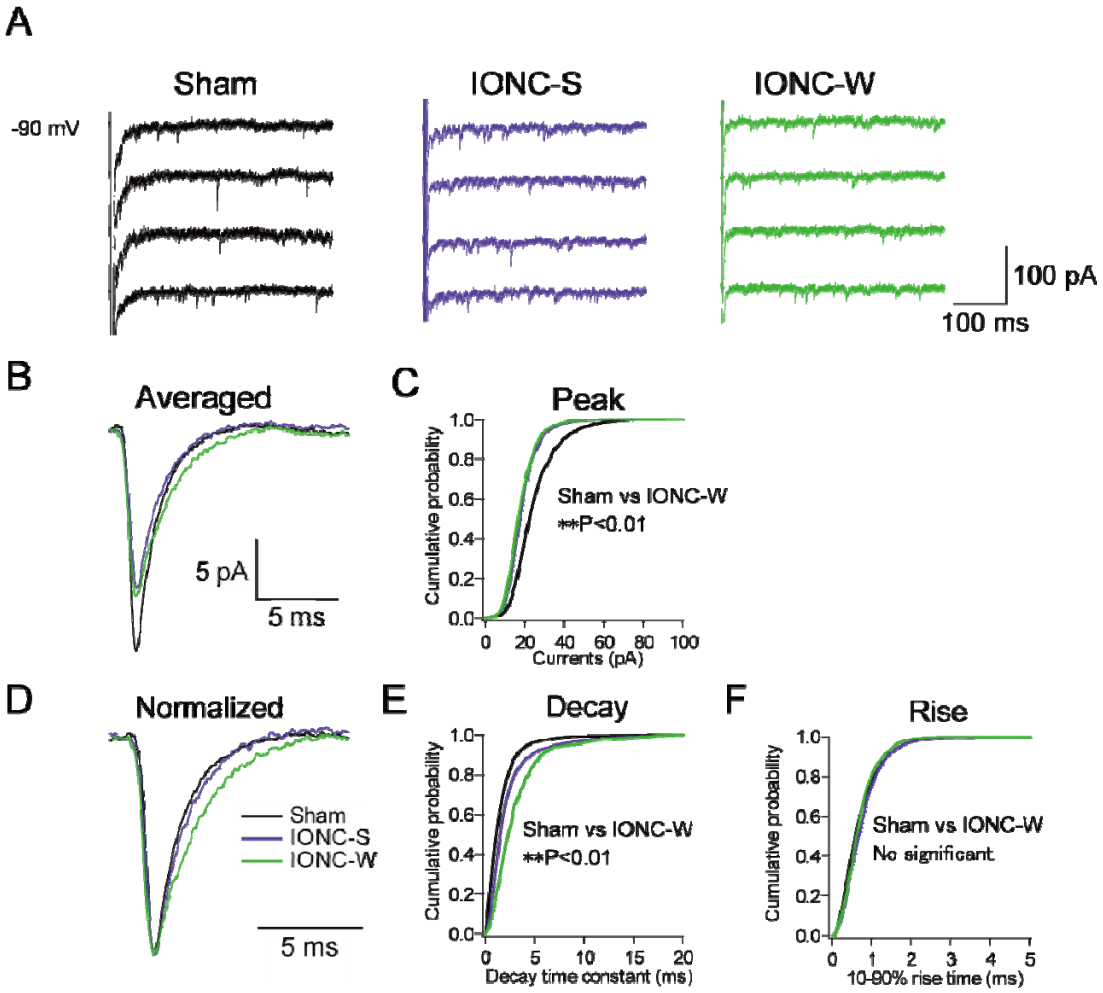
A
Sham
IONC-S
IONC-W
-90 mV
100 pA
100 ms
B
Averaged
5 pA
5 ms
C
Peak
Cumulative probability
Sham vs IONC-W
**P<0.01
Currents (pA)
D
Normalized
Sham
IONC-S
IONC-W
5 ms
E
Decay
Cumulative probability
Sham vs IONC-W
**P<0.01
Decay time constant (ms)
F
Rise
Cumulative probability
Sham vs IONC-W
No significant
10-90% rise time (ms)

Figure 16

Figure 17. Relatively abundant GluR2 containing AMPAR compositions at Weak fiber synapses

Pure AMPAR-mediated lemniscal EPSCs were isolated in the presence of 100 μM APV. *A*, Representative raw traces of AMPAR-mediated lemniscal EPSCs at various holding potentials ranged ±60 mV in 10 mV steps. The pipette solution included 0.1 mM spermine. The liquid junction potential was compensated. *B*, Current-voltage relationships of AMPAR-mediated lemniscal EPSCs. Asterisks indicate significant difference between sham and IONC-W.*C*, Summary bar graph showing rectification indexes defined as amplitude at +40 mV per that of at -40 mV. *D*, Representative traces in the presence (thick) and absence (thin) of exogenously applied 1 mM spermine. Each trace is the average of six consecutive raw traces. *E*, Summary inhibitory effects of spermine on amplitude of lemniscal EPSCs. *F*, *G*, Same as (D, E), respectively, but 100 μM pentobarbital instead of spermine. All data are represented as the mean ± S.E.M. Statistical significance was tested by multiple *t*-test with Bonferroni correction following one-way ANOVA. *$P < 0.05$; **$P < 0.01$ (two-tailed).

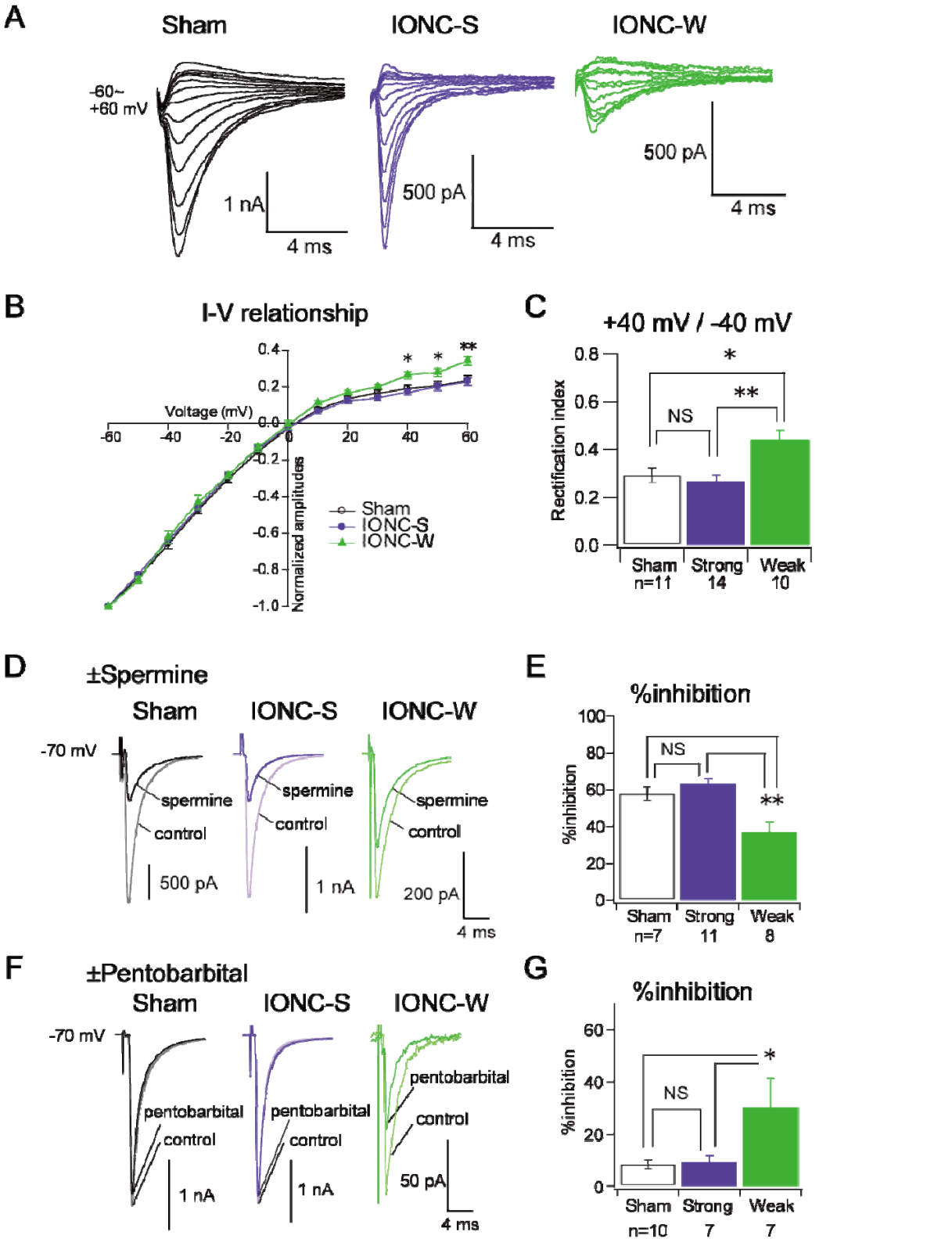
A
Sham
IONC-S
IONC-W
-60~
+60 mV
1 nA
4 ms
500 pA
4 ms
500 pA
4 ms
B
I-V relationship
Voltage (mV)
Normalized amplitudes
Sham
IONC-S
IONC-W
C
+40 mV / -40 mV
Rectification index
NS
Sham
n=11
Strong
14
Weak
10
D
±Spermine
Sham
IONC-S
IONC-W
-70 mV
spermine
control
500 pA
1 nA
200 pA
4 ms
E
%inhibition
%inhibition
NS
Sham
n=7
Strong
11
Weak
8
F
±Pentobarbital
Sham
IONC-S
IONC-W
-70 mV
pentobarbital
control
1 nA
50 pA
4 ms
G
%inhibition
%inhibition
NS
Sham
n=10
Strong
7
Weak
7

Figure 17

Figure 18. AMPA receptor splice variants are not equally distributed among fibers.

Pure AMPAR-mediated lemniscal EPSCs were isolated in the presence of 100 μM APV. CTZ and PEPA are inhibitors of AMPA receptor desensitization, and selective for the flip and flop variants of AMPA receptor subunits, respectively. *A*, Representative traces of lemniscal EPSCs in the presence of 100 μM CTZ (thick line) are overlaid with control traces (thin line). Each trace is the average of six consecutive raw traces. *C*, Same as (A) but in the presence of 100 μM PEPA instead of CTZ. *B*, Percent increments of area under the curve by CTZ. *D*, Same as (B) but in the presence of 100 μM PEPA instead of CTZ. Each column represents the mean ± S.E.M. Statistical significance was tested by multiple *t*-test with Bonferroni correction following one-way ANOVA. $*P < 0.05$ (two-tailed).

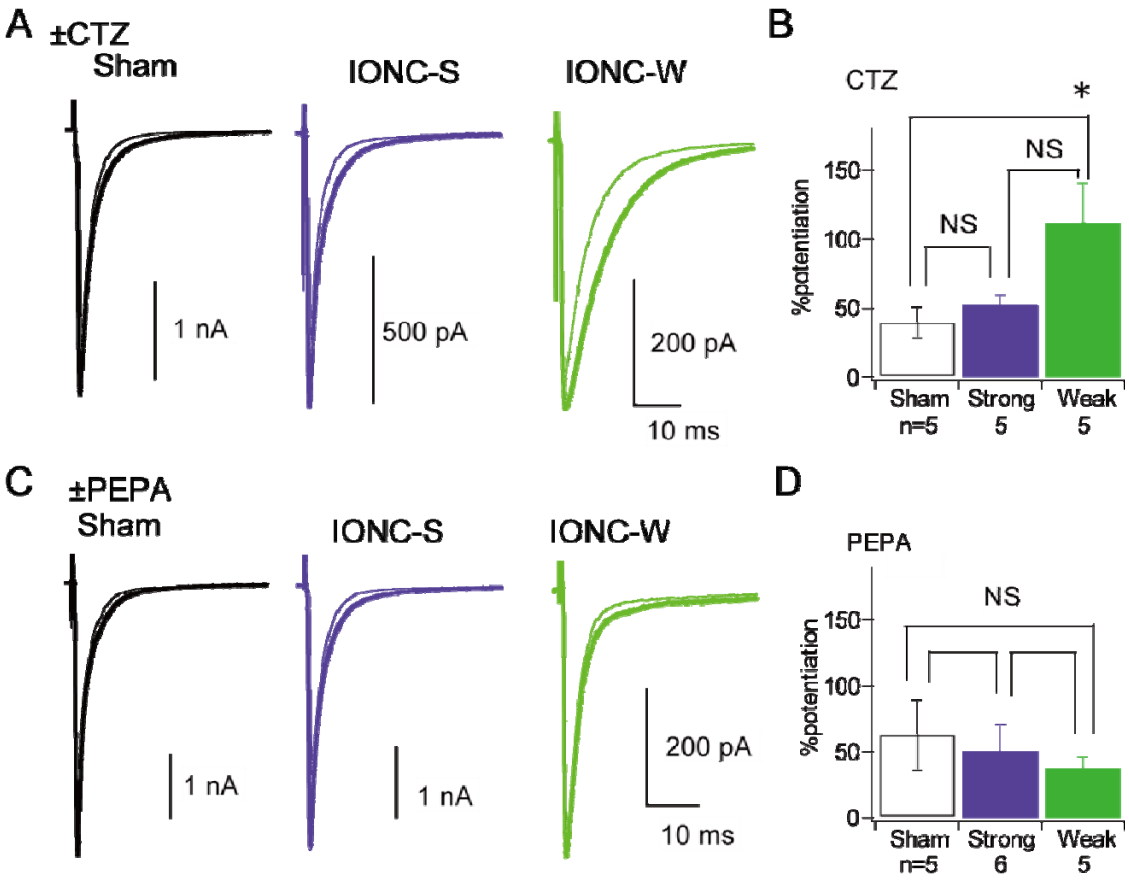
A
±CTZ
Sham
IONC-S
IONC-W
1 nA
500 pA
200 pA
10 ms
B
CTZ
*
NS
NS
%potentiation
150
100
50
0
Sham
n=5
Strong
5
Weak
5
C
±PEPA
Sham
IONC-S
IONC-W
1 nA
1 nA
200 pA
10 ms
D
PEPA
NS
%potentiation
150
100
50
0
Sham
n=5
Strong
6
Weak
5

Figure 18

Figure 19. NMDA receptor compositions are not different among the fibers.

Twenty micromolar NBQX was present in ACSF. *A*, Representative raw traces of NMDAR-mediated lemniscal EPSCs at various holding potentials between from +40 mV to -100 mV in 10 mV decrements. *B*, Current-voltage relationships of NMDAR-mediated lemniscal EPSCs. The liquid junction potential was compensated. *C*, Representative traces at 40 mV are normalized by their peak amplitude. Peaks are 671 pA, 1321 pA, and 261 pA for sham, IONC-S, and IONC-W fiber, respectively. *D*, Decay time constants of NMDAR-mediated EPSCs from each fiber are summarized. Statistical significance was tested by multiple *t*-test with Bonferroni correction following one-way ANOVA. NS: $P > 0.05$. All data are expressed as the mean ± S.E.M.

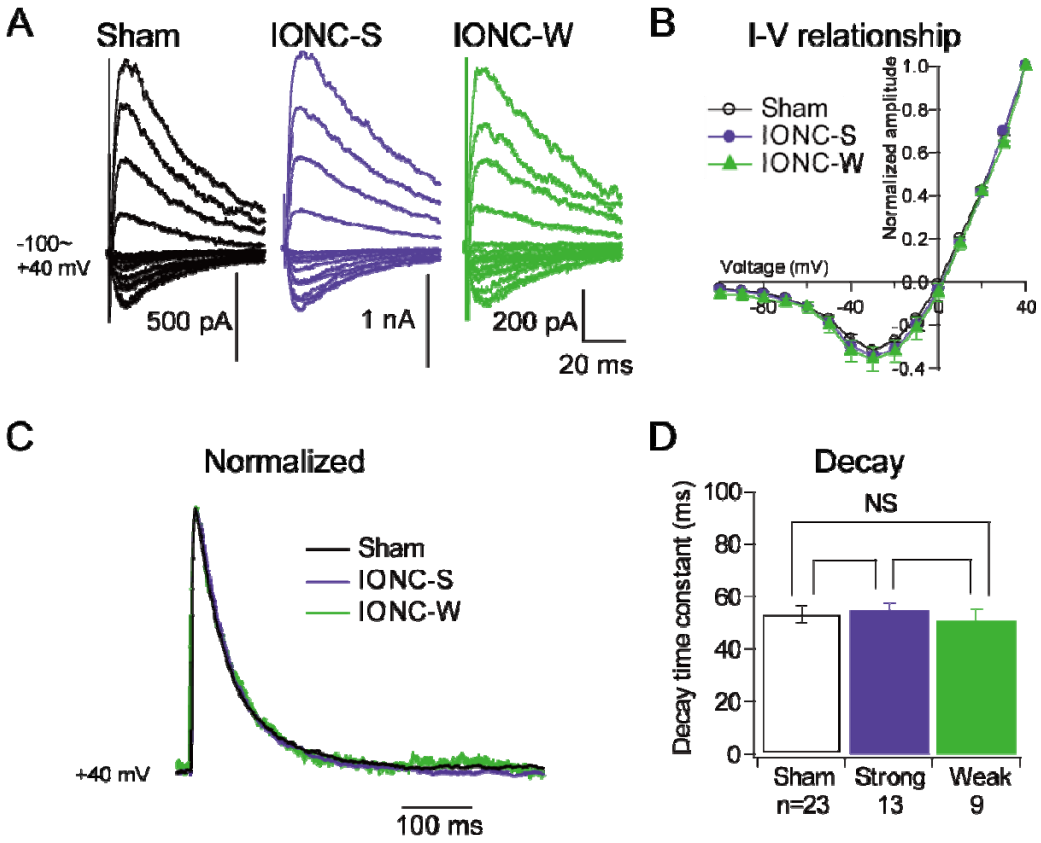
A
Sham
IONC-S
IONC-W
-100~
+40 mV
500 pA
1 nA
200 pA
20 ms
B
I-V relationship
Sham
IONC-S
IONC-W
Normalized amplitude
1.0
0.8
0.6
0.4
0.2
0.0
-0.4
Voltage (mV)
-80
-40
0
40
C
Normalized
Sham
IONC-S
IONC-W
+40 mV
100 ms
D
Decay
NS
Decay time constant (ms)
100
80
60
40
20
0
Sham
n=23
Strong
13
Weak
9

Figure 19

Figure 20. The elevated paired-pulse ratio and coefficient of variation of lemniscal EPSCs at IONC-W synapses

A, Representative raw traces of single fiber-mediated lemniscal EPSCs evoked by paired pulse stimulation, the interpulse interval of which is 50 ms. Traces are normalized by their peak height of the first EPSCs (2101 pA, 5829 pA, and 381 pA for sham, IONC-S, and IONC-W, respectively). *B*, The mean of paired-pulse ratio is plotted as a function of interpulse interval. Numbers of experiments are 6, 10, and 6 for sham, IONC-S, and IONC-W. Each point represents the mean ± S.E.M. Paired-pulse ratio of IONC-W fiber was significantly different from that of sham and IONC-S (*$P < 0.05$ vs. sham; **$P < 0.01$ vs. IONC-S, two-way repeated ANOVA). *C*, The coefficient of variation of 30 consecutive EPSC amplitude was calculated and summarized. Each column represents the mean ± S.E.M. of 25 separate cells. Statistical significance was tested by multiple *t*-test with Bonferroni correction following one-way ANOVA. **$P < 0.01$ (two-tailed).

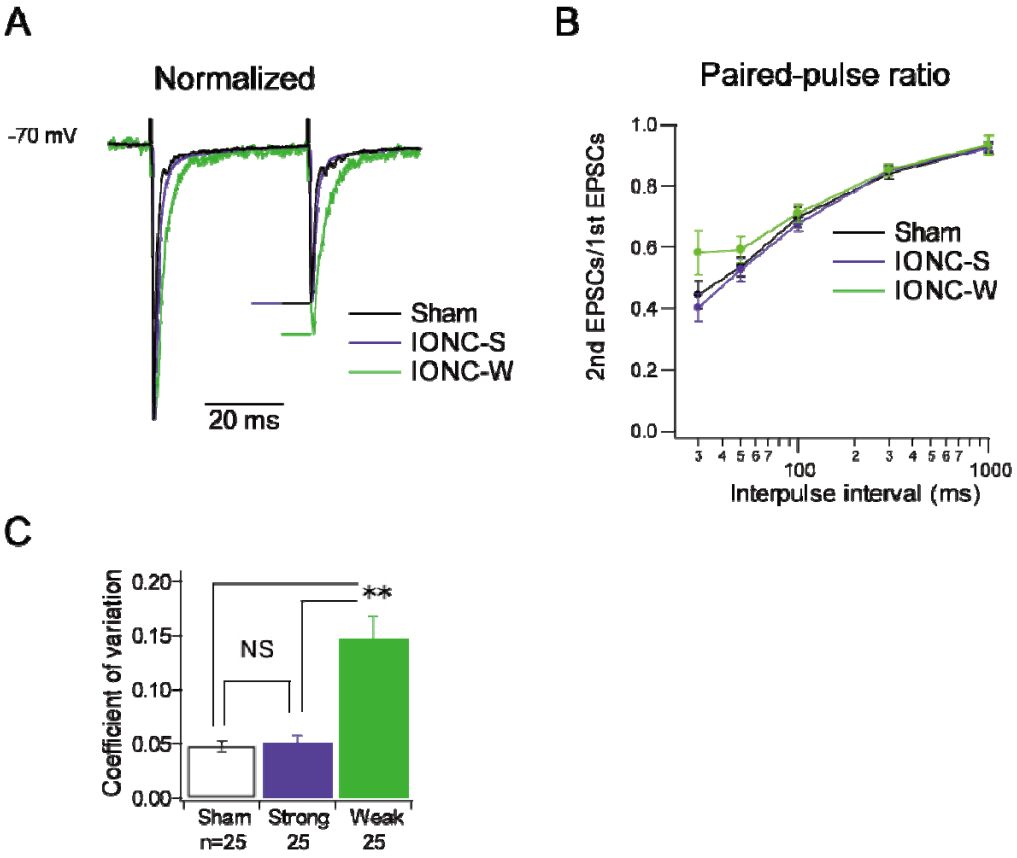
A
Normalized
-70 mV
20 ms
Sham
IONC-S
IONC-W
B
Paired-pulse ratio
2nd EPSCs/1st EPSCs
1.0
0.8
0.6
0.4
0.2
0.0
3 4 5 6 7 100 2 3 4 5 6 7 1000
Interpulse interval (ms)
Sham
IONC-S
IONC-W
C
Coefficient of variation
0.20
0.15
0.10
0.05
0.00
NS
**
Sham n=25
Strong 25
Weak 25

Figure 20

Figure 21. No effect of whisker deprivation on lemniscal fiber innervation

A, The experimental schedule of whisker deprivation. Whisker deprivation was done every day from P21 to the recording day. *B*, Representative traces of lemniscal EPSCs from a deprived mouse. Several raw traces with different stimulus intensities are superimposed. The holding potential was +40 mV or -70 mV. *C*, Summary histograms showing the number of discrete steps of EPSCs. No significant difference was observed between two group ($P = 0.74$, two-tailed, Wilcoxon-Mann-Whitney two-sample rank test).

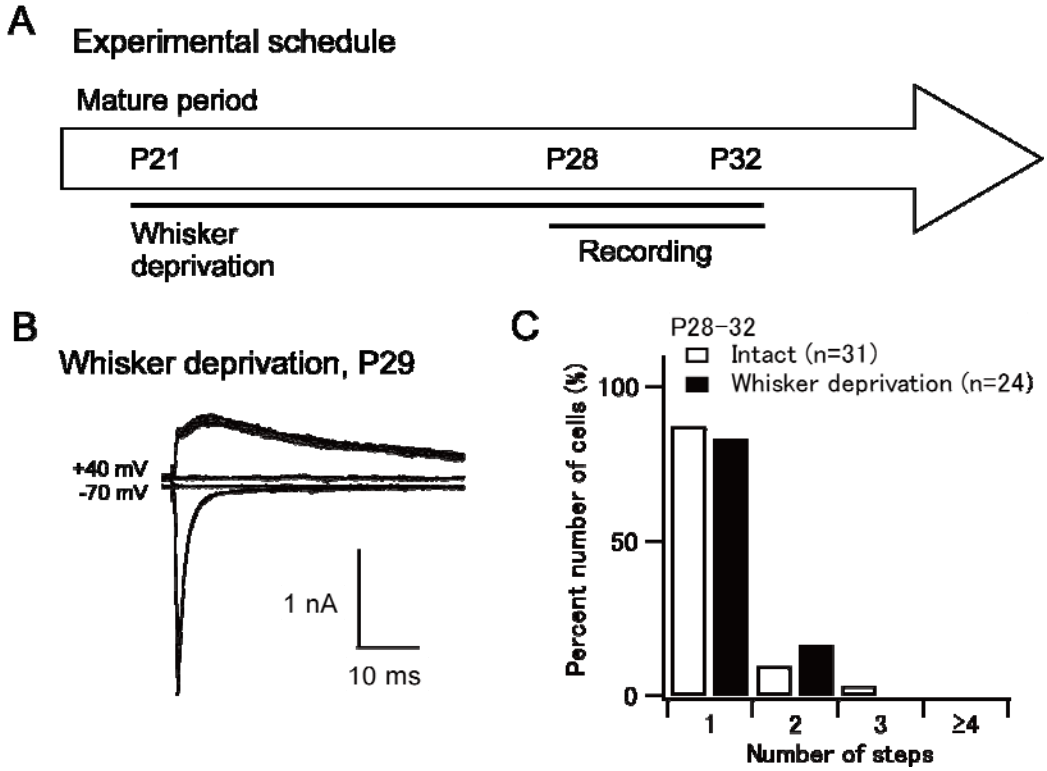
A
Experimental schedule
Mature period
P21
P28
P32
Whisker deprivation
Recording
B
Whisker deprivation, P29
+40 mV
-70 mV
1 nA
10 ms
C
P28–32
Intact (n=31)
Whisker deprivation (n=24)
Percent number of cells (%)
100
50
0
1
2
3
≥4
Number of steps

Figure 21

Figure 22. No morphological change of relay neuron after deafferentation

A, Camera lucida reconstructed projection images of relay neurons. Red traces indicate putative axons of relay neurons. *B*, *C*, Summary bar graphs showing projected area of soma and dendrite, respectively. Each column represents the mean ± S.E.M. of 6 - 7 separate cells.

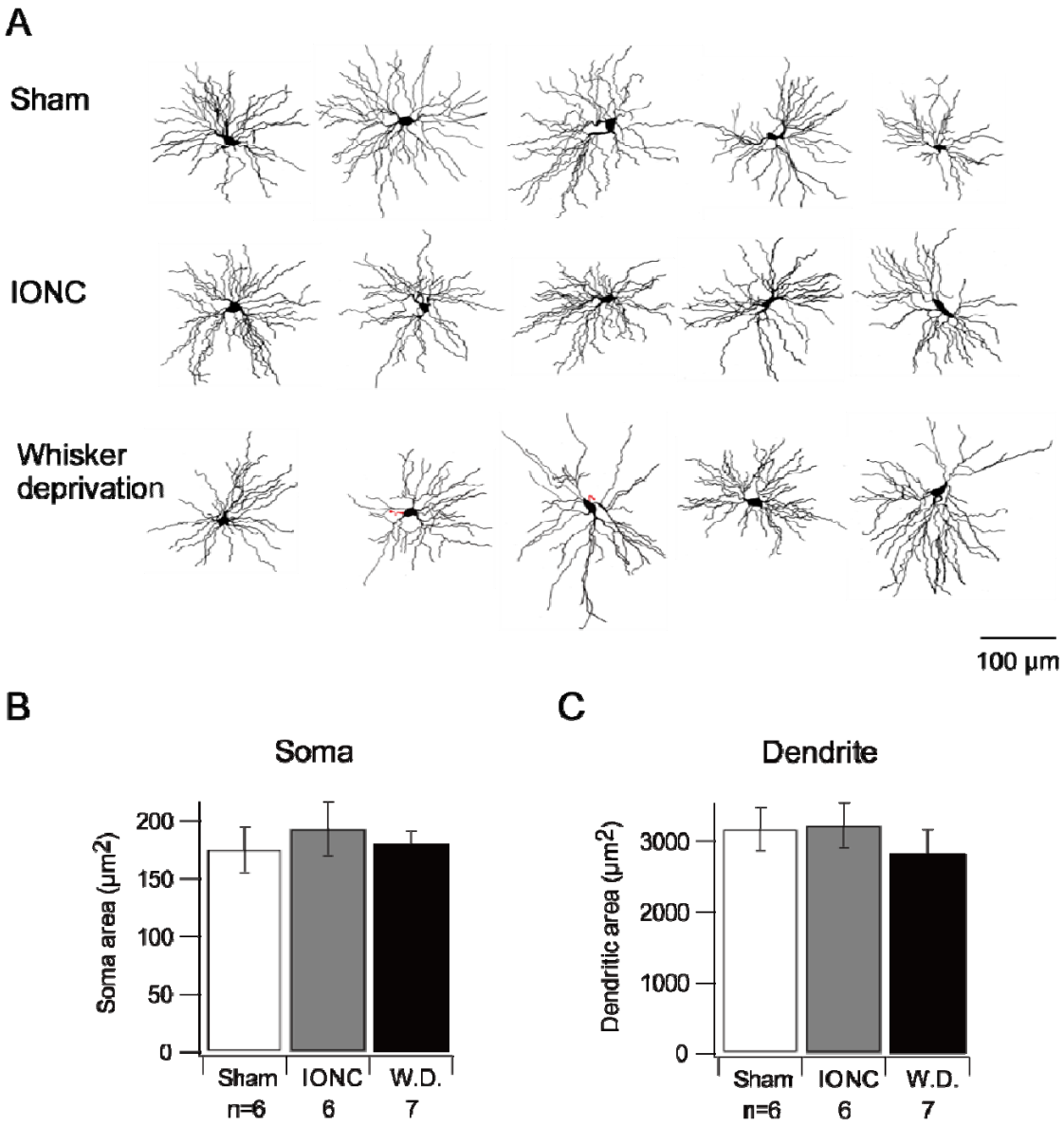
A
Sham
IONC
Whisker deprivation
100 µm
B
Soma
Soma area (µm2)
200
150
100
50
0
Sham
n=6
IONC
6
W.D.
7
C
Dendrite
Dendritic area (µm2)
3000
2000
1000
0
Sham
n=6
IONC
6
W.D.
7

Figure 22

Chapter 3: General discussion

In the present study, the peripheral nerve injury induced the remodeling of lemniscal fibers. The remodeled lemniscal fibers exhibited immature-like properties, including the multiple innervation, the small AMPA/NMDA ratio, and the relatively abundant GluR2-containing flip-type AMPA receptor compositions (summarized in Fig. 23 and Table 1). These observations are well consistent with the general concept that the developing and remodeled nervous systems share common features (Brown et al., 1981; Waxman et al., 1994; Nabekura, 1997; Chang and Balice-Gordon, 2000; Furukawa et al., 2000; Nabekura et al., 2002; Coull et al., 2003; Yoshimura et al., 2004; Chen et al., 2005; Mowery and Garraghty, 2009; Yamahachi et al., 2009). In this chapter, first, I compare the developing and remodeled lemniscal synapses. I then compare my data on lemniscal synapses and the data on other particular synapses, and discuss the similarity between the developing and pathologically remodeled (by nerve injury etc.) nervous systems. Furthermore, I discuss the functional significance of multiple innervations in both the developing and remodeled nervous systems.

Are the developing and remodeled lemniscal synapses identical?

The IONC operation induced immature-like synapses (IONC-W synapses) (Fig. 23 and Table 1). However, the remodeled state does not simply correspond to a particular developmental stage. That is, one week after the IONC operation, the number of innervation and the total

EPSC amplitude are similar to those on P15 - 18 (Fig. 1, 3, 8, and 11). On the other hand, the properties of AMPAR-mediated EPSCs of IONC-W synapses and the AMPA/NMDA ratio are similar to those on much earlier developmental stages (P0 - 9) (Fig. 3 – 5 and 14 - 18). In addition, at the IONC-W synapses, the immature type AMPA receptors and the mature type NMDA receptors coexist (Fig. 19). Thus, although it exhibits the immature-like features, the remodeled state is not completely same as a developmental stage but a particular pathological state.

Multiple innervations at various synapses in both the developmental and the remodeling stages

Developmental synapse elimination and nerve injury-induced remodeling are observed in both the peripheral (PNS) and central nervous systems (CNS). In newborn animals, each skeletal muscle fiber receives multiple axons of motor neurons. Redundant motor axons are then eliminated and each skeletal muscle fiber becomes innervated by a single motor axon during the first few weeks after the birth (Redfern, 1970; Brown et al., 1976; Purves and Lichtman, 1980; Thompson, 1983). Even after the establishment of the monoinnervation, the lesion (crush or cut) of motor nerves induces the multiple reinnervation of motor axons onto a skeletal muscle fiber (Brown et al., 1981; Rich and Lichtman, 1989). Thus, at the adult neuromuscular junctions, the lesion of motor nerve can induce the active remodeling toward

an immature phenotype in synaptic connection. In the CNS, lesions of peripheral nerves can induce sprouting of axons in the cerebral cortex and the active remodeling of spines on dendrites of pyramidal neurons, which are most frequently observed during the postnatal development (Darian-Smith and Gilbert, 1994; Florence et al., 1998; Metz et al., 2009; Yamahachi et al., 2009). In the case of the cerebellum, it is well known that a neonatal Purkinje cell receives multiple climbing fibers. The Purkinje cell is then subject to developmental synapse elimination during the first two postnatal weeks to become innervated by a single climbing fiber (Crepel et al., 1976; Hashimoto and Kano, 2005). Translocation of a climbing fiber from soma to distal dendrites of the Purkinje cell also characterizes the postnatal development of climbing fiber synapses (Hashimoto et al., 2009). The developmental elimination of climbing fiber synapses is very similar to that of lemniscal synapses in the VPM (*see chapter 1*). However, the injury-induced changes of both of which are not identical. The cut of olivo-cerebellar projection or the subtotal lesion of the inferior olive nucleus, which is the origin of climbing fibers, induces reinnervation of surviving climbing fibers onto Purkinje cells (Rossi *et al.*, 1991b; Rossi *et al.*, 1991a; Letellier *et al.*, 2007). A surviving climbing fiber after the lesion first innervates Purkinje cell soma, and then moves toward the Purkinje cell dendrites, as a climbing fiber does during the normal postnatal development. However, each mature Purkinje cell receives only one climbing fiber after the lesion, whereas a grafted immature Purkinje cell receives multiple climbing fibers.

Correctively, multiple reinnervation after nerve lesions are generally observed at various synapses in both the PNS and the CNS, as the normal development is recapitulated. The study in the cerebellum suggests that the maturity of postsynaptic cells is one of the determinants whether the multiple reinnervation occurs.

Reversion to the immature receptor compositions after the nerve injury

I found relatively abundant of GluR2-containing flip-type receptors at the remodeled lemniscal synapses, which dominantly express in the immature thalamus. In the PNS, nicotinic acetylcholine receptors at the neuromuscular synapses are subject to the developmental change in subunit composition (from αβγδ to αβεδ type), which contributes to the developmental speeding of neuromuscular EPSCs (Sakmann and Brenner, 1978; Mishina et al., 1986). The lesion of motor axons induces the reversion toward the immature composition (αβγδ type) (Witzemann et al., 1991). In the CNS, GluR2-containg AMPA receptors of the cerebral cortex are developmentally up-regulated, notably which is the reverse direction in the thalamus (Pellegrini-Giampietro et al., 1992). The retinal lesion induces the retrogression of the developmental switch of AMPA receptors in the cerebral cortex (Mowery and Garraghty, 2009). NR2B-dominant NMDA receptors, the expression of which is an immature phenotype in the cortex, are also up-regulated in the adult cerebral cortex by the peripheral tissue inflammation (Wu et al., 2005b). Such nerve injury-induced

reappearance of immature NMDA receptor composition is also observed in the brainstem (Furukawa et al., 2000; Nabekura et al., 2002). However, the remodeled lemniscal synapse did not exhibit change in NMDA receptor composition (Fig. 19 in chapter 2). Thus, it may depend on brain regions whether composition changes of NMDA receptors occur after peripheral nerve lesions. Taken together, also in the receptor level, the remodeling toward immature phenotypes is presumably general after the adult nervous system undergoes pathological conditions.

Functional significance of multiple innervation in both the developing and remodeled nervous systems

Multiple innervations observed in both the developing and remodeled nervous systems appear to have different functional significance. In the developing nervous system, the general goal of multiple innervation and subsequent synapse elimination is considered to be the establishment of functional circuits. For instance, the rewiring in the developing nervous system produces the frequency-dependent topographic map in the auditory brainstem (Kim and Kandler, 2003; Kandler et al., 2009) and the eye-specific segregation in the visual thalamus (Shatz, 1983; Sretavan and Shatz, 1984; Huberman, 2007). On the other hand, the significance of the remodeling in the adult nervous system can be an appropriate adaptation to a new environment, including peripheral nerve lesions (Rossi *et al.*, 1991b; Rossi *et al.*,

1991a; Nakatsuka *et al.*, 1999; Letellier *et al.*, 2007; Nishimura *et al.*, 2007; Yamahachi *et al.*, 2009). The multiple reinnervation of lemniscal fibers observed after the peripheral nerve injury (*see Chapter 2*) may be a synaptic basis of the long-lasting functional changes of the thalamus and the cortex, including the change in receptive field (Merzenich *et al.*, 1984; Pons *et al.*, 1991; Jones and Pons, 1998). Because surroundings (e.g. the mature neuropile) are different from those in the developing state, such remodeling may, however, fall in to maladaptation, which may underlie pathological conditions, such as phantom pain (Davis et al., 1998; Flor et al., 2006).

In conclusion, although the normal development and the remodeling after peripheral nerve lesions would have different functional significance, they appear to have common neural mechanisms by which the nervous system actively reorganizes itself. This self-renewing ability appears to be one of the most important functions of the nervous system.

Figures and Tables

Figure 23. Schema of results

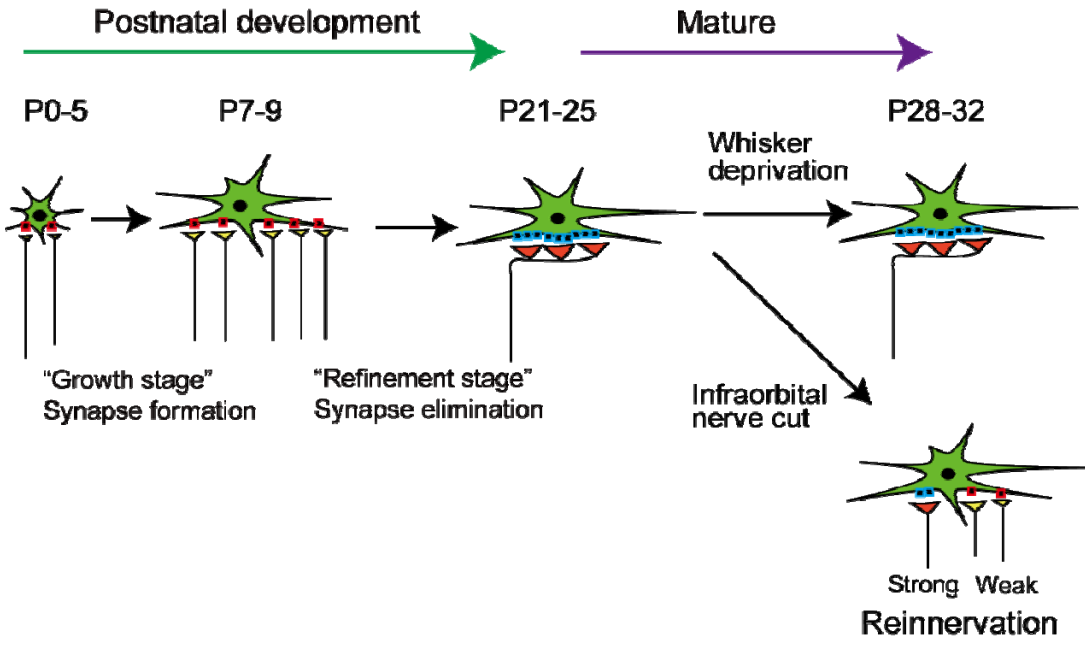

Figure 23

Summary table showing properties of lemniscal synapses

	Immature	Mature	Sham	IONC-Strong	IONC-Weak
Multiple innervation	+++	-	-	++	
Single fiber-mediated EPSCs	Small	Large	Large	Large	Small
miniature EPSCs	N.D. (Small[1*])	N.D. (Large[1*])	Large	Small	Small
AMPA/NMDA ratio	Small	Large	Large	Large	Small
Decay time of NMDAR-mediated EPSCs	Slower (NR2B[2])	Faster (NR2A[2])	Faster	Faster	Faster
Decay time of AMPAR-mediated EPSCs	Slower	Faster	Faster	Faster	Slower
GluR2 containing receptors	N.D. (+ [3,4*])	N.D. (- [3,4*,5])	-	-	+
flip/flop splice variants	flip	flop	flop	flop	flip

* Data from retinogeniculate synapses

1. Chen C, Regehr WG (2000) Developmental remodeling of the retinogeniculate synapse. Neuron 28:955-966.

2. Arsenault D, Zhang ZW (2006) Developmental remodeling of the lemniscal synapse in the ventral basal thalamus of the mouse. J Physiol 573:121-132.

3. Pellegrini-Giampietro DE, Bennett MV, Zukin RS (1992) Are Ca^{2+}-permeable kainate/AMPA receptors more abundant in immature brain? Neurosci Lett 144:65-69.

4. dos Louros SR, Hooks BM, Chen C (2009) Understanding the role of stargazin in the retinogeniculate synapse remodeling. In: Society for Neuroscience. Chicago.

[5. Yamasaki M (2009); *personal communication*]

Table 1

Future direction

To establish further evidence for the multiple reinnervation of lemniscal fibers, I will introduce a tracer technique (Rockland, 2002) from trigeminal nuclei to the VPM (Williams et al., 1994; Veinante and Deschênes, 1999). A paired recording from adjacent relay neurons will reveal sprouting collaterals of lemniscal fibers in the IONC-operated VPM. A functional expanse of lemniscal fibers in IONC-operated mice and its impact on the thalamus can be examined using a functional multineuron calcium imaging technique, while a single lemniscal fiber is stimulated (Ikegaya et al., 2005). However, a pilot study revealed that an AM-ester dye (OGB488-AM) hardly labeled VPM relay neurons even in P7 slices (data not shown). Employment of genetically encoded calcium probes such as G-CaMP family could overcome the problem (Hodgkin and Huxley, 1952; Nakai et al., 2001).

To know whether the IONC operation alters the VPM functionally, basic passive and active membrane properties of relay neurons should be investigated. *In vivo* intracellular voltage recordings are also desired.

To investigate the exact cause or causes (activity or lesion?) which induce(s) multiple innervation of lemniscal fibers, blockade of infraorbital nerve using TTX-Elvax^{TM} and crush of infraorbital nerve should be employed. It can be helpful to examine whether multiple innervation of lemniscal fibers correlate with activities of trigeminal nuclei, the VPM, and cortex after the three operations (cut, crush, and blockade).

Acknowledgements

I would like to express my sincere appreciation to Prof. Mariko Miyata for her continuous support and supervising this study.

I wish to thank Prof. Keiji Imoto for his support, encouragement, and reading this thesis.

I would like to express many thanks to Ms. Naraba, Ms. Mikuniya, and Ms. Ishihara for their technical assistance.

I would like to express many thanks to all members of department of physiology in the Tokyo Women's Medical University and division of Neural Signaling in the National Institute of Physiological Sciences for fruitful discussion.

This study was supported by KAKENHI (18500316 and 20021029) and Takeda Science Foundation for Prof. Miyata. This study was also supported by Grant-in-Aid for JSPS Fellows (21·32).

References

Ahissar E, Sosnik R, Haidarliu S (2000) Transformation from temporal to rate coding in a somatosensory thalamocortical pathway. Nature 406:302-306.

Allen CB, Celikel T, Feldman DE (2003) Long-term depression induced by sensory deprivation during cortical map plasticity in vivo. Nat Neurosci 6:291-299.

Allen PG (2003) the Allen Brain Atlas (http://www.brain-map.org/). In. Seattle, WA, U.S.A.: Allen Institute for Brain Science.

Andjus PR, Zhu L, Cesa R, Carulli D, Strata P (2003) A change in the pattern of activity affects the developmental regression of the Purkinje cell polyinnervation by climbing fibers in the rat cerebellum. Neuroscience 121:563-572.

Arsenault D, Zhang Z-W (2006) Developmental remodelling of the lemniscal synapse in the ventral basal thalamus of the mouse. J Physiol 573:121-132.

Babalian A, Vibert N, Assie G, Serafin M, Mühlethaler M, Vidal P-P (1997) Central vestibular networks in the guinea-pig: functional characterization in the isolated whole brain in vitro. Neuroscience 81:405-426.

Bagnall MW, McElvain LE, Faulstich M, du Lac S (2008) Frequency-independent synaptic transmission supports a linear vestibular behavior. Neuron 60:343-352.

Bekkers JM, Clements JD (1999) Quantal amplitude and quantal variance of strontium-induced asynchronous EPSCs in rat dentate granule neurons. J Physiol 516 (Pt 1):227-248.

Belford GR, Killackey HP (1980) The sensitive period in the development of the trigeminal system of the neonatal rat. J Comp Neurol 193:335-350.

Bender KJ, Allen CB, Bender VA, Feldman DE (2006) Synaptic basis for whisker deprivation-induced synaptic depression in rat somatosensory cortex. J Neurosci 26:4155-4165.

Bowie D, Mayer ML (1995) Inward rectification of both AMPA and kainate subtype glutamate receptors generated by polyamine-mediated ion channel block. Neuron 15:453-462.

Bowie D, Lange GD, Mayer ML (1998) Activity-dependent modulation of glutamate receptors by polyamines. J Neurosci 18:8175-8185.

Brown KE, Arends JJ, Wasserstrom SP, Zantua JB, Jacquin MF, Woolsey TA (1995) Developmental transformation of dendritic arbors in mouse whisker thalamus. Brain Res Mol Brain Res 86:335-339.

Brown MC, Jansen JK, Van Essen D (1976) Polyneuronal innervation of skeletal muscle in new-born rats and its elimination during maturation. J Physiol 261:387-422.

Brown MC, Holland RL, Hopkins WG (1981) Motor nerve sprouting. Annu Rev Neurosci 4:17-42.

Buffelli M, Burgess RW, Feng G, Lobe CG, Lichtman JW, Sanes JR (2003) Genetic evidence that relative synaptic efficacy biases the outcome of synaptic competition. Nature 424:430-434.

Bureau I, Dieudonné S, Coussen F, Mulle C (2000) Kainate receptor-mediated synaptic currents in cerebellar Golgi cells are not shaped by diffusion of glutamate. Proc Natl Acad Sci U S A 97:6838-6843.

Burnashev N, Monyer H, Seeburg PH, Sakmann B (1992) Divalent ion permeability of AMPA receptor channels is dominated by the edited form of a single subunit. Neuron 8:189-198.

Cajal SRy (1995) Histology of the nervous system of man and vertebrates. New York: Oxford University Press.

Carvell GE, Simons DJ (1990) Biometric analyses of vibrissal tactile discrimination in the rat. J Neurosci 10:2638-2648.

Castillo PE, Malenka RC, Nicoll RA (1997) Kainate receptors mediate a slow postsynaptic current in hippocampal CA3 neurons. Nature 388:182-186.

Castro-Alamancos MA (2002) Properties of primary sensory (lemniscal) synapses in the ventrobasal thalamus and the relay of high-frequency sensory inputs. J Neurophysiol 87:946-953.

Cathala L, Brickley S, Cull-Candy S, Farrant M (2003) Maturation of EPSCs and intrinsic membrane properties enhances precision at a cerebellar synapse. J Neurosci 23:6074-6085.

Chang Q, Balice-Gordon RJ (2000) Gap junctional communication among developing and injured motor neurons. Brain research Brain research reviews 32:242-249.

Chen C (2009) Impaired synaptic refinement in the thalamus of MeCP2 null mice. In: Neuroscience 2009: Society for Neuroscience. Chicago.

Chen C, Regehr WG (2000) Developmental remodeling of the retinogeniculate synapse. Neuron 28:955-966.

Chen C, Blitz DM, Regehr WG (2002) Contributions of receptor desensitization and saturation to plasticity at the retinogeniculate synapse. Neuron 33:779-788.

Chen J, Leong S-Y, Schachner M (2005) Differential expression of cell fate determinants in neurons and glial cells of adult mouse spinal cord after compression injury. Eur J Neurosci 22:1895-1906.

Chiaia NL, Bennett-Clarke CA, Rhoades RW (1992) Differential effects of peripheral damage on vibrissa-related patterns in trigeminal nucleus principalis, subnucleus interpolaris, and subnucleus caudalis. Neuroscience 49:141-156.

Chiaia NL, Bennett-Clarke CA, Crissman RS, Zheng L, Chen M, Rhoades RW (1996) Effect of neonatal axoplasmic transport attenuation in the infraorbital nerve on vibrissae-related patterns in the rat's brainstem, thalamus and cortex. Eur J Neurosci 8:1601-1612.

Cho CH, St-Gelais F, Zhang W, Tomita S, Howe JR (2007) Two families of TARP isoforms that have distinct effects on the kinetic properties of AMPA receptors and synaptic currents. Neuron 55:890-904.

Clem RL, Celikel T, Barth AL (2008) Ongoing in vivo experience triggers synaptic metaplasticity

in the neocortex. Science 319:101-104.

Coull JA, Boudreau D, Bachand K, Prescott SA, Nault F, Sik A, De Koninck P, De Koninck Y (2003) Trans-synaptic shift in anion gradient in spinal lamina I neurons as a mechanism of neuropathic pain. Nature 424:938-942.

Coull JA, Beggs S, Boudreau D, Boivin D, Tsuda M, Inoue K, Gravel C, Salter MW, De Koninck Y (2005) BDNF from microglia causes the shift in neuronal anion gradient underlying neuropathic pain. Nature 438:1017-1021.

Crepel F, Mariani J, Delhaye-Bouchaud N (1976) Evidence for a multiple innervation of Purkinje cells by climbing fibers in the immature rat cerebellum. J Neurobiol 7:567-578.

Darian-Smith C, Gilbert CD (1994) Axonal sprouting accompanies functional reorganization in adult cat striate cortex. Nature 368:737-740.

Davis KD, Kiss ZH, Luo L, Tasker RR, Lozano AM, Dostrovsky JO (1998) Phantom sensations generated by thalamic microstimulation. Nature 391:385-387.

De Biasi S, Amadeo A, Arcelli P, Frassoni C, Meroni A, Spreafico R (1996) Ultrastructural characterization of the postnatal development of the thalamic ventrobasal and reticular nuclei in the rat. Anat Embryol (Berl) 193:341-353.

del Castillo J, Katz B (1954) Quantal components of the end-plate potential. J Physiol 124:560-573.

Desai NS, Cudmore RH, Nelson SB, Turrigiano GG (2002) Critical periods for experience-dependent synaptic scaling in visual cortex. Nat Neurosci 5:783-789.

Dodge FA, Jr., Miledi R, Rahamimoff R (1969) Strontium and quantal release of transmitter at the neuromuscular junction. J Physiol 200:267-283.

dos Louros SR, Hooks BM, Chen C (2009) Understanding the role of stargazin in the retinogeniculate synapse remodeling. In: Neuroscience 2009: Society for Neuroscience. Chicago.

Durand GM, Kovalchuk Y, Konnerth A (1996) Long-term potentiation and functional synapse induction in developing hippocampus. Nature 381:71-75.

Englitz B, Tolnai S, Typlt M, Jost J, Rübsamen R (2009) Reliability of synaptic transmission at the synapses of Held in vivo under acoustic stimulation. PLoS One 4:e7014.

Flor H, Nikolajsen L, Staehelin Jensen T (2006) Phantom limb pain: a case of maladaptive CNS plasticity? Nat Rev Neurosci 7:873-881.

Florence SL, Taub HB, Kaas JH (1998) Large-scale sprouting of cortical connections after peripheral injury in adult macaque monkeys. Science 282:1117-1121.

Florence SL, Hackett TA, Strata F (2000) Thalamic and cortical contributions to neural plasticity after limb amputation. J Neurophysiol 83:3154-3159.

Foster KA, Crowley JJ, Regehr WG (2005) The influence of multivesicular release and postsynaptic receptor saturation on transmission at granule cell to Purkinje cell synapses. J Neurosci 25:11655-11665.

Fox K (1992) A critical period for experience-dependent synaptic plasticity in rat barrel cortex. J Neurosci 12:1826-1838.

Fox K (2008) Barrel cortex. Cambridge: Cambridge University Press.

Fox K, Schlaggar BL, Glazewski S, O'Leary DDM (1996) Glutamate receptor blockade at cortical synapses disrupts development of thalamocortical and columnar organization in somatosensory cortex. Proc Natl Acad Sci U S A 93:5584-5589.

Furukawa Y, Okada M, Akaike N, Hayashi T, Nabekura J (2000) Reduction of voltage-dependent magnesium block of *N*-methyl-D-aspartate receptor-mediated current by *in vivo* axonal injury. Neuroscience 96:385-392.

Futai K, Okada M, Matsuyama K, Takahashi T (2001) High-fidelity transmission acquired via a developmental decrease in NMDA receptor expression at an auditory synapse. J Neurosci 21:3342-3349.

Geiger JR, Melcher T, Koh D-S, Sakmann B, Seeburg PH, Jonas P, Monyer H (1995) Relative abundance of subunit mRNAs determines gating and Ca^{2+} permeability of AMPA receptors in principal neurons and interneurons in rat CNS. Neuron 15:193-204.

Giummarra MJ, Gibson SJ, Georgiou-Karistianis N, Bradshaw JL (2007) Central mechanisms in phantom limb perception: the past, present and future. Brain Res Rev 54:219-232.

Goda Y, Stevens CF (1994) Two components of transmitter release at a central synapse. Proc Natl Acad Sci U S A 91:12942-12946.

Goel A, Lee H-K (2007) Persistence of experience-induced homeostatic synaptic plasticity through adulthood in superficial layers of mouse visual cortex. J Neurosci 27:6692-6700.

Grüsser SM, Winter C, Mühlnickel W, Denke C, Karl A, Villringer K, Flor H (2001) The relationship of perceptual phenomena and cortical reorganization in upper extremity amputees. Neuroscience 102:263-272.

Granseth B, Ahlstrand E, Lindström S (2002) Paired pulse facilitation of corticogeniculate EPSCs in the dorsal lateral geniculate nucleus of the rat investigated in vitro. J Physiol 544:477-486.

Graziano A, Jones EG (2009) Early withdrawal of axons from higher centers in response to peripheral somatosensory denervation. J Neurosci 29:3738-3748.

Graziano A, Liu X-B, Murray KD, Jones EG (2008) Vesicular glutamate transporters define two sets of glutamatergic afferents to the somatosensory thalamus and two thalamocortical projections in the mouse. J Comp Neurol 507:1258-1276.

Greene EC (1955) Anatomy of the rat. New York: Hafner.

Harris RM (1986) Morphology of physiologically identified thalamocortical relay neurons in the rat ventrobasal thalamus. J Comp Neurol 251:491-505.

Hashimoto K, Kano M (2003) Functional differentiation of multiple climbing fiber inputs during synapse elimination in the developing cerebellum. Neuron 38:785-796.

Hashimoto K, Kano M (2005) Postnatal development and synapse elimination of climbing fiber to

Purkinje cell projection in the cerebellum. Neurosci Res 53:221-228.

Hashimoto K, Ichikawa R, Kitamura K, Watanabe M, Kano M (2009) Translocation of a "winner" climbing fiber to the Purkinje cell dendrite and subsequent elimination of "losers" from the soma in developing cerebellum. Neuron 63:106-118.

Henderson TA, Woolsey TA, Jacquin MF (1992) Infraorbital nerve blockade from birth does not disrupt central trigeminal pattern formation in the rat. Brain Res Dev Brain Res 66:146-152.

Hodgkin AL, Huxley AF (1952) A quantitative description of membrane current and its application to conduction and excitation in nerve. J Physiol 117:500-544.

Hollmann M, Heinemann S (1994) Cloned glutamate receptors. Annu Rev Neurosci 17:31-108.

Hooks BM, Chen C (2006) Distinct roles for spontaneous and visual activity in remodeling of the retinogeniculate synapse. Neuron 52:281-291.

Hooks BM, Chen C (2008) Vision triggers an experience-dependent sensitive period at the retinogeniculate synapse. J Neurosci 28:4807-4817.

Huberman AD (2007) Mechanisms of eye-specific visual circuit development. Curr Opin Neurobiol 17:73-80.

Huh GS, Boulanger LM, Du H, Riquelme PA, Brotz TM, Shatz CJ (2000) Functional requirement for class I MHC in CNS development and plasticity. Science 290:2155-2159.

Ikegaya Y, Le Bon-Jego M, Yuste R (2005) Large-scale imaging of cortical network activity with calcium indicators. Neurosci Res 52:132-138.

Isa T, Iino M, Ozawa S (1996) Spermine blocks synaptic transmission mediated by Ca^{2+}-permeable AMPA receptors. Neuroreport 7:689-692.

Isa T, Iino M, Itazawa S, Ozawa S (1995) Spermine mediates inward rectification of Ca^{2+}-permeable AMPA receptor channels. Neuroreport 6:2045-2048.

Isaac JT, Crair MC, Nicoll RA, Malenka RC (1997) Silent synapses during development of thalamocortical inputs. Neuron 18:269-280.

Jain N, Florence SL, Qi H-X, Kaas JH (2000) Growth of new brainstem connections in adult monkeys with massive sensory loss. Proc Natl Acad Sci U S A 97:5546-5550.

Jain N, Qi H-X, Collins CE, Kaas JH (2008) Large-scale reorganization in the somatosensory cortex and thalamus after sensory loss in macaque monkeys. J Neurosci 28:11042-11060.

Jones EG (2000) Cortical and subcortical contributions to activity-dependent plasticity in primate somatosensory cortex. Annu Rev Neurosci 23:1-37.

Jones EG (2007) The thalamus, 2nd Edition. Cambridge: Cambridge University Press.

Jones EG, Pons TP (1998) Thalamic and brainstem contributions to large-scale plasticity of primate somatosensory cortex. Science 282:1121-1125.

Jones EG, Tighilet B, Tran B-V, Huntsman MM (1998) Nucleus- and cell-specific expression of NMDA and non-NMDA receptor subunits in monkey thalamus. J Comp Neurol 397:371-393.

Jones LM, Depireux DA, Simons DJ, Keller A (2004) Robust temporal coding in the trigeminal system. Science 304:1986-1989.

Kaas JH, Florence SL, Jain N (1999) Subcortical contributions to massive cortical reorganizations. Neuron 22:657-660.

Kandler K, Clause A, Noh J (2009) Tonotopic reorganization of developing auditory brainstem circuits. Nat Neurosci 12:711-717.

Kano M, Hashimoto K (2009) Synapse elimination in the central nervous system. Curr Opin Neurobiol 19:154-161.

Kano M, Hashimoto K, Kurihara H, Watanabe M, Inoue Y, Aiba A, Tonegawa S (1997) Persistent multiple climbing fiber innervation of cerebellar Purkinje cells in mice lacking mGluR1. Neuron 18:71-79.

Kano M, Hashimoto K, Chen C, Abeliovich A, Aiba A, Kurihara H, Watanabe M, Inoue Y, Tonegawa S (1995) Impaired synapse elimination during cerebellar development in PKCγ mutant mice. Cell 83:1223-1231.

Kano M, Hashimoto K, Watanabe M, Kurihara H, Offermanns S, Jiang H, Wu Y, Jun K, Shin HS, Inoue Y, Simon MI, Wu D (1998) Phospholipase Cβ4 is specifically involved in climbing fiber synapse elimination in the developing cerebellum. Proc Natl Acad Sci U S A 95:15724-15729.

Katz LC, Shatz CJ (1996) Synaptic activity and the construction of cortical circuits. Science 274:1133-1138.

Keinänen K, Wisden W, Sommer B, Werner P, Herb A, Verdoorn TA, Sakmann B, Seeburg PH (1990) A family of AMPA-selective glutamate receptors. Science 249:556-560.

Kerchner GA, Nicoll RA (2008) Silent synapses and the emergence of a postsynaptic mechanism for LTP. Nat Rev Neurosci 9:813-825.

Kidd FL, Isaac JT (1999) Developmental and activity-dependent regulation of kainate receptors at thalamocortical synapses. Nature 400:569-573.

Kidd FL, Isaac JT (2001) Kinetics and activation of postsynaptic kainate receptors at thalamocortical synapses: role of glutamate clearance. J Neurophysiol 86:1139-1148.

Killackey HP, Rhoades RW, Bennett-Clarke CA (1995) The formation of a cortical somatotopic map. Trends Neurosci 18:402-407.

Kim G, Kandler K (2003) Elimination and strengthening of glycinergic/GABAergic connections during tonotopic map formation. Nat Neurosci 6:282-290.

Koike-Tani M, Saitoh N, Takahashi T (2005) Mechanisms underlying developmental speeding in AMPA-EPSC decay time at the calyx of Held. J Neurosci 25:199-207.

Krupa DJ, Wiest MC, Shuler MG, Laubach M, Nicolelis MA (2004) Layer-specific somatosensory cortical activation during active tactile discrimination. Science 304:1989-1992.

Leamey CA, Ho SM (1998) Afferent arrival and onset of functional activity in the trigeminothalamic pathway of the rat. Brain Res Mol Brain Res 105:195-207.

Letellier M, Bailly Y, Demais V, Sherrard RM, Mariani J, Lohof AM (2007) Reinnervation of late postnatal Purkinje cells by climbing fibers: neosynaptogenesis without transient multi-innervation. J Neurosci 27:5373-5383.

Li P, Wilding TJ, Kim SJ, Calejesan AA, Huettner JE, Zhuo M (1999) Kainate-receptor-mediated sensory synaptic transmission in mammalian spinal cord. Nature 397:161-164.

Li X, Glazewski S, Lin X, Elde R, Fox K (1995) Effect of vibrissae deprivation on follicle innervation, neuropeptide synthesis in the trigeminal ganglion, and S1 barrel cortex plasticity. J Comp Neurol 357:465-481.

Liao D, Hessler NA, Malinow R (1995) Activation of postsynaptically silent synapses during pairing-induced LTP in CA1 region of hippocampal slice. Nature 375:400-404.

Liu S-QJ, Cull-Candy SG (2000) Synaptic activity at calcium-permeable AMPA receptors induces a switch in receptor subtype. Nature 405:454-458.

Liu SJ, Zukin RS (2007) Ca^{2+}-permeable AMPA receptors in synaptic plasticity and neuronal death. Trends Neurosci 30:126-134.

Liu X, Chen C (2008) Different Roles for AMPA and NMDA Receptors in Transmission at the Immature Retinogeniculate Synapse. J Neurophysiol 99:629-643.

Lo F-S, Erzurumlu RS (2007) Conversion of functional synapses into silent synapses in the trigeminal brainstem after neonatal peripheral nerve transection. J Neurosci 27:4929-4934.

Lorenzetto E, Caselli L, Feng G, Yuan W, Nerbonne JM, Sanes JR, Buffelli M (2009) Genetic perturbation of postsynaptic activity regulates synapse elimination in developing cerebellum. Proc Natl Acad Sci U S A 106:16475-16480.

Manabe T, Wyllie DJ, Perkel DJ, Nicoll RA (1993) Modulation of synaptic transmission and long-term potentiation: effects on paired pulse facilitation and EPSC variance in the CA1 region of the hippocampus. J Neurophysiol 70:1451-1459.

Manger PR, Woods TM, Jones EG (1996) Plasticity of the somatosensory cortical map in macaque monkeys after chronic partial amputation of a digit. Proc Biol Sci 263:933-939.

Matthews MA, Faciane CL (1977) Electron microscopy of the development of synaptic patterns in the ventrobasal complex of the rat. Brain Res Mol Brain Res 135:197-215.

Merzenich MM, Nelson RJ, Stryker MP, Cynader MS, Schoppmann A, Zook JM (1984) Somatosensory cortical map changes following digit amputation in adult monkeys. J Comp Neurol 224:591-605.

Metz AE, Yau H-J, Centeno MV, Apkarian AV, Martina M (2009) Morphological and functional reorganization of rat medial prefrontal cortex in neuropathic pain. Proc Natl Acad Sci U S A 106:2423-2428.

Mishina M, Takai T, Imoto K, Noda M, Takahashi T, Numa S, Methfessel C, Sakmann B (1986) Molecular distinction between fetal and adult forms of muscle acetylcholine receptor. Nature 321:406-411.

Miyata M, Imoto K (2006) Different composition of glutamate receptors in corticothalamic and lemniscal synaptic responses and their roles in the firing responses of ventrobasal thalamic neurons in juvenile mice. J Physiol 575:161-174.

Miyata M, Imoto K (2009) Contrary roles of kainate receptors in transmitter release at corticothalamic synapses onto thalamic relay and reticular neurons. J Physiol 587:999-1012.

Miyata M, Kashiwadani H, Fukaya M, Hayashi T, Wu D, Suzuki T, Watanabe M, Kawakami Y (2003) Role of thalamic phospholipase Cβ4 mediated by metabotropic glutamate receptor type 1 in inflammatory pain. J Neurosci 23:8098-8108.

Miyazaki T, Fukaya M, Shimizu H, Watanabe M (2003) Subtype switching of vesicular glutamate transporters at parallel fibre-Purkinje cell synapses in developing mouse cerebellum. Eur J Neurosci 17:2563-2572.

Montemurro MA, Panzeri S, Maravall M, Alenda A, Bale MR, Brambilla M, Petersen RS (2007) Role of precise spike timing in coding of dynamic vibrissa stimuli in somatosensory thalamus. J Neurophysiol 98:1871-1882.

Mosbacher J, Schoepfer R, Monyer H, Burnashev N, Seeburg PH, Ruppersberg JP (1994) A molecular determinant for submillisecond desensitization in glutamate receptors. Science 266:1059-1062.

Mowery TM, Garraghty PE (2009) Nerve-Injury Induced Changes to GluR1 and GluR2/3 Sub-unit Expression in Area 3b of Adult Squirrel Monkeys: Developmental Recapitulation? Front Syst Neurosci 3:1.

Muñoz A, Liu XB, Jones EG (1999) Development of metabotropic glutamate receptors from trigeminal nuclei to barrel cortex in postnatal mouse. J Comp Neurol 409:549-566.

Nabekura J (1997) Reversible changes of the neural pathways and receptor functions associated with development and regeneration following nerve injuries. Fukuoka Igaku Zasshi 88:267-273.

Nabekura J, Ueno T, Katsurabayashi S, Furuta A, Akaike N, Okada M (2002) Reduced NR2A expression and prolonged decay of NMDA receptor-mediated synaptic current in rat vagal motoneurons following axotomy. J Physiol 539:735-741.

Nakagawa T, Iino M, Sekiguchi M, Wada K, Ozawa S (1999) Potentiating effects of 4-[2-(phenylsulfonylamino)ethylthio]-2,6-difluoro-phenoxyaceta mide (PEPA) on excitatory synaptic transmission in dentate granule cells. Neurosci Res 35:217-223.

Nakai J, Ohkura M, Imoto K (2001) A high signal-to-noise Ca^{2+} probe composed of a single green fluorescent protein. Nat Biotechnol 19:137-141.

Nakatsuka T, Park JS, Kumamoto E, Tamaki T, Yoshimura M (1999) Plastic changes in sensory inputs to rat substantia gelatinosa neurons following peripheral inflammation. Pain 82:39-47.

Narushima M, Uchigashima M, Tanimura A, Hashimoto K, Aiba A, Watanabe M, Kano M (2008)

Involvement of type 1 metabotoropic glutamate receptor in developmental synapse elimination in the lateral geniculate nucleus. Neurosci Res 61S:S57.

Nishimura Y, Onoe H, Morichika Y, Perfiliev S, Tsukada H, Isa T (2007) Time-dependent central compensatory mechanisms of finger dexterity after spinal cord injury. Science 318:1150-1155.

Offermanns S, Hashimoto K, Watanabe M, Sun W, Kurihara H, Thompson RF, Inoue Y, Kano M, Simon MI (1997) Impaired motor coordination and persistent multiple climbing fiber innervation of cerebellar Purkinje cells in mice lacking Gαq. Proc Natl Acad Sci U S A 94:14089-14094.

Oliet SHR, Malenka RC, Nicoll RA (1996) Bidirectional control of quantal size by synaptic activity in the hippocampus. Science 271:1294-1297.

Pan B, Zucker RS (2009) A general model of synaptic transmission and short-term plasticity. Neuron 62:539-554.

Partin KM, Patneau DK, Mayer ML (1994) Cyclothiazide differentially modulates desensitization of α-amino-3-hydroxy-5-methyl-4-isoxazolepropionic acid receptor splice variants. Mol Pharmacol 46:129-138.

Paxinos G, Franklin KBJ (2001) The Mouse Brain in Stereotaxic Coordinates, 2nd Edition. San Diego: Academic Press.

Paxinos G, Halliday G, Watson C, Koutcherov Y, Wang H (2007) Atlas of the developing mouse brain at E 17.5, P0, and P6. Amsterdam: Academic Press.

Pellegrini-Giampietro DE, Bennett MV, Zukin RS (1992) Are Ca^{2+}-permeable kainate/AMPA receptors more abundant in immature brain? Neurosci Lett 144:65-69.

Pelletier JC, Hesson DP, Jones KA, Costa A-M (1996) Substituted 1,2-dihydrophthalazines: potent, selective, and noncompetitive inhibitors of the AMPA receptor. J Med Chem 39:343-346.

Peschanski M, Lee CL, Ralston HJ, 3rd (1984) The structural organization of the ventrobasal complex of the rat as revealed by the analysis of physiologically characterized neurons injected intracellularly with horseradish peroxidase. Brain Res Mol Brain Res 297:63-74.

Petersen CCH (2007) The functional organization of the barrel cortex. Neuron 56:339-355.

Petersen RS, Brambilla M, Bale MR, Alenda A, Panzeri S, Montemurro MA, Maravall M (2008) Diverse and temporally precise kinetic feature selectivity in the VPm thalamic nucleus. Neuron 60:890-903.

Pons TP, Garraghty PE, Ommaya AK, Kaas JH, Taub E, Mishkin M (1991) Massive cortical reorganization after sensory deafferentation in adult macaques. Science 252:1857-1860.

Purves D, Lichtman JW (1980) Elimination of synapses in the developing nervous system. Science 210:153-157.

Quirk JC, Siuda ER, Nisenbaum ES (2004) Molecular determinants responsible for differences in desensitization kinetics of AMPA receptor splice variants. J Neurosci 24:11416-11420.

Ramachandran VS, Hirstein W (1998) The perception of phantom limbs. The D. O. Hebb lecture.

Brain 121 (Pt 9):1603-1630.

Rancz EA, Ishikawa T, Duguid I, Chadderton P, Mahon S, Hausser M (2007) High-fidelity transmission of sensory information by single cerebellar mossy fibre boutons. Nature 450:1245-1248.

Redfern PA (1970) Neuromuscular transmission in new-born rats. J Physiol 209:701-709.

Rhoades RW, Strang V, Bennett-Clarke CA, Killackey HP, Chiaia NL (1997) Sensitive period for lesion-induced reorganization of intracortical projections within the vibrissae representation of rat's primary somatosensory cortex. J Comp Neurol 389:185-192.

Rich MM, Lichtman JW (1989) *In vivo* visualization of pre- and postsynaptic changes during synapse elimination in reinnervated mouse muscle. J Neurosci 9:1781-1805.

Rockland KS (2002) Visual cortical organization at the single axon level: a beginning. Neurosci Res 42:155-166.

Rossi F, Wiklund L, van der Want JJL, Strata P (1991a) Reinnervation of cerebellar Purkinje cells by climbing fibres surviving a subtotal lesion of the inferior olive in the adult rat. I. Development of new collateral branches and terminal plexuses. J Comp Neurol 308:513-535.

Rossi F, van der Want JJL, Wiklund L, Strata P (1991b) Reinnervation of cerebellar Purkinje cells by climbing fibres surviving a subtotal lesion of the inferior olive in the adult rat. II. Synaptic organization on reinnervated Purkinje cells. J Comp Neurol 308:536-554.

Rozov A, Zilberter Y, Wollmuth LP, Burnashev N (1998) Facilitation of currents through rat Ca^{2+}-permeable AMPA receptor channels by activity-dependent relief from polyamine block. J Physiol 511 (Pt 2):361-377.

Rumpel S, Hatt H, Gottmann K (1998) Silent synapses in the developing rat visual cortex: evidence for postsynaptic expression of synaptic plasticity. J Neurosci 18:8863-8874.

Sakmann B, Brenner HR (1978) Change in synaptic channel gating during neuromuscular development. Nature 276:401-402.

Sakmann B, Stuart G (1995) Patch-Pipette Recordings from Soma, Dendrites, and Axon of Neurons in Brain Slices. In: Single-Channel Recording, 2nd Edition (Sakmann B, Neher E, eds), pp 199-211. New York: Plenum Press.

Sanes JR, Lichtman JW (1999) Development of the vertebrate neuromuscular junction. Annu Rev Neurosci 22:389-442.

Schlaggar BL, Fox K, O'Leary DDM (1993) Postsynaptic control of plasticity in developing somatosensory cortex. Nature 364:623-626.

Sekiguchi M, Fleck MW, Mayer ML, Takeo J, Chiba Y, Yamashita S, Wada K (1997) A novel allosteric potentiator of AMPA receptors: 4-[2-(phenylsulfonylamino)ethylthio]-2,6-difluoro-phenoxyaceta mide. J Neurosci 17:5760-5771.

Sengelaub DR, Muja N, Mills AC, Myers WA, Churchill JD, Garraghty PE (1997)

Denervation-induced sprouting of intact peripheral afferents into the cuneate nucleus of adult rats. Brain Res Mol Brain Res 769:256-262.

Shatz CJ (1983) The prenatal development of the cat's retinogeniculate pathway. J Neurosci 3:482-499.

Sherrard RM, Dixon KJ, Bakouche J, Rodger J, Lemaigre-Dubreuil Y, Mariani J (2009) Differential expression of TrkB isoforms switches climbing fiber-Purkinje cell synaptogenesis to selective synapse elimination. Dev Neurobiol 69:647-662.

Silver RA, Momiyama A, Cull-Candy SG (1998) Locus of frequency-dependent depression identified with multiple-probability fluctuation analysis at rat climbing fibre-Purkinje cell synapses. J Physiol 510 (Pt 3):881-902.

Sommer B, Keinänen K, Verdoorn TA, Wisden W, Burnashev N, Herb A, Köhler M, Takagi T, Sakmann B, Seeburg PH (1990) Flip and flop: a cell-specific functional switch in glutamate-operated channels of the CNS. Science 249:1580-1585.

Soto D, Coombs ID, Kelly L, Farrant M, Cull-Candy SG (2007) Stargazin attenuates intracellular polyamine block of calcium-permeable AMPA receptors. Nat Neurosci 10:1260-1267.

Špaček J, Lieberman AR (1974) Ultrastructure and three-dimensional organization of synaptic glomeruli in rat somatosensory thalamus. J Anat 117:487-516.

Sretavan D, Shatz CJ (1984) Prenatal development of individual retinogeniculate axons during the period of segregation. Nature 308:845-848.

Stevens B, Allen NJ, Vazquez LE, Howell GR, Christopherson KS, Nouri N, Micheva KD, Mehalow AK, Huberman AD, Stafford B, Sher A, Litke AM, Lambris JD, Smith SJ, John SW, Barres BA (2007) The classical complement cascade mediates CNS synapse elimination. Cell 131:1164-1178.

Thompson W (1983) Synapse elimination in neonatal rat muscle is sensitive to pattern of muscle use. Nature 302:614-616.

Tolnai S, Englitz B, Scholbach J, Jost J, Rübsamen R (2009) Spike transmission delay at the calyx of Held in vivo: rate dependence, phenomenological modeling, and relevance for sound localization. J Neurophysiol 102:1206-1217.

Tomita S, Sekiguchi M, Wada K, Nicoll RA, Bredt DS (2006) Stargazin controls the pharmacology of AMPA receptor potentiators. Proc Natl Acad Sci U S A 103:10064-10067.

Tomita S, Chen L, Kawasaki Y, Petralia RS, Wenthold RJ, Nicoll RA, Bredt DS (2003) Functional studies and distribution define a family of transmembrane AMPA receptor regulatory proteins. J Cell Biol 161:805-816.

Tsuda M, Shigemoto-Mogami Y, Koizumi S, Mizokoshi A, Kohsaka S, Salter MW, Inoue K (2003) $P2X_4$ receptors induced in spinal microglia gate tactile allodynia after nerve injury. Nature 424:778-783.

Turetsky D, Garringer E, Patneau DK (2005) Stargazin modulates native AMPA receptor functional properties by two distinct mechanisms. J Neurosci 25:7438-7448.

Turner JP, Salt TE (1998) Characterization of sensory and corticothalamic excitatory inputs to rat thalamocortical neurones *in vitro*. J Physiol 510 (Pt 3):829-843.

Turrigiano GG (2008) The self-tuning neuron: synaptic scaling of excitatory synapses. Cell 135:422-435.

Van Der Loos H (1976) Barreloids in mouse somatosensory thalamus. Neurosci Lett 2:1-6.

Veinante P, Deschênes M (1999) Single- and multi-whisker channels in the ascending projections from the principal trigeminal nucleus in the rat. J Neurosci 19:5085-5095.

Verdoorn TA, Burnashev N, Monyer H, Seeburg PH, Sakmann B (1991) Structural determinants of ion flow through recombinant glutamate receptor channels. Science 252:1715-1718.

Wadiche JI, Jahr CE (2001) Multivesicular release at climbing fiber-Purkinje cell synapses. Neuron 32:301-313.

Wang H, Zhang Z-W (2008) A critical window for experience-dependent plasticity at whisker sensory relay synapse in the thalamus. J Neurosci 28:13621-13628.

Wang H, Chan GCK, Storm DR, Zhang Z-W (2009) Destinctive roles of adenylyl cyclase 1 in synapse elimination and consolidation. In: Neuroscience 2009: Society for Neuroscience. Chicago.

Washburn MS, Dingledine R (1996) Block of α-amino-3-hydroxy-5-methyl-4-isoxazolepropionic acid (AMPA) receptors by polyamines and polyamine toxins. J Pharmacol Exp Ther 278:669-678.

Waxman SG, Kocsis JD, Black JA (1994) Type III sodium channel mRNA is expressed in embryonic but not adult spinal sensory neurons, and is reexpressed following axotomy. J Neurophysiol 72:466-470.

Williams MN, Zahm DS, Jacquin MF (1994) Differential foci and synaptic organization of the principal and spinal trigeminal projections to the thalamus in the rat. Eur J Neurosci 6:429-453.

Wiser AK, Callaway EM (1996) Contributions of individual layer 6 pyramidal neurons to local circuitry in macaque primary visual cortex. J Neurosci 16:2724-2739.

Witzemann V, Brenner HR, Sakmann B (1991) Neural factors regulate AChR subunit mRNAs at rat neuromuscular synapses. J Cell Biol 114:125-141.

Woolsey TA, van der Loos H (1970) The structural organization of layer IV in the somatosensory region (SI) of mouse cerebral cortex. The description of a cortical field composed of discrete cytoarchitectonic units. Brain Res Mol Brain Res 17:205-242.

Woolsey TA, Anderson JR, Wann JR, Stanfield BB (1979) Effects of early vibrissae damage on neurons in the ventrobasal (VB) thalamus of the mouse. J Comp Neurol 184:363-380.

Wu G-Y, Malinow R, Cline HT (1996) Maturation of a central glutamatergic synapse. Science 274:972-976.

Wu L-J, Zhao M-G, Toyoda H, Ko SW, Zhuo M (2005a) Kainate receptor-mediated synaptic transmission in the adult anterior cingulate cortex. J Neurophysiol 94:1805-1813.

Wu L-J, Toyoda H, Zhao M-G, Lee Y-S, Tang J, Ko SW, Jia YH, Shum FW, Zerbinatti CV, Bu G, Wei F, Xu T-L, Muglia LJ, Chen Z-F, Auberson YP, Kaang BK, Zhuo M (2005b) Upregulation of forebrain NMDA NR2B receptors contributes to behavioral sensitization after inflammation. J Neurosci 25:11107-11116.

Yamahachi H, Marik SA, McManus JNJ, Denk W, Gilbert CD (2009) Rapid axonal sprouting and pruning accompany functional reorganization in primary visual cortex. Neuron 64:719-729.

Yamakado M (1985) Postnatal development of barreloid neuropils in the ventrobasal complex of mouse thalamus: a histochemical study for cytochrome oxidase. No To Shinkei 37:497-506.

Yamakura T, Sakimura K, Mishina M, Shimoji K (1995) The sensitivity of AMPA-selective glutamate receptor channels to pentobarbital is determined by a single amino acid residue of the α2 subunit. FEBS Lett 374:412-414.

Yoshimura M, Furue H, Nakatsuka T, Matayoshi T, Katafuchi T (2004) Functional reorganization of the spinal pain pathways in developmental and pathological conditions. Novartis Found Symp 261:116-124; discussion 124-131, 149-154.

Young AB, Standaert DG, Testa C, Wüllner U, Catania M, Penney JB (1995) Excitatory amino acid receptor distribution: quantitative autoradiographic ligand binding and *In situ* hybridization studies. In: Excitatory Amino Acids and Synaptic Transmission, 2nd Edition (Wheal HV, Thomson AM, eds), pp 29-40. New York: Academic Press.

Zantua JB, Wasserstrom SP, Arends JJ, Jacquin MF, Woolsey TA (1996) Postnatal development of mouse "whisker" thalamus: ventroposterior medial nucleus (VPM), barreloids, and their thalamocortical relay neurons. Somatosens Mot Res 13:307-322.

Zucker RS, Regehr WG (2002) Short-term synaptic plasticity. Annu Rev Physiol 64:355-405.